

# Review of Tensor Network Contraction Approaches

## Shi-Ju Ran

E-mail: [Shi-Ju.Ran@icfo.eu](mailto:Shi-Ju.Ran@icfo.eu)

ICFO-Institut de Ciències Fotoniques, The Barcelona Institute of Science and Technology,  
08860 Castelldefels (Barcelona), Spain

## Emanuele Tirrito

E-mail: [Emanuele.Tirrito@icfo.eu](mailto:Emanuele.Tirrito@icfo.eu)

ICFO-Institut de Ciències Fotoniques, The Barcelona Institute of Science and Technology,  
08860 Castelldefels (Barcelona), Spain

## Cheng Peng

E-mail: [Pengcheng12@mailsucas.ac.cn](mailto:Pengcheng12@mailsucas.ac.cn)

Theoretical Condensed Matter Physics and Computational Materials Physics Laboratory,  
School of Physical Sciences, University of Chinese Academy of Sciences, Beijing 100049,  
China

## Xi Chen

E-mail: [Chenxi213@mailsucas.ac.cn](mailto:Chenxi213@mailsucas.ac.cn)

Theoretical Condensed Matter Physics and Computational Materials Physics Laboratory,  
School of Physical Sciences, University of Chinese Academy of Sciences, Beijing 100049,  
China

## Gang Su

E-mail: [Gsu@ucas.ac.cn](mailto:Gsu@ucas.ac.cn)

Theoretical Condensed Matter Physics and Computational Materials Physics Laboratory,  
School of Physical Sciences, University of Chinese Academy of Sciences, Beijing 100049,  
China

Kavli Institute for Theoretical Sciences, and CAS Center for Excellence in Topological  
Quantum Computation, University of Chinese Academy of Sciences, Beijing 100190, China

## Maciej Lewenstein

E-mail: [Maciej.lewenstein@icfo.eu](mailto:Maciej.lewenstein@icfo.eu)

ICFO-Institut de Ciències Fotoniques, The Barcelona Institute of Science and Technology,  
08860 Castelldefels (Barcelona), Spain

ICREA, Passeig Lluís Companys 23, 08010 Barcelona, Spain

16 October 2019

**Abstract.** Tensor network (TN), a young mathematical tool of high vitality and great potential, has been undergoing extremely rapid developments in the last two decades, gaining tremendous success in condensed matter physics, atomic physics, quantum information science, statistical physics, and so on. This review is designed to give an insightful and practical introduction to TN contraction algorithms. Starting from basic concepts and definitions, we first explain the relations between TN and physical systems, including the TN representations of classical partitions, non-trivial quantum states, time evolution simulations, etc. These problems, which are challenging to solve, can be reduced to TN contraction problems. Then, we present two different but closely-related kinds of algorithms for computing TN contractions: those inspired by numerical renormalization group and those based on self-consistent eigenvalue problems. Their physical implications and practical implementations are discussed in detail. Particularly, the mathematical connections between tensor network encoding and multi-linear algebra are presented.

The readership is expected to range from beginners to specialists, with two main goals. One goal is to provide a systematic introduction of TN contraction algorithms (motivations, implementations, relations, implications, etc.), for those who want to further develop TN algorithms. The other goal is to provide a practical guidance to those, who want to learn and to use TN algorithms to solve practical problems. We expect that the review will be useful to anyone devoted to the interdisciplinary sciences with related numerics.

## 1. Introduction

### 1.1. Numerics: the third way to see the world

One characteristic that defines us, human beings, is the curiosity of the unknown. Since our birth, we have been trying to use any methods that human brains can comprehend to explore the nature: to mimic, to understand and to utilize in a controlled and repeatable way. One of the most ancient means lies in the nature herself, experiments, leading to tremendous achievements from the creation of fire to the scissors of genes. Then comes mathematics, a new world we made by numbers and symbols, where the nature is reproduced by laws and theorems in an extremely simple, beautiful and unprecedentedly accurate manner. With the explosive development of digital sciences, computer was created. It provided us the third way to investigate the nature, a digital world whose laws can be ruled by ourselves with codes and *algorithms* to numerically mimic the real universe.

The best algorithms are often of both efficiency and simplicity, where most variants of the situations they are designed for can be well handled. One example in physics as well as in chemistry provide *ab-initio* principle simulations, based on density functional theory (DFT) [1, 2, 3]. It provides a reliable solution to the simulations of almost all materials that can be described by the mean field theory. Monte Carlo method [4], named after a city famous of gambling in Monaco, is another example, whose applications have covered almost every corner of science, where numerics are needed. In modern physics, however, there are still many “hard nuts to crack”, especially for systems with strong correlations that lead to exciting and important phenomena like high-temperature superconductivity [5, 6] and fractional excitations [7].

Huge progress has been made in the last twenty years benefiting from a fresh-born numeric tool, called tensor network (TN). Generally speaking, a TN is defined as the contraction of local tensors. It can be a scalar, a vector, or even a tensor labeled by infinite number of indexes. Thus, many challenging problems, e.g., simulations of ground and thermal states, and even some problems outside physics can be reduced to computing TN's. Such a unification makes the TN algorithms one of the central topics of modern physics. In this chapter, we follow the history line, and briefly review how the TN algorithms has been advanced in a “find-and-solve-problem” manner.

### 1.2. Numeric renormalization group in one dimension

In 1975, Wilson published a revolutionary paper, where he generalized the idea of renormalization group in high energy physics to a numeric method later called numeric renormalization group (NRG) [8]. The idea of NRG is that starting from a small system, one adds several spins each time and updates the optimal subspace with fixed number of basis by integrating the high-energy states. Its precision was further improved by combining with expansion theory [9, 10, 11]. NRG successfully tackles the Kondo problem in one dimension [12], however, it was soon found to only have limited accuracy for other systems including Heisenberg chains.

In the nineties, White and Noack pointed out that NRG fails to properly consider the boundary conditions [13], and then proposed the famous density matrix renormalization group (DMRG) that is recognized as the most efficient and accurate algorithms for one-dimensional (1D) models (see the original works [14, 15] and several reviews [16, 17] of the algorithm). Instead of using energy spectrum as the reference, White constructed two blocks when doing renormalization and chose the spectrum of the reduced density matrix of one block to locate the important subspace. In other words, the space of one block is renormalized by taking the other block as *environment*, which becomes one of the most important concepts in the NRG-based algorithms. Important generalizations of DMRG were then developed, including the transfer matrix renormalization group by Wang and Xiang [18], and corner transfer matrix renormalization group by Nishino and Okunishi [19].

Several years later \*, DMRG was further understood in the language of quantum entanglement † and matrix product state (MPS) [24]. The relations among entanglement and many-body simulations were discussed in, e.g., [25, 26, 27, 28]. Generally speaking, an MPS is defined as the contraction of local tensors aligned as a chain in one dimension. The indexes of the local tensors can be categorized into two kinds: physical indexes that are open and represent the physical Hilbert space, and geometrical indexes that carry the entanglement, and are contracted. In DMRG, the renormalization of each step is written as a local tensor, forming an MPS as the total ground-state wave function. Thus, the MPS in DMRG can be

\*We recommend a web page built by Tomotoshi Nishino, <http://quattro.phys.sci.kobe-u.ac.jp/dmrg.html>, where one exhaustively can find the progresses related to DMRG.

†For the general theory of quantum entanglement and its role in the many body systemns, see for instance [20, 21, 22, 23].

understood as not only a 1D state ansatz, but also a TN representation of the NRG flows ([17, 24, 29, 30, 31, 32], for a recent review see [33]). One interesting thing to note is that the “prototype” of MPS appeared in the work of Baxter for statistic physics [34, 35], which is even much earlier than Wilson’s NRG. Similar structure also appeared in several works in 1993 [36, 37].

The importance of MPS is not only justified by the success of DMRG, itself gives a non-trivial representation of many-body states. On one hand, MPS has been utilized to do some analytical investigations. One example is constructing the MPS of the Affleck-Kennedy-Lieb-Tasaki (AKLT) state [38, 39] as well as its higher-spin / higher-dimensional generalizations [40, 41, 42, 43, 27, 44]. Another example is studying the field theories in 1D suggested by Verstraete and Cirac in 2011 [45].

On the other hand, MPS is widely utilized as a variational state ansatz for numerically studying 1D systems. In 2004 and 2007, respectively, Hastings proved that correlation functions in a gapped system decay exponentially [46, 47], and the entanglement is bounded for the ground states of gapped 1D quantum systems [48, 49]. Furthermore, Verstraete and Cirac pointed out that MPS is faithful to capture the 1D gapped ground states [50]. Now people have a better knowledge about the underlying reasons for the efficiency of MPS in 1D system, it is satisfying the area law of entanglement entropy [51, 52, 53, 54, 55, 56].

During the same time, many MPS-based algorithms were developed, where the tensor elements of an MPS are considered as variational parameters [57]. DMRG itself belongs to the alternating-least-square variational methods for finding the ground states. Another way is to do imaginary time evolution of an MPS till the fixed point is reached, where there are the time-evolving block decimation [58, 59, 60, 61] and time-dependent variational principle of MPS [62]. Note these two schemes can be applied to both imaginary and real time evolutions. Scheme based on MPS were proposed for the excitation spectrum [63].

Another important issue to our topic is that by Trotter-Suzuki decomposition [64, 65, 66], the time evolution of an MPS is transferred into a 2D TN . If one considers that a classical partition function can also be written as a TN with all indexes contracted (see, e.g., Ref. [67]), there emerges an explicit equivalence between a 1D quantum theory and a 2D classical partition function, which more importantly, in some sense unifies the computation of time evolutions with TN.

Even though an MPS with finite bond dimensions can only describe gapped systems, the criticality and the central charge of the underlying conformal field theory can still be accessed efficiently by the scaling behaviors of the entanglement and correlation functions [68, 69, 53, 48, 70, 71, 72, 73, 74]. This advantage benefits from the underlying relation between MPS and quantum entanglement

### *1.3. Tensor network states in two dimensions*

The simulations of two-dimensional (2D) systems are much more complicated and tricky, where analytical solutions are extremely rare and mean field approximations often fail to consider the long-range fluctuations. For numeric simulations, exact diagonalization can

only access a small system; quantum Monte Carlo (QMC) approaches are hindered by the notorious “negative sign” problem on frustrated spin models and fermionic models away from half-filling, causing an exponential increase of the computing time with the number of particles [75, 76].

While very elegant and extremely powerful in 1D systems, the 2D version of DMRG [77, 78, 79] suffers some severe restrictions. The ground state obtained by DMRG is an MPS that is essentially a 1D state representation. Consequently, the ground state only satisfies the 1D area law of entanglement entropy [52, 48, 80, 49]. However, due to the lack of alternative approaches, 2D DMRG is still one of the most important 2D algorithms, producing a large number of astonishing work including discovering the numeric evidence of quantum spin liquid [81, 82, 83] on kagomé lattice (see, e.g., [84, 85, 86, 87, 88, 89]).

Besides directly using DMRG in 2D, another natural way is to extend the MPS representation, leading to the tensor product state [90, 91, 92, 93] or projected entangled pair state (PEPS) proposed [94, 95]. While an MPS is made up of tensors aligned in a chain, a PEPS is formed by tensors located in a 2D plain, forming a TN. Thus, PEPS can be regarded as one type of 2D tensor network states. Note the work of Affleck *et al* [38, 39, 96] can be considered as a prototype of PEPS.

The network structure of the PEPS allows us to construct 2D states that strictly fulfill the area law of entanglement entropy [97]. It implies that PEPS is able to represent 2D gapped states, and even critical and topological states, with only finite bond dimensions. Examples include resonating valence bond states [97, 98, 99, 100, 101] originally proposed by Anderson *et al* for super-conductivity [102, 103, 104, 105, 106], string-net states [107, 108, 109] proposed by Wen *et al* for gapped topological orders [110, 111, 112, 113, 114, 115, 116], and so on.

The network structure makes PEPS so powerful that it can encode difficult computational problems including NP-hard ones [97, 117, 118]. What is even more important for physics is that, according to lots of numerical benchmarks, PEPS provides an efficient representation as the ansatz for calculating ground states of many non-trivial 2D models. However, accessing the area law costs something else: the computational complexity rises [97, 117, 119]. For instance, after having determined the ground state (either by construction or variation), one wants typically to extract physical informations by computing, e.g., energies, order parameters or entanglement. For MPS, we did not discuss much these computations, because most of the tasks are matrix manipulations and products which can be easily done by computers. For PEPS, one needs to contract a TN stretching in a 2D plain, unfortunately, most of which cannot be neither done exactly or nor even efficiently. The reason for this complexity is what brings the physical advantage to PEPS: the network structure. Thus, algorithms to compute the TN contractions need to be developed.

For the TN contractions, we here specifically consider those where all bonds are contracted. A general way of applying such TN’s to different problems is to *write the cost functions as the contractions of TN’s*. A cost function is usually a scalar function, whose maximal or minimal point gives the solution of the targeted problem. For example, the cost function of the ground-state simulation can be the energy (e.g., [120, 121]); for finite-

temperature simulations, it can be the partition function or free energy (e.g., [122, 123]); for the dimension reduction problems, it can be the distance before and after the reduction or truncation error (e.g., [59, 67, 124]); for the supervised machine learning problems, it can be the accuracy (e.g., [125]). TN can then be generally considered as a specific structure of the parameters in the cost functions.

Before reaching the TN algorithms, there are a few more things worth mentioning. MPS and PEPS are not the only TN state representations in one or two dimensions. As a generalization of PEPS, projected entangled simplex state was proposed, where some redundancy of the local entanglement is integrated to reach a better efficiency [126, 127]. Except for a chain or 2D lattice, TN can be defined with some other geometries, such as trees or fractals. Tree TN state is one example with non-trivial properties and applications [40, 41, 128, 129, 130, 131, 132, 133, 134, 135, 136, 137, 138]. Another example is multi-scale entanglement renormalization ansatz (MERA) proposed by Vidal [139, 140, 141, 142, 143, 144, 145, 146, 147], which is a powerful tool especially for studying criticality [148, 149, 150, 151, 152, 153, 154, 155, 156], and AdS/CFT and holographic theories ([157, 158, 159, 160, 161, 162, 163, 164, 165], for general introduction see [166]). TN has also been applied to compute exotic properties of the physical models on fractal lattices [167, 168].

The second thing concerns the fact that some TN's can indeed be contracted exactly. Tree TN is one example, since there is no loop of a tree graph. This might be the reason that a tree TN state can only have a finite correlation length [132], thus cannot efficiently access criticality in two dimensions. MERA modifies the tree in a brilliant way so that the criticality can be accessed without giving up the exactly contractible structure [144]. Some other exactly contractible examples have also been found, where exact contractibility is not due to the geometry but due to some algebraic properties of the local tensors [169].

Thirdly, a TN can represent operators, usually dubbed as tensor network operator (TNO). Generally speaking, a TN state can be considered as a linear mapping from the physical Hilbert space to a scalar given by the contraction of tensors. A TNO is regarded as a mapping from the *bra* to the *ket* Hilbert space. Transfer matrix renormalization group [18] generalizes the DMRG to finite temperatures by computing the renormalization of both *bra* to the *ket* Hilbert space. Many algorithms explicitly employ the TNO form, including the matrix product density operator for simulating thermodynamics of 1D systems [170, 171, 172, 173, 174, 175, 176, 177], tensor product density operator (also called projected entangled pair operators) in for higher-systems [178, 179, 124, 180, 122, 181, 182, 183, 184, 185, 186, 187], and multiscale entangled renormalization ansatz [188, 189].

#### 1.4. Tensor renormalization group approaches

Since most of TN's cannot be contracted exactly (with #P-complete computational complexity [118]), efficient algorithms are strongly desired. In 2007, Levin and Nave generalized the NRG idea to TN and proposed tensor renormalization group (TRG) approach [67]. Numerically speaking, TRG consists of two main steps in each RG iteration: contraction and

truncation. In this paper, we generally call all the TN algorithms with such a characteristic the NRG-inspired algorithms.

In the contraction step, the TN is deformed by singular value decomposition (SVD) of matrix in such a way that certain adjacent tensors can be contracted without changing the geometry of the TN graph. This procedure reduces the number of tensors  $N$  to  $N/\nu$ , with  $\nu$  an integer that depends on the way of contracting. After reaching the fixed point, one tensor represents in fact the contraction of infinite number of original tensors, which can be seen as the approximation of the whole TN.

After each contraction, the dimensions of local tensors increase exponentially, and then truncations are needed. To do so in an optimized way, one should consider the “environment”, a concept which appears in DMRG and is crucially important in NRG-inspired schemes to determine how optimal the truncations are. In the truncation step of Levin’s TRG, one only keeps the basis corresponding to the  $\chi$ -largest singular values from the SVD in the contraction step, with  $\chi$  called dimension cut-off. In other words, the environment of the truncation here is the tensor that is decomposed by SVD. Such a local environment only permits local optimizations of the truncations, which hinders the accuracy of Levin’s TRG on the systems with long-range fluctuations. Nevertheless, TRG is still one of the most important and computationally-cheap approaches for both classical (e.g., Ising and Potts models) and quantum (e.g., Heisenberg models) simulations in two and higher dimensions [190, 191, 192, 193, 194, 195, 196, 197, 198, 199, 200]. It is worth mentioning that for 3D classical models, the accuracy of the TRG algorithms have surpassed other methods [195, 198], such as QMC.

With this basic idea in mind, the further developments of more efficient and accurate NRG-inspired algorithms concern mainly two aspects: more reasonable ways of contracting, and more optimized ways of truncating. Roughly speaking, the TRG algorithms can be divided into three kinds by how the number of tensors decreases: exponential, linearized and polynomial renormalization,

While Levin’s TRG “coarse-grains” a TN in an exponential way (the number of tensors decreases exponentially with the renormalization steps), Vidal’s time-evolving block decimation (TEBD) scheme [58, 59, 60, 61] implements the TN contraction with the help of MPS in a linearized way [173]. Then, instead of using the singular values of local tensors, one uses the entanglement of the MPS to find the optimal truncation, meaning the environment is a (non-local) MPS, leading to a better precision than Levin’s TRG. In this case, the MPS at the fixed point is the dominant eigenstate of the transfer matrix of the TN.

Another group of TRG algorithms, called corner transfer matrix renormalization group (CTMRG) [201], are based on the corner transfer matrix idea originally proposed by Baxter in 1978 [202], and developed by Nishina and Okunishi in 1996 [19]. In CTMRG, the contraction reduces the number of tensors in a polynomial way and the environment can be considered as a finite MPS defined on the boundary. CTMRG has a compatible accuracy compared with TEBD.

With a certain way of contracting, there is still high flexibility of choosing the environment. Thus, independent of the contraction ways, the TRG algorithms can be

generally separated into three kinds in the sense of environment, termed simple, cluster and full decimations. The word “decimation” means the reduction of the basis, borrowed from the time-evolving block decimation algorithm. The words “simple”, “cluster” and “full” are taken from the variational update schemes of quantum states (MPS, PEPS, etc.), which also refer to different ways of considering the environment. Here, we generalize the concepts to the TN contraction problems that could be physical-independent.

For example, Levin’s TRG and its variants [67, 190, 191, 192, 193, 195] belong to the simple decimation. Xie *et al* proposed the second renormalization group [203], which belongs to the full decimation, where another global TN contraction is introduced for considering globally the environment [195]. For the ground-state simulations with PEPS, it was proposed to use TEBD (or its variants) [204, 205, 206] or CTMRG [201, 179, 207, 208, 209] to compute the truncations, which also belong to the full decimation (or update).

Though with a better treatment of the environment, one drawback of the full decimation schemes is the expensive computational cost, which strongly limits the dimensions of the tensors one can keep. A compromise between simple and full decimations is the cluster decimation (update) [135, 210, 211, 206], where one considers a reasonable subsystem as the environment to find a balance between the efficiency and precision.

### 1.5. Tensor network contraction with self-consistent eigenvalue equations

Interestingly, to iteratively contract (and truncate) is not the only clue to solve a TN contraction problem. Another idea rises from the question: *can the contraction of an infinite TN be transformed optimally to the contraction of certain local tensors that can be exactly computed?*

Before talking about the specific TN algorithms, we would like to talk about an important and closely-related idea that is frequently used almost everywhere in physics: self-consistency. Considering this is a huge topic, allow us constrain our discussions within the numerical schemes in condensed matter physics.

Let us begin with one of the most successful algorithms in physics as well as chemistry, DFT, also frequently called *ab-initio principle simulations* in the sense of numeric tool (see some of the recent reviews in Refs. [1, 2, 3]). DFT can be traced back to 1926 with the birth of Thomas-Fermi theory [212, 213]. Then, countless progresses were made in the following decades; a seminal milestone, for example, is the Kohn-Sham DFT, which defines self-consistent equations solved for a set of orbitals. We would not go into too much details of DFT but to stress that one key factor of its huge success relies on the simplicity and unification, *using a popular code, a standard basis, and a standard functional approximation* [2].

Since the approximation of DFT is based on the mean-field theory with non-interacting wave functions, it is very difficult to access the strongly-correlated systems. For these reasons, dynamic mean-field theory (DMFT) was proposed [214, 215, 216], which is a natural extension of the standard mean-field theory (Hartree-Fock approximation) to Hubbard models. The basic idea of DMFT is to map the lattice models onto quantum impurity models subject to a self-consistency condition, which is exact in infinite dimensions. For



finite-dimensional cases, one has to employ other numeric approaches to solve such impurity models, including quantum Monte Carlo [217], Wilson’s NRG [8] or White’s DMRG [218].

Later, density matrix embedding theory (DMET) was proposed in 2012 by Knizia and Chan [219, 220] as an alternative of DMFT with some important improvements on efficiency and the range of applications. The key concepts in DMET are the density matrix and entanglement (note that the spectrum of density matrix gives entanglement). The idea is to embed a subsystem in a *bath* determined self-consistently, which mimics the quantum entanglement between the subsystem and the environment.

After entering the era of TN, the idea of self-consistency has been combined with quantum entanglement, aiming at the efficient simulations of strongly-correlated quantum systems. Particularly, algorithms were developed to compute TN contractions solving by self-consistent eigenvalue equations (SEE’s) that reconstruct the TN. Such an idea is very different from the NRG-inspired algorithms, because one can actually forget about the contractions and truncations, as well as the concepts of renormalization transformations and truncation environments.

The related progresses were stimulated a lot by the NRG-inspired methods, and many works of Baxter (e.g., [221, 222]), Nishino (e.g., [19, 223, 224]), and many others, made without the concept of TN clearly emerges. But allow us to restrain our discussions to the works with a clear concept of TN. Let us firstly go back to Vidal’s TEBD [58, 59, 60, 61] for 1D models, where the canonicalization of MPS was proposed for non-unitary evolutions. The central canonical form of an MPS is the fixed point of two SEE’s, where the entanglement of the MPS explicitly appears and can be used to do optimal truncations of the bond dimensions [61].

Such a scheme (as well as the SEE’s) was directly generalized to systems defined on trees with a directed canonical form [131]. Then, the algorithm for center canonical form of trees (also called super-orthogonal form) was proposed [124]. It was later realized that the (super-orthogonal) entanglement of a tree system provides a good approximation of the entanglement between a supercell and the rest [122]. In other words, the entanglement of a tree system provides a faithful bath to mimic the entanglement between a supercell and the rest in a 2D lattice.

The contraction of a tree TN can be easily “encoded” in local SEE’s, since there are no loops in a tree graph. For a TN with a lattice geometry, e.g., square lattice, the local SEE’s for solving the TN contraction was proposed in 2016 [123]. Such equations lead to a natural generalization of rank-1 decomposition [225] called *tensor ring decomposition* [123]. Such a scheme unifies different NRG-based algorithms (iDMRG[14, 15, 226], iTEBD [60], and CTMRG [201, 209]) by the same set of SEE’s, based on which the “*ab-initio* optimization principle” for classical/quantum simulations of many-body systems was suggested [227].

Interestingly, the SEE-based TN algorithms are found to bear close relations to the techniques in multi-linear algebra (MLA) (see a review of MLA [228]). Instead of restrained with linear algebra, it is quite natural but important to consider the multi-linear techniques, since we are dealing with TN. MLA was originally targeted on developing high-order generalization of the linear algebra (e.g., the higher-order version of singular value or

eigenvalue decomposition [225, 229, 230, 231]), and now has been successfully used in a large number of fields, including data mining (e.g., [232, 233, 234, 235, 236]), image processing (e.g., [237, 238, 239, 240]), machine learning (e.g., [241]), and so on. The interesting connections between the fields of TN and MLA will provide boundless space for interdisciplinary researches that cover a huge range of sciences.

To summarize the astonishing achievements, we would like to say that TN has been recognized as one of the most important tools in physics, as its role is as fundamental as numbers, matrices, tensors, and such. There are many ongoing researches whose number is still growing in an explosive way. It is impossible to mention all of the contributions related to TN here. Allow us to give several examples: describing exotic states of matter (e.g., quantum spin liquids and hall states [107, 108, 99, 98, 242, 101, 243, 244, 245, 246, 247, 248, 84, 249, 89, 87, 85, 250, 100, 251, 252]), introducing the symmetries of quantum Hamiltonians [107, 108, 109, 253, 254, 255, 256, 257, 258, 259, 260, 246] or quantum fields [261, 262, 256, 263, 264, 265, 266] in the TN for novel simulation or classification schemes (see a review [267]), simulating dynamic properties in and out of equilibrium [268, 59, 170, 171, 269, 270, 271, 272, 62, 273, 274, 205, 275, 276, 277, 278, 279, 280, 281, 282, 283, 284, 285, 286], applying TN to (classical or quantum) machine learning ([287, 125, 288, 289, 290, 291, 292, 293, 294] and a recent review [295, 296]), solving counting problems (see a review [297]), and so on. Especially in computational physics, TN algorithms have solved lots of challenging problems that could not be accessed before. But, there are still many issues to be tackled, especially the high computational complexity. One prospect could be that someday, there would be a TN algorithm, so powerful and simple, that we could, like the DFT in nowadays, *use a popular code, a standard scheme, and a standard approximation*, to explore the untouched fields.

### 1.6. Organization of the review

This review will be concentrated on the algorithms for TN contractions, and is organized as following. In Chap. 2, we will introduce the basic concepts and definitions of tensor and TN states/operators, as well as their graphic representations. Some important applications of using the TN to represent physical objects (e.g., partition functions and non-trivial quantum states) will be given as examples. The relation between TN and quantum entanglement will be discussed.

In Chap. 3, we will show some special TN's that can be exactly contracted, and then explain the difficulties of contracting TN's in general. Three kinds of NRG-inspired algorithms will be explained, which are categorized as exponential, linearized and polynomial contraction algorithms. Finally, we will relate these algorithms to the exactly contractable TN's.

In Chap. 4, we will explain the SEE-based TN schemes. We will start from the canonicalization of MPS in one dimension, and its generalization to the super-orthogonalization of PEPS in higher dimensions. We will show that the contraction of a tree TN can be implemented by the rank-1 decomposition, which further leads to the "Bethe-

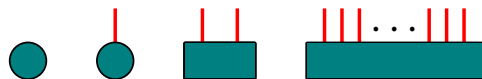


**Figure 1.** (Color online) From left to right, the graphic representations of a scalar, vector, matrix and tensor.

like” approximation of the PEPS defined on the regular lattice. Then, we will explain the tensor ring decomposition, and how it unifies iDMRG[14, 15, 226], iTEBD[60], and CTMRG [201, 209]. Then based on this scheme, we will explain the *ab-initio* optimization principle for the classical/quantum simulations of the ground states of many-body systems in one and higher dimensions.

In Chap. 5, we give the summary of our review.

## 2. Tensor Network: Basic Definitions

In this chapter, we give some basic definitions of tensor and tensor network (TN) with their graphic representations. Then we show that the TN can be used to represent quantum states, where we explain MPS in 1D and PEPS in 2D systems, as well as the generalizations to thermal states and operators.

### 2.1. Scalar, vector, matrix, and tensor

Generally speaking, a tensor is defined as a series of numbers labeled by  $N$  indexes, with  $N$  called the *order* of the tensor  $*$ . In this context, a scalar, which is one number and labeled by zero index, is a 0th-order tensor. Many physical quantities are scalars, including energy, free energy, magnetization and so on. Graphically, we use a dot to represent a scalar (Fig. 1).

A  $D$ -component vector consists of  $D$  numbers labeled by one index, and thus is a 1st-order tensor. For example, one can write the state vector of a spin-1/2 in a chosen basis (say the eigenstates of the spin operator  $\hat{S}^{[z]}$ ) as

$$|\psi\rangle = C_1|0\rangle + C_2|1\rangle = \sum_{s=0,1} C_s|s\rangle, \quad (1)$$

with the coefficients  $C$  a two-component vector. Here, we use  $|0\rangle$  and  $|1\rangle$  to represent spin up and down states. Graphically, we use a dot with one open bond to represent a vector (Fig. 1).

What if we have two spins? Of course the state vector can be written under an irreducible representation as a four-dimension vector. Instead, under the local basis of each spin, we write it as

$$|\psi\rangle = C_{00}|0\rangle|0\rangle + C_{01}|0\rangle|1\rangle + C_{10}|1\rangle|0\rangle + C_{11}|1\rangle|1\rangle = \sum_{ss'=0}^1 C_{ss'}|s\rangle|s'\rangle, \quad (2)$$

with  $C_{ss'}$  a matrix with two indexes. Here, one can see that the difference between a  $(D \times D)$  matrix and a  $D^2$ -component vector in our context is just the way of labeling the

\*Note that in some references,  $N$  is called the *tensor rank*. Here, the word *rank* is used in another meaning, which will be explained later.

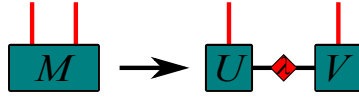


**Figure 2.** (Color online) The graphic representation of the Schmidt decomposition (singular value decomposition of a matrix). The positive-defined diagonal matrix  $\lambda$ , which gives the entanglement spectrum (Schmidt numbers), is defined on a virtual bond (dumb index) generated by the decomposition.

elements. Transferring among vector, matrix and tensor like this will be frequently used later. Graphically, we use a dot with two bonds to represent a matrix and its two indexes (Fig.1).

If we consider, e.g.,  $N$  spins, the  $2^N$  coefficients can be written as a  $N$ -th order tensor  $C$ \*, satisfying

$$|\psi\rangle = \sum_{s_1 \dots s_N=0}^1 C_{s_1 \dots s_N} |s_1\rangle \dots |s_N\rangle. \quad (3)$$

Similarly, such a tensor can be *reshaped* into a  $2^N$ -component vector. Graphically, an  $N$ -th order tensor is represented by a dot connected with  $N$  open bonds (Fig.1).

In above, we use states of spin-1/2 as examples, where each index can take two values. For a spin- $S$  state, each index can take  $d = 2S + 1$  values, with  $d$  called the *physical bond dimension*. Besides quantum states, operators can also be written as tensors. A spin-1/2 operator  $\hat{S}^\alpha$  ( $\alpha = x, y, z$ ) is a  $(2 \times 2)$  matrix by fixing the basis, where we have  $S_{s'_1 s'_2 s_1 s_2}^\alpha = \langle s'_1 s'_2 | \hat{S}^\alpha | s_1 s_2 \rangle$ . In the same way, an  $N$ -spin operator can be written as a  $2N$ -th order tensor, with  $N$  *bra* and  $N$  *ket* indexes †.

We would like to stress some conventions about the “indexes” of a tensor (including matrix) and those of an operator. A tensor is just a group of numbers, where their indexes are defined as the labels labeling the elements. Here, we always put all indexes as the lower symbols, and the upper “indexes” of a tensor (if exist) are just a part of the symbol to distinguish different tensors. For an operator which is defined in a Hilbert space, it is represented by a hatted letter, and there will be no “true” indexes, meaning that both upper and lower “indexes” are just parts of the symbol to distinguish different operators.

## 2.2. Tensor network and tensor network states

### 2.2.1. A simple example of two spins and Schmidt decomposition

After introducing tensor (and its diagram representation), now we are going to talk about TN, which is defined as a contraction of tensors. One will see that the indexes contracted in a TN carry the quantum entanglement [25, 26, 27, 28].

Let us start with the simplest situation, two spins, and consider to study the quantum entanglement properties for instance. Quantum entanglement, mostly simplified

\*If there is no confuse, we use the symbol without all its indexes to refer to a tensor for conciseness, e.g., use  $C$  to represent  $C_{s_1 \dots s_N}$ .

†Note that here, we do not distinguish *bra* and *ket* indexes deliberately in a tensor, if not necessary

as entanglement, is defined by the *Schmidt decomposition* [298, 299, 300] of the state (Fig. 2) as

$$|\psi\rangle = \sum_{ss'=0}^1 C_{ss'} |s\rangle |s'\rangle = \sum_{ss'=0}^1 \sum_{a=1}^{\chi} U_{sa} \lambda_{aa'} V_{as'}^* |s\rangle |s'\rangle, \quad (4)$$

where  $U$  and  $V$  are unitary matrices,  $\lambda$  is a positive-defined diagonal matrix in descending order  $*$ , and  $\chi$  is called the *Schmidt number*.  $\lambda$  is also called the entanglement spectrum since in the new basis after the decomposition, the state is written in a summation of  $\chi$  product states as  $|\psi\rangle = \sum_a |u\rangle_a |v\rangle_a$ , with the new basis  $|u\rangle_a = \sum_s U_{sa} |s\rangle$  and  $|v\rangle_a = \sum_{s'} V_{sa}^* |s'\rangle$ .

Graphically, we have a small TN, where we use green squares to represent the unitary matrices  $U$  and  $V$ , and a red diamond to represent the diagonal matrix  $\lambda$ . There are two bonds in the graph shared by two objects, standing for the summations (contractions) of the two indexes in Eq. (4),  $a$  and  $a'$ . Unlike  $s$  (or  $s'$ ), The space of the index  $a$  (or  $a'$ ) is not from any physical Hilbert space. To distinguish these two kinds, we call the indexes like  $s$  the *physical indexes* and those like  $a$  the *geometrical indexes*. Meanwhile, since each physical index is only connected to one tensor, it is also called an *open bond*.

In the case of Schmidt decomposition,  $a$  (also  $a'$  since  $\lambda$  is diagonal) carries the entanglement [301, 58, 59]. What about a more general case like  $C_{ss'} = \sum_a M_{sa} M'_{as'}$  without putting any constraints on  $M$  and  $M'$ ? Then the dimension of  $a$  (denoted by  $\chi$ ) gives the upper bound of the entanglement [58]. One can see the upper bond immediately by assuming that the matrix  $C$  has a flat spectrum.

Instead of Schmidt decomposition, it is more convenient to use another language to present later the algorithms: *singular value decomposition* (SVD), a matrix decomposition in linear algebra. The Schmidt decomposition of a state is the SVD of the coefficient matrix  $C$ , where  $\lambda$  is called the *singular value spectrum* and its dimension  $\chi$  is called the *rank* of the matrix.

In quantum information sciences, entanglement is regarded as a quantum version of correlation [21], which is very important to understand the physical implications of TN. In linear algebra, SVD gives the optimal lower-rank approximations of a matrix, which is more useful and important to TN algorithms. Specifically speaking, with a given matrix  $C$  of rank- $\chi$ , one wants to find a rank- $\tilde{\chi}$  matrix  $C'$  ( $\tilde{\chi} \leq \chi$ ) that minimizes the norm

$$\mathcal{D} = |M - M'| = \sqrt{\sum_{ss'} (M_{ss'} - M'_{ss'})^2}, \quad (5)$$

the optimal solution is given by SVD as

$$M'_{ss'} = \sum_{a=0}^{\chi'-1} U_{sa} \lambda_{aa} V_{s'a}^*. \quad (6)$$

In other words,  $M'$  is the optimal rank- $\chi'$  approximation of  $M$ , and the error is given by

$$\varepsilon = \sqrt{\sum_{a=\chi'}^{\chi-1} \lambda_a^2}, \quad (7)$$

\*Sometime,  $\lambda$  is treated directly as a  $\chi$ -component vector.

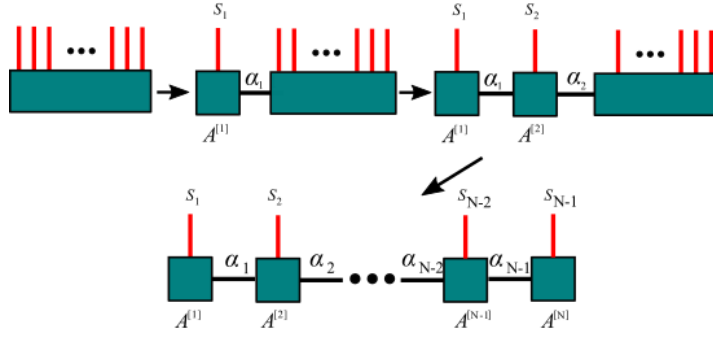


**Figure 3.** (Color online) An impractical way to obtain an MPS from a many-body wave function is to repetitively use the SVD.

which will be called the *truncation error* in the TN algorithms.

**2.2.2. Matrix product states (MPS)** For the system with  $N$  spins, we can write its coefficients as a TN given by the contraction of  $N$  tensors. One way to obtain such a TN is by repetitively using SVD (Fig. 3). First, we group the first  $N - 1$  indexes together as one large index, and write the coefficients as a  $2^{N-1} \times 2$  matrix. Then implement SVD or any other decomposition (for example QR decomposition) as the contraction of  $C^{[N-1]}$  and  $A^{[N]}$

$$C_{s_1 \cdots s_{N-1} s_N} = \sum_{a_{N-1}} C_{s_1 \cdots s_{N-1}, a_{N-1}}^{[N-1]} A_{s_N, a_{N-1}}^{[N]}. \quad (8)$$

Note that as a convention in this paper, we always put the physical indexes in front of geometrical indexes and use a comma to separate them. For the tensor  $C^{[N-1]}$ , one can do the similar thing by grouping the first  $N - 2$  indexes and decompose again as

$$C_{s_1 \cdots s_{N-1} a_{N-1}}^{[N-1]} = \sum_{a_{N-2}} C_{s_1 \cdots s_{N-2}, a_{N-2}}^{[N-2]} A_{s_{N-1}, a_{N-2} a_{N-1}}^{[N-1]}. \quad (9)$$

Then the total coefficients becomes the contraction of three tensors as

$$C_{s_1 \cdots s_{N-1} s_N} = \sum_{a_{N-2} a_{N-1}} C_{s_1 \cdots s_{N-2}, a_{N-2}}^{[N-2]} A_{s_{N-1}, a_{N-2} a_{N-1}}^{[N-1]} A_{s_N, a_{N-1}}^{[N]}. \quad (10)$$

Repeat decomposing in the above way until each tensor only contains one physical index, we have the *matrix product state* (MPS) representation of the state as

$$C_{s_1 \cdots s_{N-1} s_N} = \sum_{a_1 \cdots a_{N-1}} A_{s_1, a_1}^{[1]} A_{s_2, a_1 a_2}^{[2]} \cdots A_{s_{N-1}, a_{N-2} a_{N-1}}^{[N-1]} A_{s_N, a_{N-1}}^{[N]}. \quad (11)$$

One can see that an MPS is a TN formed by the contraction of  $N$  tensors. Graphically, MPS is represented by a 1D graph with  $N$  open bonds.

Such a way of obtaining MPS with decompositions is called tensor train decomposition (TTD) in multi-linear algebra (MLA), and MPS is also called tensor-train form [302]. One main aim of TTD is investigating algorithms to determine the optimal tensor train form of a given tensor. Interestingly, TTD is much younger than MPS and MPS-based techniques in physics, where more interdisciplinary researches are to be explored.

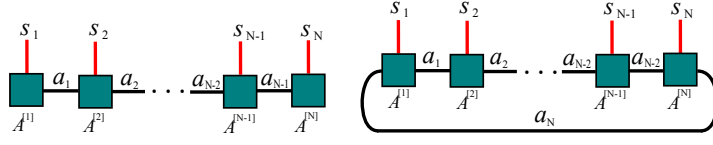


**Figure 4.** (Color online) The graphic representations of the matrix product states with open (left) and periodic (right) boundary conditions.



**Figure 5.** (Color online) One possible configuration of the sparse anti-ferromagnetic ordered state. A dot represents the  $S = 0$  state. Without looking at all the  $S = 0$  states, the spins are arranged in the anti-ferromagnetic way.

In physics, the above way guarantees that any states can be written in a MPS, as long as we do not limit the dimensions of the geometrical indexes. However, it is extremely impractical and inefficient, since in principle, the dimensions of the geometrical indexes  $\{a\}$  increase exponentially with the system size  $N$ . What is useful is the mathematic form of the MPS itself. In fact, an MPS given by Eq. (11) has open boundary condition, and can be generalized to periodic boundary condition (Fig. 4) as

$$C_{s_1 \dots s_{N-1} s_N} = \sum_{a_1 \dots a_N} A_{s_1, a_N a_1}^{[1]} A_{s_2, a_1 a_2}^{[2]} \dots A_{s_{N-1}, a_{N-2} a_{N-1}}^{[N-1]} A_{s_N, a_{N-1} a_N}^{[N]}, \quad (12)$$

where all tensors are 3rd-order. Moreover, one can introduce translational invariance to the MPS, i.e.  $A^{[n]} = A$  for  $n = 1, 2, \dots, N$ . We use  $\chi$ , dubbed as *bond dimension* of the MPS, to represent the dimension of each geometrical index.

Now we introduce a simplified notation of MPS that has been widely used in the community of physics. In fact with fixed physical indexes, the contractions of geometrical indexes are just inner products of matrices (this is where its name comes from). In this sense, we write a quantum state given by Eq. (11) as

$$|\psi\rangle = \text{tTr} A^{[1]} A^{[2]} \dots A^{[N]} |s_1 s_2 \dots s_N\rangle = \text{tTr} \prod_{n=1}^N A^{[n]} |s_n\rangle. \quad (13)$$

tTr stands for summing over all geometrical indexes. The advantage of Eq. (13) is to give a general formula for an MPS of either finite or infinite size, with either periodic or open boundary condition.

MPS is not just a mathematic form, it can represents nontrivial physical states. One important example can be found with Affleck-Kennedy-Lieb-Tasaki (AKLT) model proposed in 1987, a generalization of spin-1 Heisenberg model [38]. For 1D systems, Mermin-Wagner theorem forbids any spontaneously breaking of continuous symmetries at finite temperature with sufficiently short-range interactions. For the ground state of AKLT model called AKLT state, it possesses the *sparse anti-ferromagnetic order* (Fig. 5), which provides a non-zero excitation gap under the framework of Mermin-Wagner theorem. Moreover, AKLT state



**Figure 6.** (Color online) An intuitive graphic representation of the AKLT state. The big circles representing  $S = 1$  spins, and the small ones are effective  $S = \frac{1}{2}$  spins. Each pair of spin-1/2 connecting by a red bond forms a singlet state. The two “free” spin-1/2 on the boundary give the edge state.

provides us a precious exactly-solvable example to understand edge states and (symmetry-protected) topological orders

AKLT state can be exactly written in an MPS with  $\chi = 2$ . Without losing generality, we assume periodic boundary condition. Let us begin with the AKLT Hamiltonian that can be given by spin-1 operators as

$$\hat{H} = \sum_n \left[ \frac{1}{2} \hat{S}_n \cdot \hat{S}_{n+1} + \frac{1}{6} (\hat{S}_n \cdot \hat{S}_{n+1})^2 + \frac{1}{3} \right]. \quad (14)$$

By introducing the non-negative-defined projector  $\hat{P}_2(\hat{S}_n + \hat{S}_{n+1})$  that projects the neighboring spins to the subspace of  $S = 2$ , Eq. (14) can be rewritten in the summation of projectors as

$$\hat{H} = \sum_n \hat{P}_2(\hat{S}_n + \hat{S}_{n+1}). \quad (15)$$

Thus, the AKLT Hamiltonian is non-negative-defined, and its ground state lies in its kernel space, satisfying  $\hat{H}|\psi_{AKLT}\rangle = 0$  with a zero energy.

Now we construct a wave function which has a zero energy. As shown in Fig. 6, we put on each site a projector that maps two (effective) spins-1/2 to a *triplet*, i.e. the physical spin-1, where the transformation of the basis obeys

$$|+\rangle = |00\rangle \quad (16)$$

$$|\tilde{0}\rangle = \frac{1}{\sqrt{2}}(|01\rangle + |10\rangle), \quad (17)$$

$$|-\rangle = |11\rangle. \quad (18)$$

The corresponding projector is determined by the Clebsch-Gordan coefficients [303], and is a  $(3 \times 4)$  matrix. Here, we rewrite it as a  $(3 \times 2 \times 2)$  tensor, whose three components (regarding to the first index) are the ascending,  $z$ -component and descending Pauli matrices of spin-1/2\*,

$$\sigma^+ = \begin{bmatrix} 0 & 1 \\ 0 & 0 \end{bmatrix}, \quad \sigma^z = \begin{bmatrix} 1 & 0 \\ 0 & -1 \end{bmatrix}, \quad \sigma^- = \begin{bmatrix} 0 & 0 \\ 1 & 0 \end{bmatrix}. \quad (19)$$

In the language of MPS, we have the tensor  $A$  satisfying

$$A_{0,aa'} = \sigma_{aa'}^+, \quad A_{1,aa'} = \sigma_{aa'}^z, \quad A_{2,aa'} = \sigma_{aa'}^-. \quad (20)$$

Then we put another projector to map two spin-1/2 to a singlet, i.e. a spin-0 with

$$|\bar{0}\rangle = \frac{1}{\sqrt{2}}(|01\rangle - |10\rangle) \quad (21)$$

\*Here, one has some degrees of freedom to choose different projectors, which is only up to a gauge transformation. But once one projector is fixed, the other is also fixed.



The projector is in fact a  $(2 \times 2)$  identity with the choice of Eq. (19),

$$I = \begin{bmatrix} 1 & 0 \\ 0 & 1 \end{bmatrix}. \quad (22)$$

Now, the MPS of the AKLT state with periodic boundary condition (up to a normalization factor) is obtained by Eq. (12), with every tensor  $A$  given by Eq. (20). For such an MPS, every projector operator  $\hat{P}_2(\hat{S}_n + \hat{S}_{n+1})$  in the AKLT Hamiltonian is always acted on a singlet, then we have  $\hat{H}|\psi_{AKLT}\rangle = 0$ .

**2.2.3. Projected entangled pair states (PEPS)** For 1D states, an MPS can be regarded as the contraction of tensors which are aligned like a chain. Such a representation can be naturally extended to two- or higher-dimensional states, called projected entangled pair state (PEPS) [95, 94]. A PEPS is defined by a number of tensors that contain physical bonds to represent the physical Hilbert space and geometrical bonds that are to be contracted. Differently, the tensors are located in, instead of a 1D chain, a d-dimensional lattice, thus graphically forming a d-dimensional tensor network. A 2D PEPS defined on a square graph, for instance, can be written as

$$|\Psi\rangle = \sum_{\{s,a\}} \prod_n P_{s_n, a_n^1 a_n^2 a_n^3 a_n^4}^{[n]} |s_n\rangle \quad (23)$$

where each geometrical bond is shared by two adjacent tensors and will be contracted. An intuitive picture of PEPS is given in Fig. 7, i.e., the tensors can be understood as projectors that map the physical spins into virtual ones. The virtual spins form the maximally entangled state in a way determined by the geometry of the TN.

Similar to MPS, let us simplify the above formula as

$$|\Psi\rangle = \text{tTr} \prod_n P^{[n]} |s_n\rangle, \quad (24)$$

where tTr means to sum over all geometrical indexes. Graphically, a shared index is again represented by a bond and the whole PEPS is illustrated by a square TN.

Such a generalization makes a lot of senses in physics. One key factor regards the *area law of entanglement entropy* [51, 52, 53, 54, 55, 56] which we will talk about later in this chapter. In the following as two straightforward examples, we show that PEPS can indeed represents non-trivial physical states including nearest-neighbor *resonating valence bond* (RVB) and  $Z_2$  *spin liquid* states.

**2.2.4. Representing non-trivial states by tensor networks** Resonating valence bond (RVB) state was firstly proposed by Anderson to explain the possible disordered ground state of the Heisenberg model on triangular lattice [102, 103]. RVB state is defined as the superposition of macroscopic configurations where all spins are paired to form the singlet states. The strong fluctuations restore all symmetric and lead to a spin liquid state without any local orders. The distance between two paired spins can be short range or long range. For nearest-neighbor RVB, the valence bonds are only be nearest neighbors (Fig. 8). RVB state are

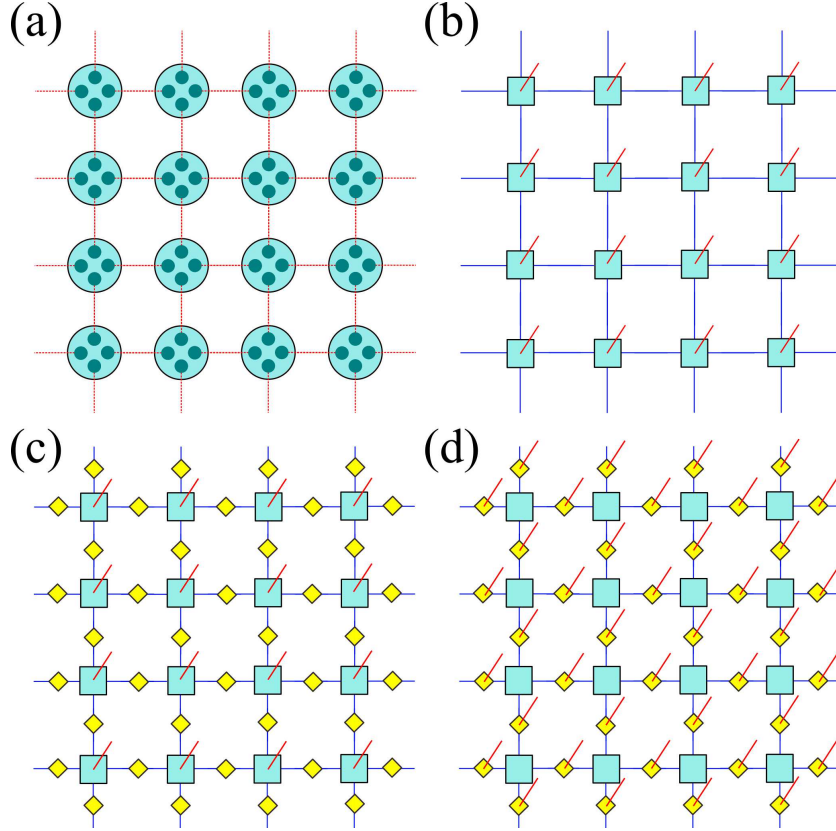


**Figure 7.** (Color online) (a) An intuitive picture of the projected entangled pair state. The physical spins (big circles) are projected to the virtual ones (small circles), which form the maximally entangled states (red bonds). (b)-(d) Three kinds of frequently used PEPS's.

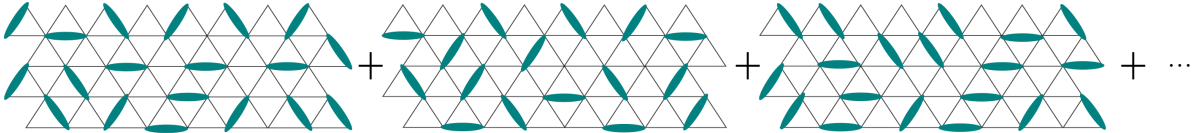


**Figure 8.** (Color online) The nearest-neighbor resonating valence bond state is the superposition of all possible configurations of nearest-neighbor singlets.

supposed to relate to high- $T_c$  copper-oxide-based superconductor, by doping the singlet pairs, the insulating RVB state can translate to a charged superconducting state [104, 105, 106].

For the nearest-neighbor situation, an RVB (defined on an infinite square lattice, for example) state can be exactly written in PEPS of  $\chi = 3$  with translational invariance (i.e., all tensors equal to each other). In detail, the tensor defined on each site whose dimensions are  $(2 \times 3 \times 3 \times 3 \times 3)$  only has five nonzero elements with explicit physical meaning, which are

$$P_{0,0000} = 1, \quad P_{1,2111} = 1, \quad P_{1,1211} = 1, \quad P_{1,1121} = 1, \quad P_{1,1112} = 1. \quad (25)$$

Here, we use the language of strings to understand the projector: the spin-up state ( $s = 0$ ) stands for the vacuum state and the spin-down ( $s = 1$ ) for the occupied state of a string. In this sense, the first element means it is vacuum in the physical space, thus all the geometrical spaces are vacuum. For the rest four elements, the physical space is occupied by a string

that is mapped to one of geometrical space with the same amplitude, leaving the rest three vacuum. For example,  $P_{1,1211} = 1$  means one possibility, where the physical string is mapped to the second geometrical space while the rest three remain vacuum \*. The rest elements are all zero, which means the corresponding configurations are forbidden.

The tensor  $P$  only maps physical strings to geometrical spaces. Then we put a projector  $B$  on each geometrical bond to form the singlets in the RVB picture.  $B$  is a  $(3 \times 3)$  matrix with only three nonzero elements as

$$B_{00} = 1, \quad B_{12} = 1, \quad B_{21} = -1. \quad (26)$$

Similarly, the first one means a vacuum state, and the rest two simply give a singlet state ( $|12\rangle - |21\rangle$ ) in a geometrical space.

Then the infinite PEPS (iPEPS) of the nearest-neighbor RVB is given by the contraction of infinite copies of  $P$ 's on the sites and  $B$ 's (Fig.7) on the bonds as

$$|\Psi\rangle = \sum_{\{s,a\}} \prod_{n \in \text{sites}} P_{s_n, a_n^1 a_n^2 a_n^3 a_n^4} \prod_{m \in \text{bonds}} B_{a_m^1 a_m^2} \prod_{j \in \text{sites}} |s_j\rangle. \quad (27)$$

After the contraction of all geometrical indexes, the state is the super-position of all possible configurations consisting of nearest-neighbor singlets. These PEPS looks different from the one given in Eq. (23) or (24) but they are essentially the same, because one can contract the  $B$ 's into  $P$ 's so that the PEPS is only formed by tensors defined on the sites.

Another example is the  $Z_2$  spin liquid state, which is one of simplest states that belong to the so-called string-net states [107, 108, 109], firstly proposed by Levin and Wen to characterize gapped topological orders [114]. Similarly with the picture of strings, the  $Z_2$  state is the super-position of all configurations of string loops. Writing such a state with TN, the tensor on each vertex is  $(2 \times 2 \times 2 \times 2)$  satisfying

$$P_{a_1 \dots a_N} = \begin{cases} 1, & a_1 + \dots + a_N = \text{even}, \\ 0, & \text{otherwise}. \end{cases} \quad (28)$$

The tensor  $P$  forces the *fusion rules* of the strings: the number of the strings connecting to a vertex must be even, so that there are no loose ends and all strings have to form loops. It is also called in some literatures the *ice rule* [304, 305] or *Gauss' law* [306]. In addition, the square TN formed solely by the tensor  $P$  gives the famous *eight-vertex model*, where the number "eight" corresponds to the eight non-zero elements (i.e. allowed sting configurations) on a vertex [307].

Similar to the RVB iPEPS given in Eq. (27), the tensors  $B$  are defined on each bond to project the strings to spins, whose non-zero elements are

$$B_{0,00} = 1, \quad B_{1,11} = 1. \quad (29)$$

The tensor  $B$  is a projector that maps the spin-up (spin-down) state to the occupied (vacuum) state of a string.

\*Note that for a geometrical space, 0 and 1 are to distinguish the vacuum and occupied states, respectively.

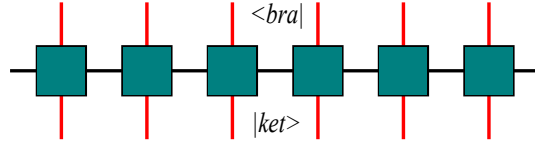


**Figure 9.** (Color online) The graphic representation of a matrix product operator, where the upward and downward indexes represent the *bra* and *ket* space, respectively.

**2.2.5. Generalizations to operators and thermal states** The MPS or PEPS can be readily generalized from representations of states to those of operators, called matrix product operator (MPO) [170, 171, 173, 174, 175] or projected entangled pair operator (PEPO) \* [178, 179, 124, 180, 122, 182, 183, 184, 185, 186, 187]. Let us begin with MPO, which is also formed by the contraction of local tensors as

$$\hat{O} = \sum_{\{s,a\}} \prod_n W_{s_n s'_n, a_n a_{n+1}}^{[n]} |s_n\rangle \langle s'_n|. \quad (30)$$

Different from MPS, each tensor has two physical indexes, of which one is a *bra* and the other is a *ket* index Fig. 10. The dimensions of the geometrical bonds (dubbed  $\chi_W$ ) can be different from each other. For open boundary conditions, the dimensions of the first and last geometrical bonds are 1.

An MPO comes from several varieties, where one example is the Hamiltonian that can be put in a lower (upper) triangular form. The Hamiltonian is usually a polynomial summation of local operators, hence the expectation value of such an operator is a polynomial function of the lattice size. It is worth mentioning that Crosswhite and Bacon [308] have also proposed a general way of constructing an MPO called *automata*.

Now we utilize some properties of a *triangular MPO* to construct the MPO of an Hamiltonian. Starting from a general lower-triangular MPO satisfying  $W_{::,00}^{[n]} = C^{[n]}$ ,  $W_{::,10}^{[n]} = B^{[n]}$ , and  $W_{::,11}^{[n]} = A^{[n]}$  with  $A^{[n]}$ ,  $B^{[n]}$ , and  $C^{[n]}$  some  $d \times d$  square matrices. Or we can write  $W^{[n]}$  in a more explicit  $2 \times 2$  block-wise form as

$$W^{[n]} = \begin{pmatrix} C^{[n]} & 0 \\ B^{[n]} & A^{[n]} \end{pmatrix} \quad (31)$$

If one puts such a  $W^{[n]}$  in Eq. (30), it will give the summation of all terms in the form of

$$\begin{aligned} \hat{O} &= \sum_{n=1}^N A^{[1]} \otimes \dots \otimes A^{[n-1]} \otimes B^{[n]} \otimes C^{[n+1]} \otimes \dots \otimes C^{[N]} \\ &= \sum_{n=1}^N \prod_{\otimes i=1}^{n-1} A^{[i]} \otimes B^{[n]} \otimes \prod_{\otimes j=n+1}^N C^{[j]}, \end{aligned} \quad (32)$$

with  $N$  the total number of tensors and  $\prod_{\otimes}$  the tensor product  $\dagger$ . Such a property can be easily generalized to a  $W$  formed by  $D \times D$  blocks.

\*Generally, a representation of an operator with a TN can be called tensor product operator (TPO). MPO and PEPO are two examples.

$\dagger A^{[0]}$  (or  $B^{[0]}$ ,  $C^{[0]}$ ) does not exist but can be defined as a scalar 1, for simplicity of the formula.

Imposing Eq. (32), we can construct the summation of one-site local terms, i.e.,  $\sum_n X^{[n]}$  \*, with

$$W^{[n]} = \begin{pmatrix} I & 0 \\ X^{[n]} & I \end{pmatrix}, \quad (33)$$

with  $X^{[n]}$  a  $d \times d$  matrix and  $I$  the  $d \times d$  identity.

If two-body terms are included, such as  $\sum_m X^{[m]} + \sum_n Y^{[n]} Z^{[n+1]}$ , we have

$$W^{[n]} = \begin{pmatrix} I & 0 & 0 \\ Z^{[n]} & 0 & 0 \\ X^{[n]} & Y^{[n]} & I \end{pmatrix}. \quad (34)$$

This can be obviously generalized to  $L$ -body terms. With open boundary conditions, the left and right tensors are

$$W^{[1]} = \begin{pmatrix} 0 & 0 & I \end{pmatrix}, \quad (35)$$

$$W^{[N]} = \begin{pmatrix} I \\ 0 \\ 0 \end{pmatrix}. \quad (36)$$

Now we apply the above technique on a Hamiltonian of, e.g., the Ising model in a transverse field

$$\hat{H} = \sum_n \hat{S}_n^z \hat{S}_{n+1}^z + h \sum_m \hat{S}_m^x. \quad (37)$$

Its MPO is given by

$$W^{[n]} = \begin{pmatrix} I & 0 & 0 \\ \hat{S}^z & 0 & 0 \\ h\hat{S}^x & \hat{S}^z & I \end{pmatrix}. \quad (38)$$

Such a way of constructing an MPO is very useful. Another example is the Fourier transformation to the number operator of Hubbard model in momentum space  $\hat{n}_k = \hat{b}_k^\dagger \hat{b}_k$ . The Fourier transformation is written as

$$\hat{n}_k = \sum_{m,n=1}^N e^{i(m-n)k} \hat{b}_m^\dagger \hat{b}_n, \quad (39)$$

with  $\hat{b}_n$  ( $\hat{b}_n^\dagger$ ) the annihilation (creation) operator on the  $n$ -th site. The MPO representation of such a Fourier transformation is given by

$$\hat{W}_n = \begin{pmatrix} \hat{I} & 0 & 0 & 0 \\ \hat{b}^\dagger & e^{ik} \hat{I} & 0 & 0 \\ \hat{b} & 0 & e^{-ik} \hat{I} & 0 \\ \hat{b}^\dagger \hat{b} & e^{+ik} \hat{b}^\dagger & e^{-ik} \hat{b} & \hat{I} \end{pmatrix} \quad (40)$$

with  $\hat{I}$  the identical operator in the corresponding Hilbert space.

\*Note that  $X^{[n_1]}$  and  $X^{[n_2]}$  are not defined in a same space with  $n_1 \neq n_2$ , Thus, precisely speaking,  $\sum$  here is the direct sum. We will not specify this when it causes no confuse

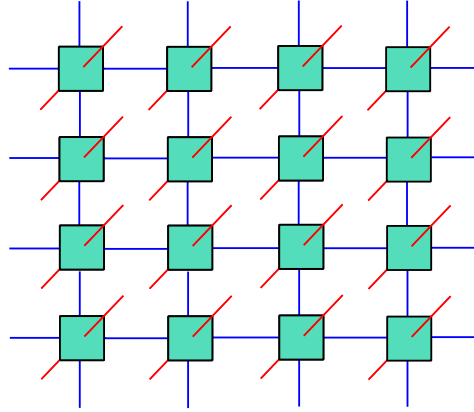


**Figure 10.** (Color online) The graphic representation of a projected entangled pair operator, where the upward and downward indexes represent the *bra* and *ket* space, respectively.

The MPO formulation also allows for a convenient and efficient representation of the Hamiltonians with longer range interactions [309]. The geometrical bond dimensions will in principle increase with the interaction length. Surprisingly, a small dimension is needed to approximate the Hamiltonian with long-range interactions that decay polynomially [Ref].

Besides, MPO can be used to represent the time evolution operator  $\hat{U}(\tau) = e^{-\tau\hat{H}}$  with *Trotter-Suzuki decomposition*, where  $\tau$  is a small positive number called *Trotter-Suzuki step* [59, 60]. Such an MPO is very useful in calculating real, imaginary, or even complex time evolutions, which we will present later in detail. An MPO can also give a mixed state.

Similarly, PEPS can also be generalized to PEPO (Fig. 10), which on a square lattice for instance can be written as

$$\hat{O} = \sum_{\{s,a\}} \prod_n W_{s_n s'_n, a_n^1 a_n^2 a_n^3 a_n^4}^{[n]} |s_n\rangle \langle s'_n|. \quad (41)$$

Each tensor has two physical indexes (*bra* and *ket*) and four geometrical indexes. Each geometrical bond is shared by two adjacent tensors and will be contracted.

### 2.3. General form of tensor network

One can see that a TN is defined as the contraction of certain tensors  $\{T^{[n]}\}$  with a general form as

$$\mathcal{T}_{\{s\}} = \sum_{\{a\}} \prod_n T_{s_1^n s_2^n \dots, a_1^n a_2^n \dots}^{[n]}. \quad (42)$$

The indexes  $\{a\}$  are actually dumb, each of which is shared by more than one tensors and will be contracted. The indexes  $\{s\}$  are open bonds, each of which only belongs to one tensor. After contracting all dumb indexes, the TN represents a  $\mathcal{N}$ -th order tensor, with  $\mathcal{N}$  the total number of open indexes.

Each tensor in the TN can possess different number of open or dumb indexes. For MPS, each tensor has one open index (called physical bond) and two dumb indexes (called virtual

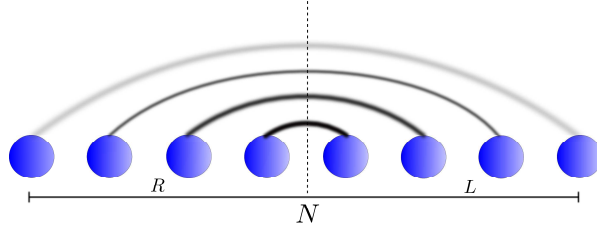


**Figure 11.** Bipartition of a 1D system into two half chains. Significant quantum correlations in gapped ground states occur only on short length scales.

or geometrical bonds); for PEPS on square lattice, it has one open and four dumb indexes. For the generalizations of operators, the number of open indexes are two for each tensor. It allows hierarchical structure of the TN, such as MERA.

One special kind of the TN's is the scalar TN with no open bonds, denoted as

$$Z = \sum_{\{a\}} \prod_n T_{a_1^n a_2^n \dots}^{[n]} \quad (43)$$

A scalar TN can be obtained from the TN's that has open bonds, such as  $Z = \sum_{\{s\}} \mathcal{T}_{\{s\}}$  or  $Z = \sum_{\{s\}} \mathcal{T}_{\{s\}}^\dagger \mathcal{T}_{\{s\}}$ . It is very important because many physical problems can be transformed to computing the contractions of scalar TN's, where  $Z$  is the cost function (e.g., energy or fidelity) to be optimized. The TN contraction algorithms mainly concern the scalar TN's.

#### 2.4. Tensor network and quantum entanglement

The numerical methods based on TN face great challenges, primarily that the dimension of Hilbert space increases exponentially with the size. Such an “*exponential wall*” has been problematic significantly for many numeric algorithms, including the density functional methods [310] and Monte Carlo approaches [76].

The power of TN has been understood in the sense of quantum entanglement: the entanglement structure of low-lying energy states can be efficiently encoded in tensor network states. It takes advantage of the fact that not all quantum states in the total Hilbert space of a many-body system are equally relevant to the low-energy or low-temperature physics. It has been found that the low-lying eigenstates of a gapped Hamiltonian with local interactions obey the area law of the entanglement entropy [311].

More precisely speaking, for a certain subregion  $\mathcal{R}$  of the system, its reduced density matrix is defined as  $\hat{\rho}_{\mathcal{R}} = \text{Tr}_{\mathcal{E}}(\hat{\rho})$ , with  $\mathcal{E}$  denotes the spatial complement of  $\mathcal{R}$ . The entanglement entropy is defined as

$$S(\rho_{\mathcal{R}}) = -\text{Tr}\{\rho_{\mathcal{R}} \log(\rho_{\mathcal{R}})\}. \quad (44)$$

Then the area law of the entanglement entropy [56, 49] reads

$$S(\rho_{\mathcal{R}}) = O(|\partial\mathcal{R}|), \quad (45)$$

with  $|\partial\mathcal{R}|$  the size of the boundary. In particular, for a  $D$ -dimensional system, one has

$$S = O(l^{D-1}), \quad (46)$$

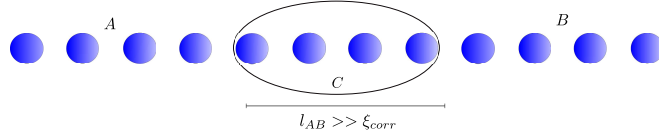


**Figure 12.** The argue the 1D area law, the chain is separated into three sub-systems denoted by  $A$ ,  $B$  and  $C$ . If the correlation length  $\xi_{corr}$  is much larger than the size of  $B$  (denoted by  $l_{AC}$ ), the reduced density matrix by tracing  $B$  approximately satisfies  $\hat{\rho}_{AC} \simeq \hat{\rho}_A \otimes \hat{\rho}_C$ .

with  $l$  the length scale. This means that for 1D systems,  $S = const$ . The area law suggests that the low-lying eigenstates stay in a “small corner” of the full Hilbert space of the many-body system, and that they can be described by a much smaller number of parameters. We shall stress that the locality of the interactions is not sufficient to the area law. Vitagliano, *et al* show that simple 1D spin models can exhibit volume law, where the entanglement entropy scales with the bulk [312].

The area law of entanglement entropy is intimately connected to another fact that a non-critical quantum system exhibits a finite correlation length. The correlation functions between two blocks in a gapped system decay exponentially as a function of the distance of the blocks [46], which is argued to lead to the area law. An intuitive picture can be seen in Fig. 11. Let us consider a 1D gapped quantum system whose ground state  $|\psi_{ABC}\rangle$  possesses a correlation length  $\xi_{corr}$ . By dividing into three subregions  $A$ ,  $B$  and  $C$ , the reduced density operator  $\hat{\rho}_{AC}$  is obtained when tracing out the block  $B$ , i.e.  $\hat{\rho}_{AC} = \text{Tr}_B |\psi_{ABC}\rangle\langle\psi_{ABC}|$  (see Fig. 12). In the limit of large distance between  $A$  and  $C$  blocks with  $l_{AC} \gg \xi_{corr}$ , one has the reduced density matrix satisfying

$$\hat{\rho}_{AC} \simeq \hat{\rho}_A \otimes \hat{\rho}_C, \quad (47)$$

up to some exponentially small corrections. Then  $|\psi_{ABC}\rangle$  is a purification  $*$  of a mixed state with the form  $|\psi_{AB_l}\rangle \otimes |\psi_{B_r C}\rangle$  that has no correlations between  $A$  and  $C$ ; here  $B_l$  and  $B_r$  sit at the two ends of the block  $B$ , which together span the original block.

It is well known that all possible purifications of a mixed state are equivalent to each other up to a local unitary transformation on the virtual Hilbert space. This naturally implies that there exists a unitary operation  $\hat{U}_B$  on the block  $B$  that completely disentangles the left from the right part as

$$\hat{I}_A \otimes \hat{U}_B \otimes \hat{I}_C |\psi_{ABC}\rangle \rightarrow |\psi_{AB_l}\rangle \otimes |\psi_{B_r C}\rangle. \quad (48)$$

$\hat{U}_B$  implies that there exists a tensor  $B_{s,aa'}$  with  $0 \leq a, a', s \leq \chi - 1$  and basis  $\{|\psi^A\rangle\}$ ,  $\{|\psi^B\rangle\}$ ,  $\{|\psi^C\rangle\}$  defined on the Hilbert spaces belonging to  $A$ ,  $B$ ,  $C$  such that

$$|\psi_{ABC}\rangle \simeq \sum_{saa'} B_{s,aa'} |\psi_s^A\rangle |\psi_s^B\rangle |\psi_{a'}^C\rangle. \quad (49)$$

This argument directly leads to the MPS description and gives a strong hint that the ground states of a gapped Hamiltonian is well represented by an MPS of finite bond

$*$ Purification: Let  $\rho$  be a density matrix acting on a Hilbert space  $\mathcal{H}_A$  of finite dimension  $n$ . Then there exist a Hilbert space  $\mathcal{H}_B$  and a pure state  $|\psi\rangle \in \mathcal{H}_A \otimes \mathcal{H}_B$  such that the partial trace of  $|\psi\rangle\langle\psi|$  with respect to  $\mathcal{H}_B$ :  $\rho = \text{Tr}_B |\psi\rangle\langle\psi|$ . We say that  $|\psi\rangle$  is the purification of  $\hat{\rho}$ .



dimensions, where  $B$  in Eq. (49) is analog to the tensor in an MPS. Let us remark that every state of  $N$  spins has an exact MPS representation if we allow  $\chi$  grow exponentially with the number of spins [27]. The whole point of MPS is that a ground state can typically be represented by an MPS where the dimension  $\chi$  is small and scales at most polynomially with the number of spins: this is the reason why MPS-based methods are more efficient than exact diagonalization.

For the 2D PEPS, it is more difficult to strictly justify the area law of entanglement entropy. However, we can make some sense of it from the following aspects. One is the fact that PEPS can exactly represent some non-trivial 2D states that satisfies the area law, such as the nearest-neighbor RVB and  $Z_2$  spin liquid mentioned above. Another is to count the dimension of the geometrical bonds  $\mathcal{D}$  between two subsystems, from which the entanglement entropy satisfies an upper bound as  $S \leq \log \mathcal{D}$  \*.

After dividing a PEPS into two subregions, one can see that the number of geometrical bonds  $N_b$  increase linearly with the length scale, i.e.  $N_b \sim l$ . It means the dimension  $\mathcal{D}$  satisfies  $\mathcal{D} \sim \chi^l$ , and the upper bound of the entanglement entropy fulfills the area law given by Eq. (46), which is

$$S \leq O(l). \tag{50}$$

However, as we will see later, such a property of PEPS is exactly the reason that makes it computationally difficult.

## 2.5. From physical problems to tensor networks

In this subsection, we show that many physical problems can be transformed into TN contraction problems. We will give three examples, which are the calculations of classical partition functions, observables of a given TN state, and ground-state/finite-temperature simulations of quantum Hamiltonians. In this way, different physical problems can be solved by implementing TN contractions.

*2.5.1. Classical partition functions* Partition function, which is a function of the variables of a thermodynamic state such as temperature, volume, and etc., contains the statistical information of a thermodynamic equilibrium system. From its derivatives of different orders, we can calculate the energy, free energy, entropy, and so on. Levin and Nave pointed out in Ref.[67] that the partition function of a lattice statistic model (such as Ising and Potts models) with local interactions can be written in a TN. In this section we will introduce how to obtain the TN representation of the partition function of different classical models. Without losing generality, we take square lattice as an example.

First, let us start from the simplest case: the classical Ising model on a single square with only four sites. The four Ising spins denoted by  $s_i$  ( $i = 1, 2, 3, 4$ ) locate separately on the four corners of the square, as shown in Fig. 13(a); each spin can be up or down, represented by

\*One can see this with simply a flat entanglement spectrum,  $\lambda_n = 1/\mathcal{D}$  for any  $n$ .

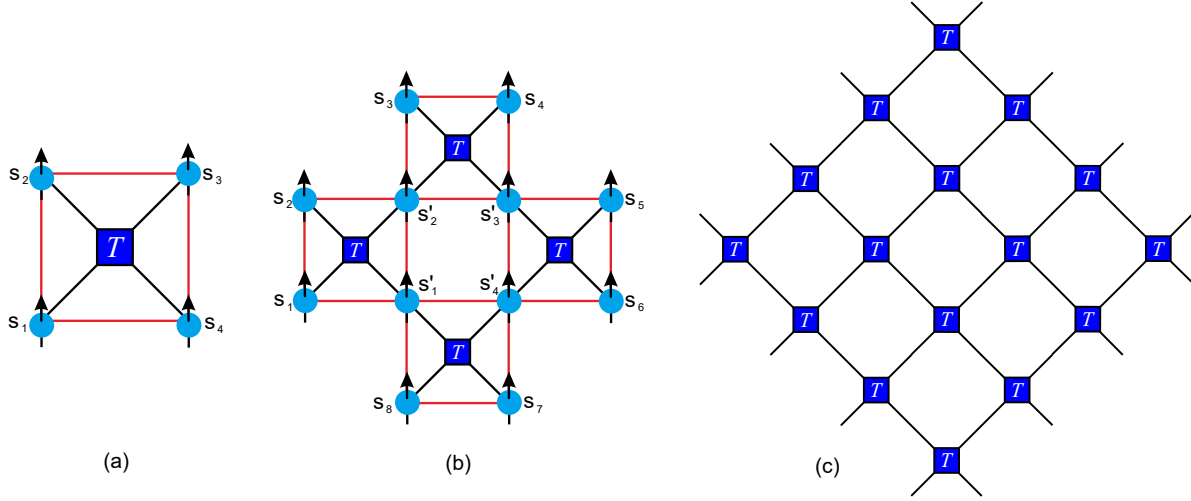


**Figure 13.** (Color online) (a) Four Ising spins (blue balls with arrows) sitting on a single square, and the red lines represent the interactions. The blue block is the tensor  $T$  [Eq. (52)], with the black lines denoting the indexes of  $T$ . (b) The graphic representation of the TN on a larger lattice with more than one squares. (c) The TN construction of the partition function on infinite square lattice.

$s_i = 0$  and  $1$ , respectively. The classical Hamiltonian of such a system reads

$$H_{s_1 s_2 s_3 s_4} = J(s_1 s_2 + s_2 s_3 + s_3 s_4 + s_4 s_1) - h(s_1 + s_2 + s_3 + s_4) \quad (51)$$

with  $J$  the coupling constant and  $h$  the magnetic field.

When the model reaches the equilibrium at temperature  $T$ , the probability of each possible spin configuration is determined by the Maxwell-Boltzmann factor

$$T_{s_1 s_2 s_3 s_4} = e^{-\beta H_{s_1 s_2 s_3 s_4}}, \quad (52)$$

with the inverse temperature  $\beta = 1/T$  \*. Obviously, Eq. (52) is a fourth-order tensor  $T$ , where each element gives the probability of the corresponding configuration.

The partition function is defined as the summation of the probability of all configurations. In the language of tensor, it is obtained by simply summing over all indexes as

$$Z = \sum_{s_1 s_2 s_3 s_4} T_{s_1 s_2 s_3 s_4}. \quad (53)$$

Let us proceed a little bit further by considering four squares, whose partition function can be written in a TN with four tensors [Fig.13(b)] as

$$Z = \sum_{\{s, s'\}} T_{s_1 s_2 s_2' s_1'} T_{s_2' s_3 s_4 s_3'} T_{s_4' s_3' s_5 s_6} T_{s_8 s_1' s_4' s_7}. \quad (54)$$

One can see that each of the indexes  $\{s'\}$  inside the TN is shared by two tensors, representing the spin that appears in both of the squares.

For the infinite square lattice, the probability of a certain spin configuration  $(s_1, s_2, \dots)$  is given by the product of the tensor elements as

$$e^{-\beta H_{\{s\}}} = e^{-\beta H_{s_1 s_2 s_3 s_4}} e^{-\beta H_{s_4 s_5 s_6 s_7}} \dots = T_{s_1 s_2 s_3 s_4} T_{s_4 s_5 s_6 s_7} \dots \quad (55)$$

\*In this paper, we set Boltzmann constant  $k_B = 1$  for convenience.

Then the partition function is given by the contraction of an infinite TN formed by the copies of  $T$  [Eq. (52)] as

$$Z = \sum_{\{s\}} \prod_n T_{s_1^n s_2^n s_3^n s_4^n}, \quad (56)$$

where two indexes satisfy  $s_j^n = s_k^m$  if they refer to the same spin. The graphic representation of Eq.56 is shown in Fig.13(c). One can see that on square lattice, the TN still has the geometry of a square lattice. In fact, such a way will give a TN that has a geometry of the dual lattice of the system (note the dual of the square lattice is itself).

For the  $Q$ -state Potts model on square lattice, the partition function has the same TN representation as that of the Ising model, except that the elements of the tensor are given by the Boltzmann weight of the Potts model and the dimension of each index is  $Q$ . Note that the Potts model with  $q = 2$  is equivalent to the Ising model.

Another example is the eight-vertex model proposed by Baxter in 1971 [307]. It is one of the “ice-type” lattice statistic model, and can be considered as the classical correspondence of the  $Z_2$  spin liquid state. Specifically speaking, the total magnetization of every four spins in a square should be even times of the single spin magnetization. The tensor that gives the TN of the partition function is also  $(2 \times 2 \times 2 \times 2)$ . It is the same as the tensor of the  $Z_2$  spin liquid defined on the sites, whose non-zero elements are

$$T_{s_1, \dots, s_N} = \begin{cases} 1, & s_1 + \dots + s_N = \text{even}, \\ 0, & \text{otherwise.} \end{cases} \quad (57)$$

We shall remark that there are more than one ways to define a TN of the partition function of a classical system. For example, when there only exist nearest-neighbor couplings, one can define a matrix  $M_{ss'} = e^{-\beta H_{ss'}}$  on each bond and put on each site a *super-digonal* tensor  $I$  (or called copy tensor) defined as

$$I_{s_1, \dots, s_N} = \begin{cases} 1, & s_1 = \dots = s_N; \\ 0, & \text{otherwise.} \end{cases} \quad (58)$$

Then the TN of the partition function is the contraction of copies of  $M$  and  $I$ , and possesses exactly the same geometry of the original lattice.

**2.5.2. Quantum observations** By utilizing TN representations, the computations of quantum observations as  $\langle \psi | \hat{O} | \psi \rangle$  and  $\langle \psi | \psi \rangle$  become TN contractions. Those TN constructions are directly linked with physical properties of the system, such as per-site energy, magnetization and so on. For 1D MPS, these are very easy to be done, since one only needs to deal with a 1D TN stripe. For 2D PEPS, such calculations become contractions of 2D TN's. Taking  $\langle \psi | \psi \rangle$  as an example, the TN of such an inner product is the contraction of the copies of the local tensor defined as

$$T_{a_1 a_2 a_3 a_4} = \sum_s P_{s, a_1' a_2'' a_3' a_4''}^* P_{s, a_1' a_2' a_3' a_4'}, \quad (59)$$

with  $P$  the tensor of the PEPS and  $a_i = (a_i', a_i'')$ . There are no open indexes left and the TN gives a scalar that is exactly  $\langle \psi | \psi \rangle$ . The TN for computing the observable  $\langle \hat{O} \rangle$  is similar. The

only difference is that we should substitute some small number of  $T_{a_1 a_2 a_3 a_4}$  in original TN for  $\langle \psi | \psi \rangle$  with “impurities” at the sites we do local observations. The single-point “impurity” tensor on the  $i$ th site can be defined as

$$\tilde{T}_{a_1 a_2 a_3 a_4}^{[i]} = \sum_{s, s'} P_{s, a'_1 a'_2 a'_3 a'_4}^* \hat{O}_{s, s'}^{[i]} P_{s', a'_1 a'_2 a'_3 a'_4}, \quad (60)$$

In such case, the single-point observables, can be represented by the TN contraction of

$$\frac{\langle \psi | \hat{O}^{[i]} | \psi \rangle}{\langle \psi | \psi \rangle} = \frac{\text{tTr } \tilde{T}^{[i]} \prod_{n \neq i} T}{\text{tTr } \prod_{n=1}^N T}, \quad (61)$$

For some non-local observable, e.g., correlation function, the contraction of  $\langle \psi | \hat{O}^{[i]} \hat{O}^{[j]} | \psi \rangle$  is nothing but adding another “impurity” by

$$\langle \psi | \hat{O}^{[i]} \hat{O}^{[j]} | \psi \rangle = \text{tTr } \tilde{T}^{[i]} \tilde{T}^{[j]} \prod_{n \neq i, j}^N T, \quad (62)$$

**2.5.3. Ground-state and finite-temperature simulations** Ground-state simulations of quantum models with short-range interactions can also be efficiently transferred to TN contractions. When minimizing the energy

$$E = \frac{\langle \psi | \hat{H} | \psi \rangle}{\langle \psi | \psi \rangle}, \quad (63)$$

$|\psi\rangle$  can be written in an MPS for 1D and a PEPS for 2D systems as a variational ansatz (see, e.g., [208, 121]). Generally speaking, there are two ways to solve the minimization problem: (i) simply treat all the tensor elements as variational parameters; (ii) simulate the imaginary-time evolution

$$|\psi_{gs}\rangle = \lim_{\beta \rightarrow \infty} \frac{e^{-\beta \hat{H}} |\psi\rangle}{\| e^{-\beta \hat{H}} |\psi\rangle \|}. \quad (64)$$

The first way can be realized by, e.g., Monte Carlo methods, where one could randomly change or choose the value of each tensor element to locate the minimal of energy. One can also use the Newton method and solve the partial-derivative equations  $\partial E / \partial x_n = 0$  with  $x_n$  standing for an arbitrary variational parameter. Anyway, it is inevitable to calculate  $\langle \psi | \hat{H} | \psi \rangle$  and  $\langle \psi | \psi \rangle$  for most cases.

We shall stress that without TN, the dimension of the ground state (i.e., the number of variational parameters) increases exponentially, which makes the ground-state simulations impossible for large systems.

The second way of computing the ground state with imaginary-time evolution is more or less like an “annealing” process. One starts from an arbitrarily chosen initial state and acts the imaginary-time operator on it to lower the “temperature” a little each step, until the state reaches a fixed point. Mathematically speaking, by using Trotter-Suzuki decomposition [65, 66], such an evolution is written in a TN defined on  $(D + 1)$ -dimensional lattice, with  $D$  the dimension of the real space of the model.

Here, we take a quantum 1D chain with nearest-neighbor interactions as an example. We assume that the Hamiltonian only contains at most nearest-neighbor couplings, which reads

$$\hat{H} = \sum_n \hat{h}_{n,n+1}, \quad (65)$$

with  $\hat{h}_n$  and  $\hat{h}_{n,n+1}$  the on-site and two-body interactions. It is useful to divide  $\hat{H}$  into two groups,  $\hat{H} = \hat{H}^e + \hat{H}^o$  as

$$\hat{H}^e \equiv \sum_{\text{even } n} \hat{h}_{n,n+1}, \quad \hat{H}^o \equiv \sum_{\text{odd } n} \hat{h}_{n,n+1}. \quad (66)$$

By doing so, each two terms in  $\hat{H}^e$  or  $\hat{H}^o$  commute with each other. Then the evolution operator  $\hat{U}(\tau)$  for infinitesimal imaginary time  $\tau \rightarrow 0$  can be written as

$$\hat{U}(\tau) = e^{-\tau\hat{H}} = e^{-\tau\hat{H}^e} e^{-\tau\hat{H}^o} + O(\tau^2)[\hat{H}^e, \hat{H}^o] \quad (67)$$

If  $\tau$  is small enough, the high-order terms are negligible, and the evolution operator becomes

$$\hat{U}(\tau) \simeq \prod_n \hat{U}(\tau)_{n,n+1}, \quad (68)$$

with the two-site evolution operator  $\hat{U}(\tau)_{n,n+1} = e^{-\tau\hat{H}_{n,n+1}}$ .

Note that higher order expansions can also be adopted. For example, the second order Trotter-Suzuki decomposition is written as

$$e^{-\tau\hat{H}} \simeq e^{-\frac{\tau}{2}\hat{H}^e} e^{-\tau\hat{H}^o} e^{-\frac{\tau}{2}\hat{H}^e}. \quad (69)$$

With Eq. (68), the time evolution can be transferred to a TN [Fig. 13 (c)], where the local tensor is actually the coefficients of  $\hat{U}(\tau)_{n,n+1}$ , satisfying

$$T_{s_n s_{n+1} s'_n s'_{n+1}} = \langle s'_n s'_{n+1} | \hat{U}(\tau)_{n,n+1} | s_n s_{n+1} \rangle. \quad (70)$$

Such a TN is defined in a plain of two dimensions that corresponds to the spatial and time, respectively. The initial state is located at the bottom of the TN ( $\beta = 0$ ) and its evolution is to do the TN contraction which can efficient solved by TN algorithms (presented later).

The evolution operator  $U(\tau)$  can be written as an MPO (also see Fig. 9 and the related texts). Then  $U(\beta)$  with  $\beta = K\tau$  becomes a TN with  $K$  layers of MPO's. To do so, we decompose  $T_{s_n s'_{n+1} s_{n+1} s'_{n+1}}$  by QR or SVD as

$$T_{s_n s'_{n+1} s_{n+1} s'_{n+1}} = \sum_{\alpha} F_{s_n s'_n, \alpha}^L F_{s_{n+1} s'_{n+1}, \alpha}^R. \quad (71)$$

By contracting as

$$T_{s_n s'_n, \alpha \alpha'}^L = \sum_s F_{s_n s, \alpha}^R F_{s s'_n, \alpha'}^L, \quad T_{s_n s'_n, \alpha \alpha'}^R = \sum_s F_{s_n s, \alpha}^L F_{s s'_n, \alpha'}^R. \quad (72)$$

We have  $U(\tau)$  as a two-site translationally invariant MPO that is formed by the copies of  $T^L$ 's and  $T^R$ 's. See Fig. 14 (a). Note in Ref. [172], the authors proposed a way to defined the one-site translationally invariant MPO, which could be very useful in certain cases.

In addition, one can readily see that the evolution operator for 2D quantum systems can also be written as a PEPO (also see Fig. 10 and the related texts). Starting from a 3D TN formed by the copies of  $T$  [Eq. (70)], one can use  $X^L$  and  $X^R$  [Eq. (71)] to obtain two sixth-ordered tensors as shown in Fig. 14 (b). Then the 3D TN contains  $K$  layers of PEPO.

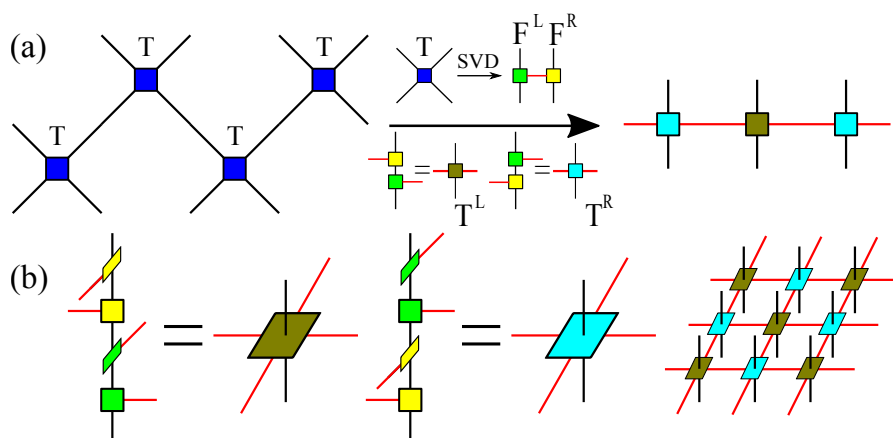


**Figure 14.** (Color online) The evolution operator  $U(\tau)$  in 1D (a) or 2D (b) can be written as an MPO or PEPO, respectively.

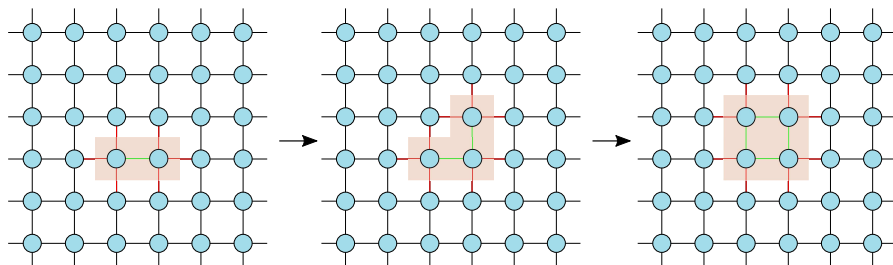


**Figure 15.** (Color online) If one starts with contracting an arbitrary bond, there will be a tensor with six bonds. As the contraction goes on, the number of bonds increases linearly with the boundary  $\partial$  of the contracted area, thus the memory increases exponentially as  $O(\chi^\partial)$  with  $\chi$  the bond dimension.

### 3. Tensor network contraction approaches inspired by numerical renormalization group

The most natural way to calculate a TN contraction is to contract the TN. Since in most cases, it is IMPOSSIBLE to contract all bonds simultaneously, one has to specify a contraction order. In this chapter, we will present some of the most important tensor renormalization group algorithms, which we categorize by the contraction orders as coarse-graining, linearized and polynomial contraction algorithms.

#### 3.1. Several exactly contractible tensor networks

Let us consider a square TN, as shown in Fig. 15. We start from contracting an arbitrary bond in the TN (yellow shadow). Consequently, we obtain a new tensor with six bonds that contains  $\chi^6$  parameters ( $\chi$  is the bond dimension). To proceed, the bonds adjacent to this tensor are probably a good choice to contract next. Then we will have to restore a new tensor with eight bonds. As the contraction goes on, the number of bonds increases linearly with the boundary

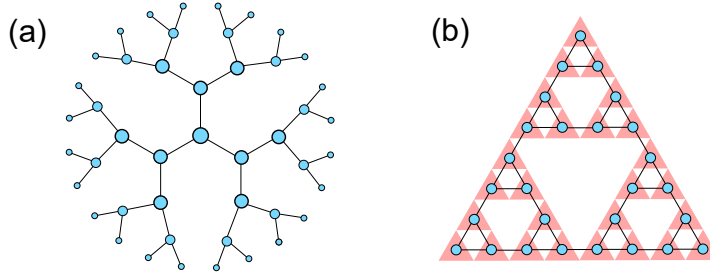


**Figure 16.** (Color online) Two kinds of TN's that can be exactly contracted: (a) tree and (b) fractal TN's. In (b), the shadow shows the Sierpiński gasket, where the tensors are defined in the triangles.

$\partial$  of the contracted area, thus the memory increases exponentially as  $O(\chi^\partial)$ . For this reason, it is impossible to exactly contract a TN, even if it only contains a small number of tensors. Thus, approximations are inevitable. This computational difficulty is closely related to the area law of entanglement entropy [56] (also see Chap. 2).

Before talking about the TN algorithms, allow us to firstly present three kinds of TN's that can be exactly contracted, which are the TN's defined on trees and fractals (Fig. 16), as well as the algebraically contractible TN's.

**Tensor networks on tree graphs.** A TN defined on a tree graph is usually called a tree TN (TTN) [Fig. 16 (a)]. To discuss the contraction, we consider a finite TTN with  $N_L$  layers of tensors and put some vectors on its boundary. The TN is written as

$$Z = \sum_{\{a\}} \prod_{n=1}^{N_L} \prod_{m=1}^{M_n} T_{a_n, m, 1, a_n, m, 2, a_n, m, 3}^{[n, m]} \prod_k v_{a_k}^{[k]}, \quad (73)$$

with  $T^{[n, m]}$  the  $m$ -th tensor on the  $n$ -th layer,  $M_n$  the number of tensors of the  $n$ -th layer, and  $v^{[k]}$  the  $k$ -th vectors on the boundary.

Now we contract each of the tensor on the  $N_L$ -th layer with the corresponding two vectors on the boundary as

$$v'_{a_3} = \sum_{a_1 a_2} T_{a_1 a_2 a_3}^{[N_L, m]} v_{a_1}^{[k_1]} v_{a_2}^{[k_2]}. \quad (74)$$

Then, the vectors are updated by the equation above, and the number of layers of the TTN becomes  $N_L - 1$ . The whole TTN can be exactly contracted by repeating this procedure.

Moreover, we can see from the above contraction that if the graph does not contain any loops, i.e. has a tree like structure, the TN defined on it can be exactly contracted. This is again related to the area law of entanglement entropy a loop-free TN satisfies. It can be seen that to separate a tree-like TN into two disconnecting parts, the number of bonds that needs to be cut is only one. It means the upper bond of the entanglement entropy between these two parts is constant, determined by the dimension of the bond that is cut. Under this circumstance, the size of the tensors that appear during the computation is limited, thus the contraction can be done without approximations.

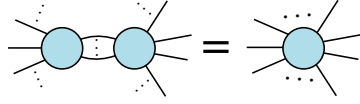


**Figure 17.** (Color online) The fusion rule of the copy tensor: the contraction of two copy tensors of  $N_1$ -th and  $N_2$ -th order gives a copy tensor of  $(N_1 + N_2 - N)$ -th order, with  $N$  the number of the contracted bonds.

**Tensor networks on fractals.** Another example that can be exactly contracted is the TN defined on the fractal called Sierpiński gasket [Fig. 16 (b)] (see, e.g. [167, 168]). The TN can represent the partition function of the statistical model defined on the Sierpiński gasket, such as Ising model. As explained in Sec. II, the tensor is given by the probability distribution of the three spins in a triangle.

Such a TN can be exactly contracted by iteratively contracting each three of the tensors located in a same triangle as

$$T'_{a_1 a_2 a_3} = \sum_{b_1 b_2 b_3} T_{a_1 b_1 b_2} T_{a_2 b_2 b_3} T_{a_3 b_3 b_1}. \quad (75)$$

After each round of contractions, the dimension of the tensors and the geometry of the network keep unchanged, but the number of the tensors in the TN decreases from  $N$  to  $N/3$ . It means we can exactly contract the whole TN by repeating the above process.

**Algebraically contractible tensor networks.** The third example is called algebraically contractible TN's [169]. The tensors that form the TN possess some special algebraic properties, so that even the bond dimensions increase after each contraction, the rank of the bonds is kept unchanged. It means one can introduce some projectors to lower the bond dimension without causing any errors.

The simplest algebraically contractible TN is the one formed by the *super-diagonal tensor*  $I$  defined as

$$I_{a_1, \dots, a_N} = \begin{cases} 1, & a_1 = \dots = a_N, \\ 0, & \text{otherwise.} \end{cases} \quad (76)$$

$I$  is also called *copy tensor*, since it only forces all its indexes to take a same value.

For a square TN of an arbitrary size formed by the fourth-order  $I$ 's, obviously we have its contraction  $Z = d$  with  $d$  the bond dimension. The reason is that the contraction is the summation of only  $d$  non-zero values (each equals to 1).

To demonstrate its contraction, we will need one important property of the copy tensor (Fig. 17): if there are  $n \geq 1$  bonds contracted between two copy tensors, the contraction gives a copy tensor,

$$I_{a_1 \dots b_1 \dots} = \sum_{c_1 \dots} I_{a_1 \dots c_1 \dots} I_{b_1 \dots c_1 \dots} \quad (77)$$

This property is called the *fusion rule*, and can be understood in the opposite way: a copy tensor can be decomposed as the contraction of two copy tensors.

With the fusion rule, one will readily have the theorem for the dimension reduction: if there are  $n \geq 1$  bonds contracted between two copy tensors, the contraction is identical after



replacing the  $n$  bonds with one bond,

$$\sum_{c_1 \dots} I_{a_1 \dots c_1 \dots} I_{b_1 \dots c_1 \dots} = \sum_c I_{a_1 \dots c} I_{b_1 \dots c}. \quad (78)$$

In other words, the dimension of the contracting bonds can be exactly reduced from  $d^n$  to  $d$ . Applying this theorem to TN contraction, it means each time when the bond dimension increases after contracting several tensors into one tensor, the dimension can be exactly reduced to  $d$ , so that the contraction can continue until all bonds are contracted.

From the TN of the copy tensors, a class of exactly contractible TN can be defined, where the local tensor is the multiplication of the copy tensor by several unitary tensors. Taking the square TN as example, we have

$$T_{a_1 a_2 a_3 a_4} = \sum_{b_1 b_2 b_3 b_4} X_{b_1} I_{b_1 b_2 b_3 b_4} U_{a_1 b_1} V_{a_2 b_2} U_{a_3 b_3}^* V_{a_4 b_4}^*, \quad (79)$$

with  $U$  and  $V$  two unitary matrices.  $X$  is an arbitrary  $d$ -dimensional vector that can be understood as the “weights” (not necessarily to be positive to define the tensor). After putting the tensors in the TN, all unitary matrices vanish to identities. Then one can use the fusion rule of the copy tensor to exactly contract the TN, and the contraction gives  $Z = \prod_b (X_b)^{N_T}$  with  $N_T$  the total number of tensors.

The unitary matrices are not trivial in physics. If we take  $d = 2$  and

$$U = V = \begin{bmatrix} \sqrt{2}/2 & \sqrt{2}/2 \\ \sqrt{2}/2 & -\sqrt{2}/2 \end{bmatrix}, \quad (80)$$

the TN is in fact the inner product of the  $Z_2$  topological state (see the definition of  $Z_2$  PEPS in Sec. 2.2.3). If one cuts the system into two sub-regions, all the unitary matrix vanish into identities inside the bulk. However, those on the boundary will survive, which could lead to exotic properties such as topological orders, edge states and so on. Note that  $Z_2$  state is only a special case. One can refer to a systematic picture given by X. G. Wen called the string-net condensation.

### 3.2. Tensor renormalization group: exponential contraction

In 2007, Levin and Nave proposed tensor renormalization group (TRG) approach [67] to contract the TN of 2D classical lattice models. TRG can be considered as a coarse-graining contraction algorithm. To introduce the TRG algorithm, let us consider a square TN formed by infinite number of copies of a forth-order tensor  $T_{a_1 a_2 a_3 a_4}$  (see Fig. 15).

**Contraction and truncation.** The idea of TRG is to iteratively “coarse-grain” the TN without changing the bond dimensions, the geometry of the network and the translational invariance. Such a process is realized by two local operations in each iteration. Let us denote the tensor in the  $t$ -th iteration as  $T^{(t)}$  (we take  $T^{(0)} = T$ ). For obtaining  $T^{(t+1)}$ , the first step is to decompose  $T^{(t)}$  by SVD in two different ways [Fig. 18] as

$$T_{a_1 a_2 a_3 a_4}^{(t)} = \sum_b U_{a_1 a_2 b} V_{a_3 a_4 b}, \quad (81)$$

$$T_{a_1 a_2 a_3 a_4}^{(t)} = \sum_b X_{a_4 a_1 b} Y_{a_2 a_3 b}. \quad (82)$$

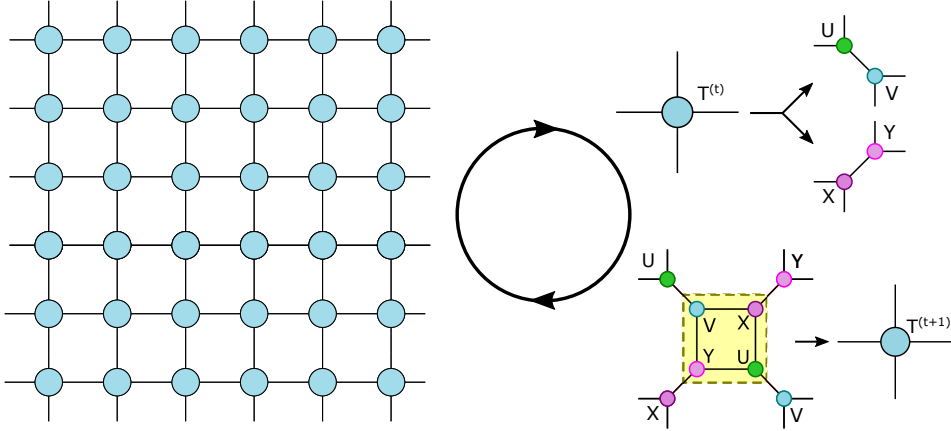


**Figure 18.** (Color online) For an infinite square TN with translational invariance, the renormalization in the TRG algorithm is realized by two local operations of the local tensor. After each iteration, the bond dimensions of the tensor and the geometry of the network keep unchanged.

Note that the singular value spectrum can be handled by multiplying it with the tensor(s), and the dimension of the new index satisfies  $\dim(b) = \chi^2$  with  $\chi$  the bond dimension of  $T^{(t)}$ .

The purpose of the first step is to deform the TN, so that in the second step, a new tensor  $T^{(t+1)}$  can be obtained by contraction the four tensors that form a square [Fig. 18] as

$$T_{b_1 b_2 b_3 b_4}^{(t+1)} \leftarrow \sum_{a_1 a_2 a_3 a_4} V_{a_1 a_2 b_1} Y_{a_2 a_3 b_2} U_{a_3 a_4 b_3} X_{a_4 a_1 b_4}. \quad (83)$$

We use an arrow instead of the equal sign, because one may need to dividing the tensor by a proper number to keep the value of the elements from being divergent. The arrows will be used in the same way below.

These two steps define the contraction strategy of TRG. By the first step, the number of tensors in the TN (i.e., the size of the TN) increases from  $N$  to  $2N$ , and by the second step, it decreases from  $2N$  to  $N/2$ . Thus, after  $t$  times of each iterations, the number of tensors decreases to the  $\frac{1}{2^t}$  of its original size. For this reason, TRG is an *exponential contraction algorithm*.

**Error and environment.** The dimension of the tensor at the  $t$ -th iteration becomes  $\chi^{2^t}$ , if no truncations are implemented. It means truncations of the bond dimensions are necessary. In its original proposal, the dimension is truncated by taking the singular vectors of the  $\chi$ -largest singular values in Eq. (82). Then the new tensor  $T^{(t+1)}$  obtained by Eq. (83) has exactly the same dimension as  $T^{(t)}$ .

Each truncation will absolutely introduce some error, which is called the *truncation error*. Consistent with Eq. (7), the truncation error is quantified by the discarded singular values  $\lambda$  as

$$\varepsilon = \frac{\sqrt{\sum_{b=\chi}^{\chi^2-1} \lambda_b^2}}{\sqrt{\sum_{b=0}^{\chi^2-1} \lambda_b^2}}. \quad (84)$$

According to the linear algebra,  $\varepsilon$  in fact gives the error of the SVD given in Eq. (82), meaning

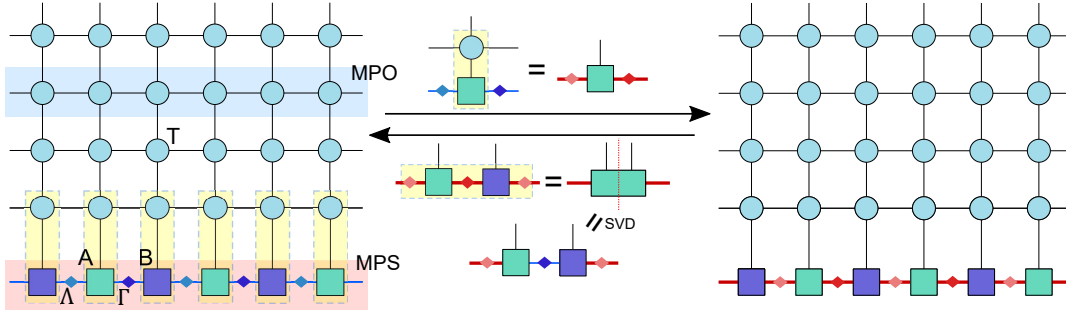


**Figure 19.** (Color online) The illustration of the contraction and truncation of the iTEBD algorithm. In each iteration step, a row of tensors in the TN are contracted to the MPS, and truncations by SVD are implemented so that the bond dimensions of the MPS keep unchanged.

that such a truncation minimizes the error of reducing the rank of  $T^{(t)}$ , which reads

$$\varepsilon = |T_{a_1 a_2 a_3 a_4}^{(t)} - \sum_{b=0}^{\chi-1} U_{a_1 a_2 b} V_{a_3 a_4 b}| \quad (85)$$

In other words, the truncation is optimized according to the tensor  $T^{(t)}$ . Thus,  $T^{(t)}$  is called the *environment* for determining the truncation.

After  $t$  times of iterations, the TN that contains  $2^t$  number of  $T$ 's is contracted into a local tensor  $T^{(t)}$ .

### 3.3. Time-evolving block decimation: linearized contraction

The time-evolving block decimation (TEBD) by Vidal was developed originally for simulating the time evolution of 1D quantum models [58, 59, 60, 61]. The (finite and infinite) TEBD algorithm has been widely applied to varieties of issues, such as criticality in quantum many body systems (e.g., [70, 71, 313]), the topological phases [314], the many-body localization [315, 316, 317] and the thermodynamic property of quantum many-body systems [318, 319, 320, 272, 321, 322].

In the language of TN, TEBD solves the TN problems in a linearized contraction manner, and the truncation is calculated in the context of MPS. Let us still take the infinite square TN formed by the copies of a fourth-order tensor  $T$  as an example, and explain the infinite TEBD (iTEBD) algorithm [60] (Fig. 19). In each step, a row of tensors (which is in fact an MPO) are contracted to an MPS. The truncations are needed to prevent the bond dimension from being exponentially large, which are calculated by minimizing the distance between the MPS before and after truncating. While converging, the MPS is considered to be the dominant eigenvector of the MPO.

**Contraction.** The MPS we use is two-site translational invariant, which is formed by the tensors  $A$  and  $B$  on the sites and the spectrum  $\Lambda$  and  $\Gamma$  on the bonds as

$$\sum_{\{a\}} \cdots \Lambda_{a_{n-1}} A_{s_{n-1}, a_{n-1} a_n} \Gamma_{a_n} B_{s_n, a_n a_{n+1}} \Lambda_{a_{n+1}} \cdots \quad (86)$$

In each step of iTEBD, the contraction part is given by

$$A_{s,\tilde{a}\tilde{a}'} \leftarrow \sum_{s'} T_{sbs'b'} A_{s',aa'}, \quad (87)$$

$$B_{s,\tilde{a}\tilde{a}'} \leftarrow \sum_{s'} T_{sbs'b'} B_{s',aa'}, \quad (88)$$

where the new virtual bonds are entangled, satisfying  $\tilde{a} = (b, a)$  and  $\tilde{a}' = (b', a')$ . Meanwhile, the spectrum are also updated as

$$\Lambda_{\tilde{a}} \leftarrow \Lambda_a \mathbf{1}_b, \quad (89)$$

$$\Gamma_{\tilde{a}'} \leftarrow \Gamma_{a'} \mathbf{1}_{b'}, \quad (90)$$

where  $\mathbf{1}$  is a vector with  $\mathbf{1}_b = 1$  for any  $b$ .

We can see that after contracting, the number of the tensors contracted is  $N$ . It means after  $t$  iterations, the number of tensors will be reduced linearly by  $tN$ . That's why we call iTBED a *linearized contraction algorithm*.

**Truncation.** Then truncation part is needed when the dimensions of the virtual bonds exceed the dimension cut-off  $\chi$ . Generally, what we need is to find the  $(d\chi \times \chi)$  isometries (denoted by  $X$  and  $Y$ ) that optimally reduces the virtual bond dimensions as

$$A_{s,aa'} = \sum_{\tilde{a}\tilde{a}'} A_{s,\tilde{a}\tilde{a}'} X_{\tilde{a}\tilde{a}a} Y_{\tilde{a}'a'}. \quad (91)$$

Here, we explain a simple way used in iTEBD to do the truncations by local SVD. To truncate the virtual bond  $\tilde{a}$  for example, we defined a matrix by contracting the tensors and spectrum connected to the target bond as

$$M_{s_1\tilde{a}_1,s_2\tilde{a}_2} = \sum_{\tilde{a}} \Lambda_{\tilde{a}_1} A_{s_1,\tilde{a}_1\tilde{a}} \Gamma_{\tilde{a}} B_{s_2,\tilde{a}\tilde{a}_2} \Lambda_{\tilde{a}_2}. \quad (92)$$

Note that it is important to have all the three spectrum in the contraction.

Then, perform SVD on  $M$ , keeping only the  $\chi$ -largest singular values and the corresponding basis as

$$M_{s_1\tilde{a}_1,s_2\tilde{a}_2} = \sum_{a=0}^{\chi-1} U_{s_1,\tilde{a}_1a} \Gamma_a V_{s_2,a\tilde{a}_2}. \quad (93)$$

The spectrum  $\Gamma$  is updated by the singular values of the above SVD. The tensors  $A$  and  $B$  are also updated as

$$A_{s_1,\tilde{a}a} = (\Lambda_{\tilde{a}})^{-1} U_{s_1,\tilde{a}a}, \quad (94)$$

$$B_{s_2,a\tilde{a}} = V_{s_2,a\tilde{a}} (\Lambda_{\tilde{a}})^{-1}. \quad (95)$$

Till now, the truncations of the spectrum  $\Gamma$  and the corresponding virtual bonds have been completed. The spectrum  $\Lambda$  and the virtual bonds can be truncated similarly.

**Error and environment.** With SVD, the truncation error is usually quantified by the discarded singular values. So are the truncations above. From the linear algebra, such truncations minimize the error of reducing the rank of  $M$  in Eq. (91), thus the environment is a finite part of the MPS formed by two tensors and three spectrum.

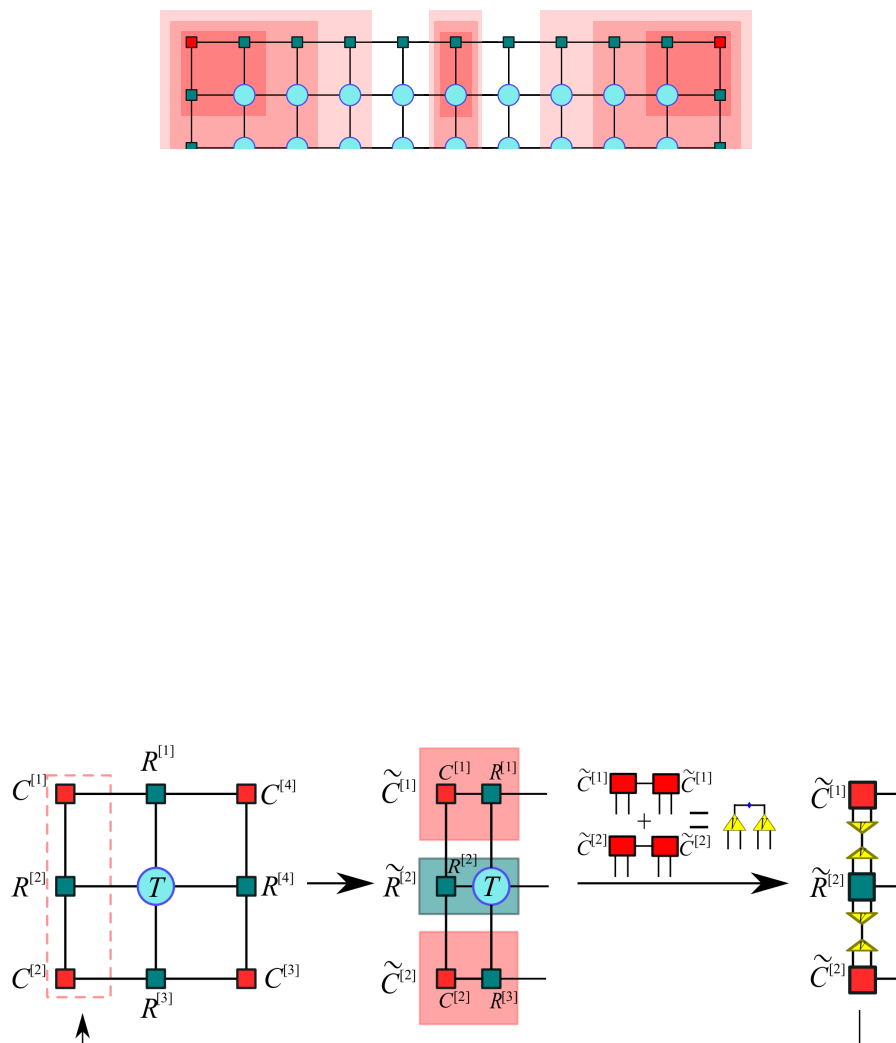


**Figure 21.** (Color online) The first arrow shows absorbing tensors  $R^{[1]}$ ,  $T$ , and  $R^{[3]}$  to renew tensors  $C^{[1]}$ ,  $R^{[2]}$ , and  $C^{[2]}$  in left operation. The second arrow shows the truncation of the enlarged bond of  $\tilde{C}^{[1]}$ ,  $\tilde{R}^{[2]}$  and  $\tilde{C}^{[2]}$ . Inset is the acquisition of the truncation matrix  $Z$ .

What is amazing is that when the MPO is unitary or near unitary, the MPS converges to a so-called *canonical form* [61]. The truncations are then optimal under the whole MPS as the environment. If the MPO is far from being unitary, Orús and Vidal proposed the *canonicalization* algorithm to transform the MPS into the canonical form before truncating. We will talk about this issue in detail in the next chapter.

### 3.4. Corner transfer-matrix renormalization group: polynomial contraction

In the sixteens, the corner transfer matrix (CTM) idea was developed originally by Baxter in ([34, 202] and a book by Baxter [323]). Such ideas and methods have been applied to various models, for example, the chiral Potts model [324, 325, 326], the 8-vertex model [307, 221, 222], and to the 3D Ising model [327]. Combining CTM with DMRG, Nishino and Okunishi proposed the corner transfer matrix renormalization group (CTMRG) [19] in

1996 and applied it on several models [19, 328, 329, 330, 331, 332, 333, 223, 334, 335, 336].

In 2009, Orús and Vidal further developed CTMRG to deal with TN's [201], where the TN is contracted in a polynomial manner. The idea is to put eight variational tensors, which are four corner transfer matrices  $C^{[1]}, C^{[2]}, C^{[3]}, C^{[4]}$  and four row (column) tensors  $R^{[1]}, R^{[2]}, R^{[3]}, R^{[4]}$ , on the boundary, and then contract the tensors in the TN to the variational tensors in a specific order (Fig. 20).

**Contraction.** In each iteration step of CTMRG, one chooses two corner matrices on the same side and the row tensor between them, e.g.,  $C^{[1]}, C^{[2]}$  and  $R^{[2]}$ . The update of these tensors (Fig.21) reads

$$\tilde{C}_{\tilde{b}_2 \tilde{b}'_1}^{[1]} \leftarrow \sum_{b_1} C_{b_1 b_2}^{[1]} R_{b_1 a_1 b'_1}^{[1]}, \quad (96)$$

$$\tilde{R}_{\tilde{b}_2 a_4 \tilde{b}_3}^{[2]} \leftarrow \sum_{a_2} R_{\tilde{b}_2 a_2 b_3}^{[2]} T_{a_1 a_2 a_3 a_4}, \quad (97)$$

$$\tilde{C}_{\tilde{b}_3 \tilde{b}'_4}^{[2]} \leftarrow \sum_{b_4} C_{b_3 b_4}^{[2]} R_{b_4 a_3 b'_4}^{[3]}, \quad (98)$$

where  $\tilde{b}_2 = (b_2, a_1)$  and  $\tilde{b}_3 = (b_3, a_1)$ .

After the contraction given above, it can be considered that one column of the TN (as well as the corresponding row tensors  $R^{[1]}$  and  $R^{[3]}$ ) are contracted. Then one chooses other corner matrices and row tensors (such as  $\tilde{C}^{[1]}, C^{[4]}$  and  $R^{[1]}$ ) and implement similar contractions. By iteratively doing so, the TN is contracted in the way shown in Fig. 20.

Note that for a finite TN, the corner matrices and row tensors should be taken as the tensors locating on the boundary of the TN. For an infinite TN, they can be taken randomly at the first step, and the contraction should be iterated until a preset convergence is reached.

From the process given above, CTMRG can be regarded as a *polynomial contraction scheme*. One can see that the number of tensors that are contracted at each step is determined by the length of the boundary of the TN at each iteration time (denoted as  $t$ ). When contracting a 2D TN defined on a  $(L \times L)$  square lattice as an example, the length of each side is  $L - 2t$  at the  $t$ -th step. The total boundary length of the TN (i.e., the number of tensors contracted at the  $t$ -th step) bears a linear relation with  $t$  as  $4(L - 2t) - 4$ . For a 3D TN such as cubic TN, the total boundary length scales as  $6(L - 2t)^2 - 12(L - 2t) + 8$ , which is a polynomial relation.

**Truncation.** One can see that after the contraction in each iteration step, the bond dimensions of the tensors increase. Truncations are then in need to prevent the excessive growth of bond dimensions. In Ref. [201], each truncation is obtained by inserting a pair of isometries  $V$  and  $V^\dagger$  in the enlarged bonds. A reasonable but not the only choice of  $V$  for translational invariant TN is to consider an eigenvalue decomposition on the sum of corner transfer matrices as

$$\sum_b \tilde{C}_{\tilde{b}\tilde{b}}^{[1]\dagger} \tilde{C}_{\tilde{b}'\tilde{b}}^{[1]} + \sum_b \tilde{C}_{\tilde{b}\tilde{b}}^{[2]\dagger} \tilde{C}_{\tilde{b}'\tilde{b}}^{[1]} \simeq \sum_{b=0}^{\chi-1} V_{\tilde{b}\tilde{b}} \Lambda_b V_{\tilde{b}'\tilde{b}}^*. \quad (99)$$

Only the  $\chi$  largest eigne values are preserved. Therefore,  $V$  is a matrix of the dimension  $D\chi \times \chi$ , where  $D$  is the bond dimension of  $T$  and  $\chi$  is the dimension cut-off. We then

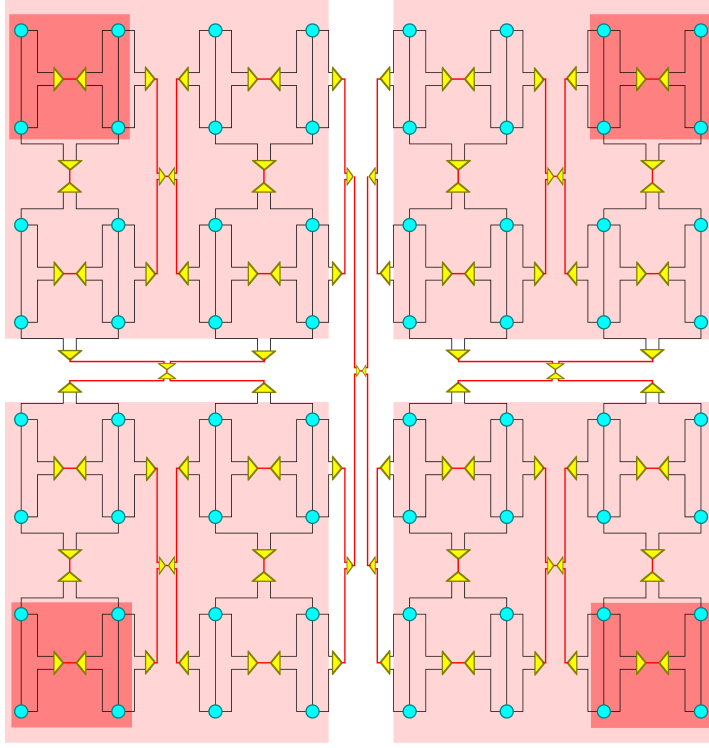


**Figure 22.** (Color online) The exactly contractible TN in the HOTRG algorithm.

truncate  $\tilde{C}^{[1]}$ ,  $\tilde{R}^{[2]}$ , and  $\tilde{C}^{[2]}$  using  $V$  as

$$C_{b'_1 b_2}^{[1]} = \sum_{\tilde{b}_2} \tilde{C}_{\tilde{b}_2 b'_1}^{[1]} V_{\tilde{b}_2 b_2}^*, \quad (100)$$

$$R_{b_2 a_4 b_3}^{[2]} = \sum_{\tilde{b}_2, \tilde{b}_3} \tilde{R}_{\tilde{b}_2 a_4 \tilde{b}_3}^{[2]} V_{\tilde{b}_2 b_2} V_{\tilde{b}_3 b_3}^*, \quad (101)$$

$$C_{b_3 b'_4}^{[2]} = \sum_{\tilde{b}_3} \tilde{C}_{\tilde{b}_3 b'_4}^{[2]} V_{\tilde{b}_3 b_3}. \quad (102)$$

**Error and environment.** Same as TRG or iTEBD, the truncations are obtained by the matrix decompositions of the corresponding tensors. Then the truncation error is minimized by the tensors that are decomposed. From Eq. (99), the environment in CTMRG is the loop formed by the corner matrices and row tensors.

Note that symmetries might be considered to accelerate the computation. For example, one may take  $C^{[1]} = C^{[2]} = C^{[3]} = C^{[4]}$  and  $R^{[1]} = R^{[2]} = R^{[3]} = R^{[4]}$  when the TN has rotational and reflection symmetries ( $T_{a_1 a_2 a_3 a_4} = T_{a'_1 a'_2 a'_3 a'_4}$  after any permutation of the indexes).

### 3.5. Relations to exactly contractible tensor networks and entanglement renormalization

The TN algorithms explained above are aimed at dealing with contracting optimally the TN's that cannot be exactly contracted. A question rises: is a classical computer really able to handle these TN's? In the following, we show that by putting the isometries for truncations

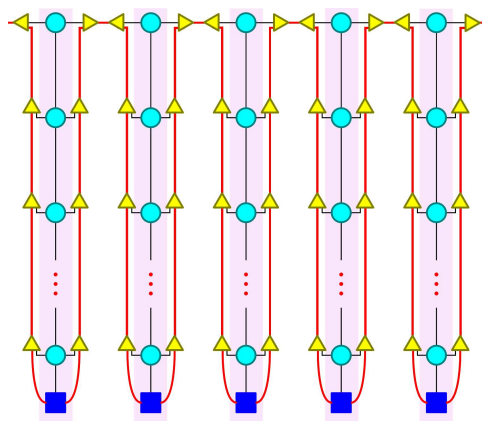


**Figure 23.** (Color online) The exactly contractible TN in the iTEBD algorithm.

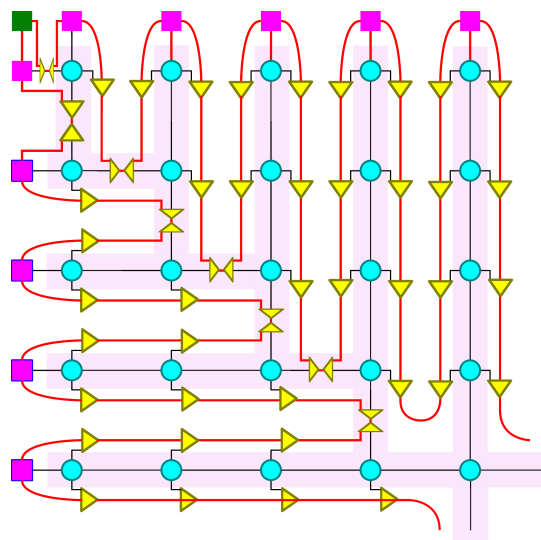
inside, the TN's that are contracted in these algorithms are eventually exactly contractible. Thus, if the algorithm have a high performance, it means that the TN can be accurately approximated by the corresponding exactly contractible TN (ECTN).

Fig. 22 shows the ECTN emerging in the HOTRG algorithm [195]. HOTRG shares a similar spirit to TRG, but with a more explicit RG procedure. For example for contracting a TN on square lattice, in each iteration step, four tensors in a square are contracted together, which leads to a new square TN with larger bond dimensions. Then, a pair of isometries (yellow triangles) are inserted in the TN to truncation the bond dimensions. By leaving these isometries inside the TN, trees appears on the boundaries of the coarse-grained plaques. Inside the smallest 2-by-2 plaques (dark red shadow), we have the tree TN's formed by one isometry. Inside the 4-by-4 plaques (light red shadow), we have the two-layer tree TN's formed by three isometries. In the 8-by-8 plaques, one tree TN has three layers with seven isometries. These tree TN's separate the original TN into different plaques, transforming it into an ECTN that is similar to the fractal TN's introduced in Sec. 3.1.

In the iTEBD algorithm [58, 59, 60, 61] (Fig. 23), one starts with an initial MPS (dark blue squares). In each iteration, one tensor (light blue square) in the TN is contracted in the MPS and then the bonds are truncated by isometries (yellow triangles). Globally seeing, the isometries separate the TN into many “tubes” (red shadow) that are connected only at the top. The length of the tubes are the times of the iterations in the iTEBD. The isomitres form two MPS's in the vertical direction in each of the tubes, which is very important in the TN encoding scheme (see Chap. 4). Obviously, this TN is exactly contractible. Such a tube-like structure also appears in the contraction algorithms based on PEPS.

For the CTMRG algorithm [201], the corresponding ECTN is a little bit complicated (see one quarter of it in Fig. 24). The initial row (column) tensors and the corner transfer matrices are represented by the pink and green squares. In each iteration step, the tensors (light blue squares) located most outside are contracted to the row (column) tensors and the corner transfer matrices, and isometries are introduced to truncate the bond dimensions. Globally seeing the picture, the isometries separate the TN into a tree-like structure (red shadow), thus is exactly contractible.





**Figure 24.** (Color online) A part of the exactly contractible TN in the CTMRG algorithm.

For these three algorithms, each of them gives an ECTN that is formed by two part: the tensors in the original TN and the isometries that make the TN exactly contractible. After optimizing the isometries, the original TN is approximated by the ECTN. The structure of the ECTN and the way of optimizing the isometries depend on the algorithm.

The ECTN picture shows us explicitly how the correlations and entanglement are approximated in different algorithms. In the ECTN, roughly speaking, the correlation properties can be read from the minimal distance of the path that connects two certain sites, and the (bipartite) entanglement can be read from the number of bonds that cross the boundary of the bipartition. How well the structure suits the correlations and entanglement should be a key factor of the performance of a NRG-inspired algorithm. Meanwhile, this picture allows us to develop new NRG-inspired algorithms by designing the ECTN and taking the whole ECTN as the environment for optimizing the isometries. These issues still need further investigations.

The unification of the TN contraction and the ECTN has been explicitly utilized in the so-called TN renormalization (TNR) [337, 338]. In TNR, isometries and unitaries (called *disentangler*) are put into the TN to make it exactly contractible. Then instead of tree TN's or MPS's, one will have MERA's inside which can better capture the entanglement of the critical systems.

### 3.6. Summary of numeric renormalization of tensor network: contraction and truncation

In this chapter, we discuss about NRG-inspired approaches for dealing with TN contractions. Such algorithms consist of two key steps: contractions (that local operations of tensors) and truncations (that are optimized locally or globally). The local contraction determines the way how the TN is contracted step by step, or in other words, how the renormalization is implemented. Different (local or global) contractions may lead to different costs, thus optimizing the contraction sequence is necessary in many cases [339, 340, 341]. The truncation is the approximation to discard less important basis so that the computational

costs are tolerable. One essential concept in the truncations is “environment”, which plays the role of the reference when determining the weights of the basis. Thus, the choice of environment concerns the balance between the accuracy and efficiency of a tensor renormalization algorithm. Finally, we argue that the NRG-inspired algorithms eventually transform the TN’s into those that can be exactly contracted by classical computers.

#### 4. Tensor network approaches with self-consistent eigenvalue problems

As discussed in the previous sections, the central task is to compute the TN contraction, which is normally NP-hard with classical computers. To implement the contraction, it seems to be necessary to choose a contraction order, as the approaches based on numerical renormalization group. Particularly to contract a TN with a regular geometry (such as square lattice), truncations are inevitable. Are there any clues other than such an iterative contraction-and-truncation way? Or, let us ask another question that is more specific: can the TN contraction be transformed to a set of eigenvalue functions that can be efficiently (or even exactly) solved by classical computers? We believe that two “*principles*” should be considered: the function must be as simple as possible; the number of input and variational parameters must be as small as possible.

The utilization of eigenvalue problems and self-consistency in condensed matter and statistic physics has quite a long history. Here, we briefly review three related examples. One is the CTM method proposed by Baxter in 1976 [221, 222] and its generalized versions by Nishino *et al* [19] and Orús [201] (see Sec. 3.5 for mode details). Another example is known as tensor product variational approaches developed by Nishino *et al* [223, 224], where self-consistent equations were built and applied to solve 3D classical models. The third example is the time-dependent variational principle (TDVP). The basic idea of TDVP was proposed by Dirac in 1930 [342], and then was cooperated with the formulation of Hamiltonian [343] and action function [344]. For more details, one could refer to a review by Langhoff *et al* [345]. In 2011, TDVP was developed to simulate the time evolution of many-body systems with the help of MPS [62].

While the methods mentioned above are for specific physical problems, we focus in this chapter on several algorithms that solve general TN contraction problems by self-consistent eigenvalue problems. Different from the NRG-inspired schemes which are implemented by iterative contractions and truncations, the idea of the following methods is to build a set of local self-consistent eigenvalue equations (SSE’s), from which the TN can be automatically contracted/reconstructed. In this way, the TN contraction is approximated by local eigenvalue problems that can be efficiently computed.

Meanwhile, the connections between these TN methods and the algorithms (including Tucker [229], rank-1 [225], and tensor-train [302] decompositions) in multi-linear algebra (MLA) are discussed. MLA (see a review [228]) is a subject of studying the properties of tensors. One of the goals is to find the optimal lower-rank approximations of a given tensor by defining a set of self-consistent equations. To deal with TN’s and understand TN methods,

it is very natural to utilize the techniques in MLA instead of the algebra of matrices. In this section, we will show the underlying relations between the algorithms in MLA and the TN algorithms. Moreover, since we work on TN instead of single tensor, the TN algorithms generalize the methods in MLA.

This section is organized as below, aiming at understanding several TN updating algorithms based on SSE's. In Sec. 4.1, we will define and motivate the main task, which is to find the optimal approximation of a given TN state with lower bond dimensions. In Sec. 4.2, we will start from a simple example with a 1D TN stripe, which can be “contracted” by solving the eigenvalue decomposition of matrix. This leads to several important MPS techniques such as canonicalization [61], which will be discussed in Sec. 4.3. Canonicalization enables to implement optimal truncations of the bond dimensions of MPS's. Then in Sec. 4.4, we will discuss super-orthogonalization [124] that was proposed to implement optimal truncations of PEPS's defined on trees, which is a higher-dimensional generalization of canonicalization. In Sec. 4.5, we will discuss based on the rank-1 decomposition [225], that super-orthogonalization can be used to obtain the “optimal” truncations of the PEPS's of regular geometries (e.g., square or honeycomb lattices) with loopless approximations [122]. This explains how the simple update algorithm for the ground-state simulations on 2D regular lattices [190] works and what cause the errors. In Sec. 4.6, we will discuss tensor ring decomposition (TRD) [123], a rank- $N$  generalization of the rank-1 decomposition. TRD naturally provides a unified description of iDMRG[14, 15, 226], iTEBD[60], and CTMRG [201, 209] when considering the contractions of 2D TN's. Note we have the full update schemes when using these algorithms to obtain optimal truncations of PEPS. In Secs. 4.7 and 4.8, we will give some examples of simulating the ground states of one- and higher-dimensional quantum systems. We will give a unified procedure of the classical/quantum simulations of many-body lattice models.

#### 4.1. Main task: finding the optimal approximation of a tensor network state with lower bond dimensions

In Sec. 3, we explained several NRG-inspired algorithms for contracting a 2D TN. In this section, the main task is to find the optimal low-bond-dimensional approximations of a given TN state, i.e., to optimally truncate the TN state. Such schemes are often called *update schemes*. For 2D TN contractions, we already show in Sec. 3.3 that optimally truncating an MPS is required in the iTEBD algorithms.

Let us consider the 3D TN contractions (including 2D quantum simulations) by taking a TN defined on a cubic lattice as an example. Such a TN can be considered as  $K$  layers of TPO, as shown in Fig 14 (b). For simplicity, we assume that the TN is formed by the copies of one inequivalent tensor denoted by  $\tilde{T}$ . A typical strategy for contraction is to contract the TN layer by layer to a 2D PEPS as

$$P_{s,a'_1 a'_2 a'_3 a'_4} = \sum_{s'} \tilde{T}_{ss',\alpha_1 \alpha_2 \alpha_3 \alpha_4} P_{s',a_1 a_2 a_3 a_4}, \quad (103)$$

with  $P$  the tensor in the PEPS and  $a'_n = (\alpha_n, a_n)$ . One can see that during the contraction, the

bond dimensions of  $P$  will increase exponentially (similar to what happened in iTEBD), and it is necessary to implement the optimal truncations of the bond dimensions of the PEPS.

The error to be minimized is the distance  $\varepsilon = (|\Psi\rangle - |\Psi'\rangle)^2$  with  $|\Psi\rangle$  and  $|\Psi'\rangle$  the PEPS before and after the truncation. Since the PEPS is normalized, this is equivalent to the maximization of  $Z = \langle \Psi | \Psi' \rangle$ , which is actually a 2D square TN formed by the copies of  $T_{\tilde{a}_1 \tilde{a}_2 \tilde{a}_3 \tilde{a}_4} = \sum_s P_{s, a'_1 a'_2 a'_3 a'_4} P_{s, a_1 a_2 a_3 a_4}$  with  $\tilde{a}'_n = (a_n, a'_n)$ . The problem becomes again the optimal contraction of the 2D TN.

Different update schemes are proposed to determine the truncations of the PEPS. These update schemes are categorized, according to the environment of the truncations, as the *simple* [190, 124], *cluster* [135, 210, 211, 206], and *full* [204, 201, 205, 179, 195, 206, 207, 208] update schemes of PEPS. In the full update scheme, the whole TN is contracted (approximately by TRG, iTEBD, CTMRG, etc.) to obtain the optimal truncation, which is accurate but extremely consuming. In the simple and cluster update schemes, certain approximations are made to avoid implementing the TN contraction. In the following, we will explain how SEE's are built in order to find the optimal truncations of the PEPS. This will also provide an alternative and systematic understanding of the NRG-based algorithms.

#### 4.2. A simplest example of solving tensor network contraction by eigenvalue decomposition

Let us begin with a trivial example by simply considering the trace of the product of  $N$  number of  $(\chi \times \chi)$  matrices  $M$  as

$$\text{Tr}\mathcal{M} = \text{Tr}(M^{[1]}M^{[2]} \dots M^{[N]}) = \text{Tr} \prod_{n=1}^N M^{[n]}, \quad (104)$$

with  $M^{[n]} = M$ . In the language of TN, this can be regarded as a 1D TN with periodic boundary condition. For simplicity, we assume that the dominant eigenstate of  $M$  is unique.

Allow us to firstly use a clumsy way to do the calculation: contract the shared bonds one by one from left to right. For each contraction, the computational cost is  $O(\chi^3)$ , thus the total cost is  $O(N\chi^3)$ .

Now let us be smarter by using the eigenvalue decomposition (assume it exists for  $M$ ) in the linear algebra, which reads

$$M = U\Lambda U^\dagger, \quad (105)$$

where  $\Lambda$  are diagonal and  $U$  is unitary satisfying  $UU^\dagger = U^\dagger U = I$ . Substituting Eq. (105) into Eq. (104), we can readily have the contraction as

$$\text{Tr}\mathcal{M} = \text{Tr}(U\Lambda U^\dagger U\Lambda U^\dagger \dots U\Lambda U^\dagger) = \text{Tr}(U\Lambda^N U^\dagger) = \sum_{a=0}^{\chi-1} \Lambda_a^N. \quad (106)$$

The computational cost is around  $O(\chi^3 + \chi)$ .

In the limit of  $N \rightarrow \infty$ , things become even easier, where we have

$$\text{Tr}\mathcal{M} = \lim_{N \rightarrow \infty} \Lambda_0^N \sum_{a=0}^{\chi-1} \left(\frac{\Lambda_a}{\Lambda_0}\right)^N = \Lambda_0^N, \quad (107)$$

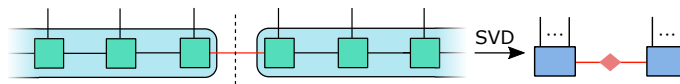


**Figure 25.** (Color online) An impractical scheme to get the global optimal truncation of the virtual bond (red). First, the MPS is cut into two parts. All the indexes on each side of the cut are grouped into one big index. Then by contracting the virtual bond and doing the SVD, the virtual bond dimension is optimally reduced to  $\chi$  by only taking the  $\chi$ -largest singular values and the corresponding vectors.

where  $\Lambda_0$  is the largest eigenvalue, and we have  $\lim_{N \rightarrow \infty} (\frac{\Lambda_a}{\Lambda_0})^N = 0$  for  $a > 0$ . It means all the contributions except for the dominant eigenvalue vanish when the TN is infinitely long. What we should do is just to compute the dominant eigenvalue. The efficiency can be further improved by many mature techniques (such as Lanczos algorithm).

Even though the example is quite trivial, we still can get some useful information by comparing these two approaches from the aspect of solving TN contraction problems. The first one is a standard TN contraction approach, where a contraction order is specified. Taking the TEBD algorithm as an example, it starts from an initial MPS, and for each time one contracts an MPO formed by one row of tensors into the MPS. In this sense, TEBD is analog to the first approach mentioned above, except for that the matrix is the MPO that possesses an exponentially huge dimension. Then, a question rises here: is there an algorithm for contracting TN that is analog to the second approach with eigenvalue decomposition?

### 4.3. Canonicalization of matrix product state

The utilizations of canonicalization are mainly in two aspects: locating optimal truncations of the MPS, and fixing the gauge degrees of freedom of the MPS for better stability and efficiency.

**4.3.1. Canonical form and globally optimal truncations of MPS** Before considering a 2D TN, let us take some more advantages of the eigenvalue decomposition on the 1D TN's, which is closely related to the *canonicalization* of MPS proposed by Orús and Vidal for non-unitary evolution of MPS [61].

As discussed in the above chapter, when using iTEBD to contract a TN, one needs to find the optimal truncations of the virtual bonds of the MPS. In other words, the problem is how to optimally reduce the dimension of an MPS.

To this end, let us divide the MPS into two parts by cutting the bond that is to be truncated (Fig. 25). Then, if we contract all the virtual bonds on the left hand side and reshape all the physical indexes there into one index, we will obtain a large matrix denoted as  $L_{\dots s_n, \alpha_n}$  that has one big physical and one virtual index. Another matrix denoted as  $R_{s_{n+1} \dots, \alpha_n}^*$  can be obtained by doing the same thing on the right hand side. The conjugate of  $R$  is taken there to obey some conventions.

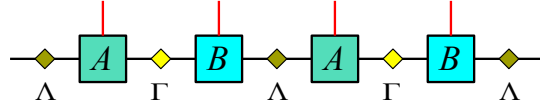


**Figure 26.** (Color online) The MPS with two-site translational invariance.

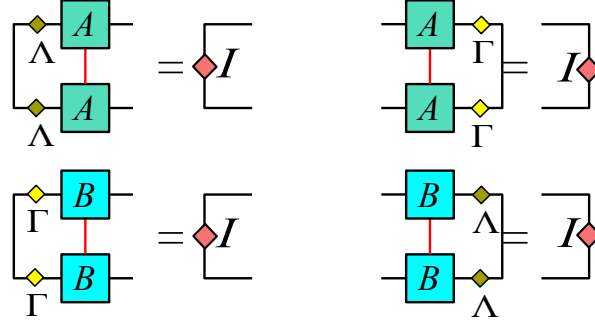


**Figure 27.** (Color online) Four canonical conditions of an MPS.

Then, by contracting the virtual bond and doing SVD as

$$\sum_{a_n} L^{\dots s_n, a_n} R_{s_{n+1}^{\dots}, a_n}^* = \sum_{a'_n} \tilde{L}^{\dots s_n, a'_n} \lambda_{a'_n} \tilde{R}_{s_{n+1}^{\dots}, a'_n}^*, \quad (108)$$

the virtual bond dimension is optimally reduced to  $\chi$  by only taking the  $\chi$ -largest singular values and the corresponding vectors. The truncation error that is minimized is the distance between the MPS before and after the truncation, thus the truncation is optimal globally concerning the whole MPS.

In practice, we do not implement the SVD above. It is actually the decomposition of the whole wave function, which is exponentially expensive. Canonicalization provides an efficient way to realize the SVD through only local operations (conditions).

Considering an infinite MPS has two-site translational invariance (Fig. 26), and is formed by the tensors  $A$  and  $B$  as well as the diagonal matrices  $\Lambda$  and  $\Gamma$  as

$$\sum_{\{a\}} \dots \Lambda_{a_{n-1}} A_{s_{n-1}, a_{n-1} a_n} \Gamma_{a_n} B_{s_n, a_n a_{n+1}} \Lambda_{a_{n+1}} \dots = \text{tTr}(\dots \Lambda \Gamma B \Lambda \dots) \quad (109)$$

This is the MPS used in the iTEBD algorithm (see Chap.3.3 and Fig.19). Note that all argument can be readily generalized to the infinite MPS's with  $n$ -site translational invariance, or even to the finite MPS's.

An MPS is in the *canonical form* if all tensors satisfy

$$\sum_{sa} \Lambda_a A_{s, aa'} \Lambda_a^* A_{s, aa''}^* = I_{a'a''}, \quad (110)$$

$$\sum_{sa} A_{s, a'a} \Gamma_a A_{s, a''a}^* \Gamma_a^* = I_{a'a''}, \quad (111)$$

$$\sum_{sa} \Gamma_a B_{s, aa'} \Gamma_a^* B_{s, aa''}^* = I_{a'a''}, \quad (112)$$

$$\sum_{sa} B_{s, a'a} \Lambda_a B_{s, a''a}^* \Lambda_a^* = I_{a'a''}, \quad (113)$$

with  $\Lambda$  and  $\Gamma$  positive-defined vectors (Fig. 27). Eqs. (110) - (113) are called the *canonical conditions* of the MPS. Note there will be  $2n$  equations with  $n$ -site translational invariance, meaning that each inequivalent tensor will obey to two (left and right) conditions.

In the canonical form,  $\Lambda$  or  $\Gamma$  directly give the singular values by cutting the MPS on the corresponding bond. To see this, let us calculate Eq. (108) from a canonical MPS. From the canonical conditions, matrices  $L$  and  $R$  are unitary, satisfying  $L^\dagger L = I$  and  $R^\dagger R = I$  (the physical indexes are contracted). Meanwhile,  $\Lambda$  (or  $\Gamma$ ) is positive-defined, thus  $L$ ,  $\Lambda$  (or  $\Gamma$ ) and  $R$  of a canonical MPS directly define the SVD, and  $\Lambda$  or  $\Gamma$  is indeed the singular value spectrum. Then the optimal truncations of the virtual bonds are reached by simply keeping  $\chi$ -largest values of  $\Lambda$  and the corresponding basis of the neighboring tensors. This is true when cutting any one of the bonds of the MPS.

There are two important issues we shall stress. For a state, its MPS representation is not unique. A simple operation for instance is to contract each  $\Lambda$  to the tensor on its right side, then we will have a new MPS that reads

$$\sum_{\{a\}} \cdots A'_{s_{n-1}, a_{n-1} a_n} B'_{s_n, a_n a_{n+1}} \cdots = \text{tTr}(\cdots A' B' \cdots), \quad (114)$$

with  $A'_{s, aa'} = \Lambda_a A_{s, aa'}$  and  $B'_{s, aa'} = \Gamma_a B_{s, aa'}$ . Since we do not actually make any changes but to contract certain bonds, this MPS with the new tensors  $A'$  and  $B'$  still gives the exactly same state. Another example is to insert a (full-rank) matrix  $U$  and its inverse  $U^{-1}$  on any of the virtual bonds and then contracted them, respectively, into the two neighboring tensors. The tensors are changed but the state given by the MPS does not, since we actually insert an identity. This is called the *gauge degrees of freedom* of the MPS. The transformations such as  $U$  and  $U^{-1}$  are called *gauge transformations*.

From the uniqueness of SVD, Eqs. (110) and (111) leads to a unique MPS representation \*, thus such a form is called “*canonical*”. In other words, the canonicalization fixes the gauge degrees of freedom of the MPS.

The second issue concerns the orthogonality of  $L$  or  $R$ . For an infinite MPS, since the dimension of the first index of  $L$  or  $R$  is infinite, we should define the orthogonality more carefully. To this end, let us define the left and right *transfer matrices*  $M^L$  of  $A$  as

$$M^L_{a_1 a'_1 a_2 a'_2} = \sum_s \Lambda_{a_1} A_{s, a_1 a_2} \Lambda_{a'_1}^* A_{s, a'_1 a'_2}^*, \quad (115)$$

$$M^R_{a_1 a'_1 a_2 a'_2} = \sum_s A_{s, a_1 a_2} \Gamma_{a_1} A_{s, a'_1 a'_2}^* \Gamma_{a'_1}^*. \quad (116)$$

Then the first canonical condition [Eq. (110)] says that the identity is the left (right) eigenvector of  $M^L$  ( $M^R$ ), satisfying

$$\sum_{a_1 a'_1} I_{a_1 a'_1} M^L_{a_1 a'_1 a_2 a'_2} = \lambda^L I_{a_2 a'_2}, \quad (117)$$

$$\sum_{a_1 a'_1} I_{a_2 a'_2} M^R_{a_1 a'_1 a_2 a'_2} = \lambda^R I_{a_1 a'_1}, \quad (118)$$

\*For any finite MPS, the uniqueness is robust. For an infinite MPS, there will be some additional complexity. This will be soon discussed below from the aspect of eigenvalue solutions.





as

$$A_{s_1, a_1 a_2} \leftarrow \sum_a A_{s_1, a_1 a} \mathcal{U}_{a a_2}, \quad (123)$$

$$B_{s_1, a_1 a_2} \leftarrow \sum_a B_{s_1, a a_2} \mathcal{V}_{a_1 a}. \quad (124)$$

Implement the same steps given above on the virtual bonds between  $B$  and  $A$ , then the MPS is transformed to the canonical form.

There are two important issues. Firstly, the canonical conditions do not require the “identity” eigenvector to be dominant. However, if the identity is not the leading one, the canonical conditions will become unstable under an arbitrarily small noise. The canonicalization algorithm given above assures that the identity is the leading eigenvector, since it transforms the leading eigenvector to an identity. Secondly, if the dominant eigenvector of  $M^L$  and  $M^R$  is degenerate, the canonical form will not be unique. See Ref.[61] for more details.

**Variants of the canonical form.** From the canonical form of an MPS, one can define the *left or right canonical forms* as

$$\text{tTr}(\dots A^L B^L A^M B^R A^R \dots). \quad (125)$$

This MPS is obtained by implementing the gauge transformations as

$$A_{s, aa'}^L = \Lambda_a A_{s, aa'}, \quad (126)$$

$$A_{s, aa'}^R = A_{s, aa'} \Gamma_{a'}, \quad (127)$$

$$B_{s, aa'}^L = \Gamma_a B_{s, aa'}, \quad (128)$$

$$B_{s, aa'}^R = B_{s, aa'} \Lambda_{a'}, \quad (129)$$

$$A_{s, aa'}^M = \Lambda_a A_{s, aa'} \Gamma_{a'}. \quad (130)$$

Compared with the canonical conditions, the first four tensors are actually non-square orthogonal matrices (e.g.,  $\sum_{sa} A_{s, aa'}^L A_{s, aa''}^{L*} = I_{a'a''}$ ), thus are called *isometries*. The last tensor is called the *central tensor* of the MPS.

This MPS form was proposed as the state ansatz behind the *density matrix renormalization group* (DMRG) algorithm [14, 15], and is very useful in TN-based methods (see for example the works of McCulloch [32, 226]). For instance, when applying DMRG to solve 1D quantum model, the tensors  $A^L$  and  $B^L$  define a left-to-right RG flow that optimally compresses the Hilbert space of the left part of the chain.  $A^R$  and  $B^R$  define a right-to-left RG flow similarly. The central tensor is between these two RG flows. Note that the canonical MPS is also called the *central canonical form*, where the directions of the RG flows can be switched arbitrarily by gauge transformations, thus there is no need to define a specific center.

**Relations to tensor train decomposition.** It is worth mentioning the *tensor-train decomposition* (TTD) [302] proposed in the field of MLA. As argued in Chap. 2, one advantage of MPS is it lowers the number of parameters from an exponential size dependence to a polynomial one. Let us consider a similar problem: for a  $N$ -th order tensor that has  $d^N$  parameters, how to find its optimal MPS representation, where there are only  $[2d\chi + (N - 2)d\chi^2]$  parameters? TTD was proposed for this aim, and it borrows many

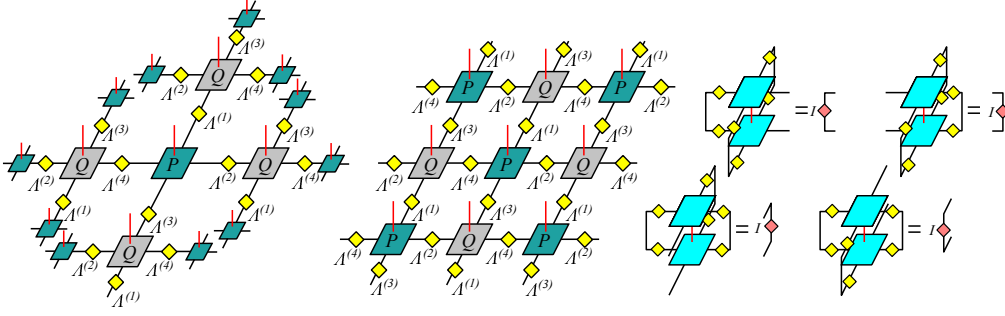


**Figure 29.** (Color online) The first two figures show the iPEPS on tree and square lattices, with two-site translational invariance. The last one shows the super-orthogonal conditions.

ideas from MPS and the related algorithms (especially DMRG which was proposed about two decades earlier). The aim of TTD is similar to that of the truncations in the TN algorithms, which is to compress the number of parameters. By decomposing a tensor into a tensor-train form that is similar to a finite open MPS, the number of parameters becomes linearly relating to the order of the original tensor.

#### 4.4. Super-orthogonalization and Tucker decomposition

Similar to canonicalization, the utilizations of super-orthogonalization are mainly in two aspects: locating optimal truncations of the PEPS, and fixing the gauge degrees of freedom of the PEPS for better stability and efficiency. In the following, we will concentrate on the first aspect.

**4.4.1. Super-orthogonalization** As discussed in the above section, the canonical form of an MPS brings a lot of advantages, such as determining the entanglement and the optimal truncations of the virtual bond dimensions by local transformations. Can we also define the canonical form for the TN state in higher dimensions, such as the PEPS defined on an infinite square lattice (Fig. 29)? If this can be done, we would know how to find the globally optimal transformations that reduces the bond dimensions of the TN, just like what we can do with an MPS. Due to the complexity of tensors, unfortunately, there is no such a form in general.

In the following, we explain the *super-orthogonal form* of iPEPS proposed in 2012 [124], which provides a compromised way for canonicalization in higher dimensions. Let us take the PEPS on the (infinite) Bethe lattice with the coordination number  $z = 4$  as an example. It is formed by two tensors  $P$  and  $Q$  on the sites as well as four spectrums  $\Lambda^{(k)}$  ( $k = 1, 2, 3, 4$ ) on the bonds, as illustrated in Fig. 29. Here, we still take the two-site translational invariance for simplicity.

There are eight *super-orthogonal conditions*, four of which associate to the tensor  $P$  and four to  $Q$ . For  $P$ , the conditions are

$$\sum_s \sum_{\dots a_{k-1} a_{k+1} \dots} P_{s, \dots a_k \dots} P_{s, \dots a'_k \dots}^* \prod_{n \neq k} \Lambda_{a_n}^{(n)} \Lambda_{a_n}^{(n)*} = I_{a_k a'_k}, \quad (\forall k), \quad (131)$$

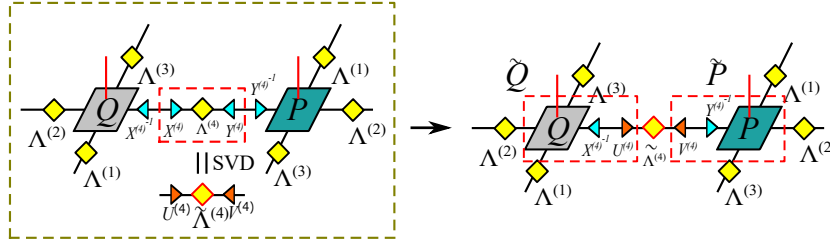


**Figure 30.** (Color online) The illustrations of gauge transformations in the super-orthogonalization algorithm.

where all the bonds along with the corresponding spectrums are contracted except for  $a_k$ . It means that by putting  $a_k$  as one index and all the rest as another, the  $k$ -rectangular matrix  $S^{(k)}$  defined as

$$S_{s \dots a_{k-1} a_{k+1} \dots, a_k}^{(k)} = P_{s, \dots, a_k} \prod_{n \neq k} \Lambda_{a_n}^{(n)}, \quad (132)$$

is an isometry, satisfying  $S^{(k)\dagger} S^{(k)} = I$ . The super-orthogonal conditions of the tensor  $Q$  are defined in the same way.  $\Lambda^{(k)}$  is dubbed *super-orthogonal spectrum* when Eq. (131) is fulfilled.

In canonicalization of MPS, the vectors on the virtual bonds give the bipartite entanglement defined by Eq. (108). Meanwhile, the bond dimensions can be optimally reduced by discarding certain smallest Schmidt numbers. In super-orthogonalization, this is not always true any more for iPEPS's. For example, given a translational invariant iPEPS defined on a tree (or called Bethe lattice, see Fig. 29 (a)) [131, 132, 133, 134, 135, 136, 137, 138], the super-orthogonal spectrum gives the bipartite entanglement spectrum by cutting the system at the corresponding place. However, when considering loopy lattices, such as the iPEPS defined on a square lattice (Fig. 29 (b)), this will no longer be true. Instead, the super-orthogonal spectrum provides an approximation of the entanglement of the iPEPS by optimally ignoring the loops. One can still truncate the bond dimensions according to the super-orthogonal spectrum, which is called simple update. We will discuss the approximation in detail in Sec. 4.4.

Besides, super-orthogonalization can be used to fix the gauge degrees of freedom of PEPS's. Similar to MPS (see the last second part of Sec. 4.2), one can be able to change the tensors of the PEPS without changing the state it represents. One way is to insert an arbitrary invertible matrix and its inverse on a virtual bond, and contract them to the adjacent tensors, respectively.

Fixing the gauge degrees of freedom will improve the stability and efficiency of the PEPS simulations. It is worth mentioning here that there are several works heading towards this direction, which were applied to solving different physical problems [124, 206, 346, 207]. In 2012, super-orthogonalization was proposed and used to optimally simulate the finite-temperature density operator for simulating the thermodynamics of infinite-size 2D quantum systems [124]. In 2014, gauge fixing of finite-size PEPS was proposed [206]. In 2015, the self-consistent equations (Eq. (131)) are applied to fix the gauge degrees of freedom of iPEPS

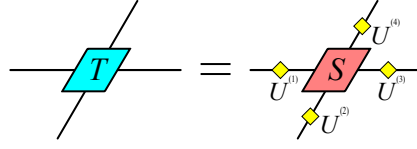


**Figure 31.** (Color online) The illustrations of Tucker decomposition [Eq. (137)].

for simulating the ground states of 2D systems, where the environment can be recycled in the simulation and better efficiency and stability can be achieved [346]. In the same year, the gauge fixing was proposed to improve the efficiency and stability of full update algorithms [207].

**4.4.2. Super-orthogonalization algorithm** Any PEPS can be transformed to the super-orthogonal form by iteratively implementing proper gauge transformations on the virtual bonds [124]. Firstly, compute the reduced matrix  $\mathcal{M}^{(k)}$  of the  $k$ -rectangular matrix of the tensor  $P$  [Eq. (132)] as

$$\mathcal{M}_{a_k a'_k}^{(k)} = \sum_s \sum_{\dots a_{k-1} a_{k+1} \dots} S_{s \dots a_{k-1} a_{k+1} \dots, a_k}^{(k)} S_{s \dots a_{k-1} a_{k+1} \dots, a'_k}^{(k)*}. \quad (133)$$

Compared with the super-orthogonal conditions in Eq. (131), one can see that  $\mathcal{M}^{(k)} = I$  when the PEPS is super-orthogonal. Similarly, we define the reduced matrix  $\mathcal{N}^{(k)}$  of the tensor  $Q$ .

When the PEPS is not super-orthogonal,  $\mathcal{M}^{(k)}$  and  $\mathcal{N}^{(k)}$  are Hermitian matrices. Decompose them as  $\mathcal{M}^{(k)} = X^{(k)} X^{(k)\dagger}$  and  $\mathcal{N}^{(k)} = Y^{(k)} Y^{(k)\dagger}$ . Then, insert the identities  $X^{(k)} [X^{(k)}]^{-1}$  and  $Y^{(k)} [Y^{(k)}]^{-1}$  on the virtual bonds to perform gauge transformations along four directions as shown in Fig. 30. Then, we can use SVD to renew the four spectrums by  $X^{(k)} \Lambda^{(k)} Y^{(k)T} = U^{(k)} \tilde{\Lambda}^{(k)} V^{(k)\dagger}$ . Meanwhile, we transform the tensors as

$$P_{s, \dots, a_k \dots} \leftarrow \sum_{a'_k a''_k} P_{s, \dots, a'_k \dots} [X^{(k)}]_{a'_k a''_k}^{-1} U_{a''_k a_k}^{(k)}, \quad (134)$$

$$Q_{s, \dots, a_k \dots} \leftarrow \sum_{a'_k a''_k} Q_{s, \dots, a'_k \dots} [Y^{(k)}]_{a'_k a''_k}^{-1} V_{a''_k a_k}^{(k)*}. \quad (135)$$

Compared with the canonicalization algorithm of MPS, one can see that the gauge transformations in the super-orthogonalization algorithm are quite similar. What is different is that one cannot transform a PEPS into the super-orthogonal form by a single step, since the transformation on one bond might cause some deviation from obeying the super-orthogonal conditions on other bonds. Thus, the above procedure should be iterated until all the tensors and spectrums converge.

**4.4.3. Relations to Tucker decomposition** Such an iterative scheme is closely related to the Tucker decomposition in MLA [229]. Tucker decomposition is considered as a generalization of (matrix) SVD to higher-order tensors, thus it is also called higher-order or multi-linear SVD. The aim is to find the optimal reductions of the bond dimensions for a single tensor.

Let us define the  $k$ -reduced matrix of a tensor  $T$  as

$$M_{a_k a'_k}^{(k)} = \sum_{a_1 \cdots a_{k-1} a_{k+1} \cdots} T_{a_1 \cdots a_{k-1} a_k a_{k+1} \cdots} T_{a_1 \cdots a_{k-1} a'_k a_{k+1} \cdots}^*, \quad (136)$$

where all except the  $k$ -th index are contracted. The Tucker decomposition (Fig. 31) of a tensor  $T$  has the form as

$$T_{a_1 a_2 \cdots} = \sum_{a_1 a_2 \cdots} S_{b_1 b_2 \cdots} \prod_k U_{a_k b_k}^{(k)}, \quad (137)$$

where the following properties should be satisfied:

- *Unitary.*  $U^{(k)}$  are unitary matrices satisfying  $U^{(k)} U^{(k)\dagger} = I$ .
- *All-orthogonality.* For any  $k$ , the  $k$ -reduced matrix  $M^{(k)}$  of the tensor  $S$  is diagonal, satisfying

$$M_{a_k a'_k}^{(k)} = \Gamma_{a_k}^{(k)} I_{a_k a'_k}. \quad (138)$$

- *Ordering.* For any  $k$ , the elements of  $\Gamma^{(k)}$  in the  $k$ -reduced matrix are positive-defined and in the descending order, satisfying  $\Gamma_0 > \Gamma_1 > \cdots$ .

From these properties, one can see that the tensor  $T$  is decomposed to the product of another tensor  $S$  with several unitary matrices on its bonds.  $S$  is called the *core tensor*. In other words, the optimal lower-rank approximation of the tensor can be simply obtained by

$$T_{a_1 a_2 \cdots} \simeq \sum_{a_1 a_2 \cdots = 0}^{\chi-1} S_{b_1 b_2 \cdots} \prod_k U_{a_k b_k}^{(k)}, \quad (139)$$

where we only take the first  $\chi$  terms in each summation of the indexes.

Such an approximations can be understood in terms of SVD of matrices. Applying the properties to the  $k$ -reduced matrix of  $T$ , we have

$$M_{a_k a'_k}^{(k)} = \sum_{b_k} U_{a_k b_k}^{(k)} \Gamma_{b_k}^{(k)} U_{a'_k b_k}^{(k)\dagger}. \quad (140)$$

Since  $U^{(k)}$  is unitary and  $\Gamma^{(k)}$  is positive-defined and in the descending order, the above equation is exactly the eigenvalue decomposition of  $M^{(k)}$ . From the relation between the SVD of a matrix and the eigenvalue decomposition of its reduced matrix, we can see that  $U^{(k)}$  and  $\Gamma^{(k)}$  in fact give the SVD of the matrix  $T_{a_1 \cdots a_{k-1} a_{k+1} \cdots, a_k}$  as

$$T_{a_1 \cdots a_{k-1} a_{k+1} \cdots, a_k} = \sum_{b_k} \mathcal{S}_{a_1 \cdots a_{k-1} a_{k+1} \cdots, b_k} \sqrt{\Gamma_{b_k}^{(k)}} U_{a_k b_k}^{(k)}. \quad (141)$$

Then, The optimal truncation of the rank of each index is reached by the corresponding SVD. The truncation error is obviously the distance defined as

$$\varepsilon^{(k)} = |T_{a_1 \cdots a_{k-1} a_{k+1} \cdots, a_k} - \sum_{b_k=1}^{\chi} \mathcal{S}_{a_1 \cdots a_{k-1} a_{k+1} \cdots, b_k} \Gamma_{b_k}^{(k)} U_{a_k b_k}^{(k)}|, \quad (142)$$

which is minimized in this SVD.

For the algorithms of Tucker decomposition, one simple way is to do the SVD of the matrix obtained by grouping the indexes correspondingly. Then for a  $K$ -th ordered tensor,  $K$

SVD's will give us the Tucker decomposition and a lower-rank approximation. This algorithm is often called *higher-order SVD* (HOSVD). However, this is not the most accurate way. Since the truncation on one index will definitely affect the truncations on other indexes, there will be some “interactions” among different indexes (modes) of the tensor. The truncations in HOSVD are calculated independently, thus such “interactions” are ignored. One way to improve the accuracy is the so-called *high-order orthogonal iteration* (HOOI), where the interactions among different modes are considered by iteratively doing SVD's until reaching the convergence. See more details in Ref. [229].

With the knowledge of Tucker decomposition, let us redefine the super-orthogonal form of a PEPS. From the super-orthogonal conditions, it can be seen that if a PEPS is super-orthogonal, we have

- *Super-orthogonality.* For any  $k$ , the reduced matrix of the  $k$ -rectangular matrix  $\mathcal{M}^{(k)}$  [Eq. (133)] is diagonal, satisfying

$$\mathcal{M}_{a_k a'_k}^{(k)} = \Gamma_{a_k}^{(k)} I_{a_k a'_k}. \quad (143)$$

- *Ordering.* For any  $k$ , the elements of  $\Gamma^{(k)}$  are positive-defined and in the descending order, satisfying  $\Gamma_0 > \Gamma_1 > \dots$ .

Note that the property “unitary” (first one in Tucker decomposition) is hidden in the fact that we use gauge transformations to transform the PEPS into the super-orthogonal form. Thus the super-orthogonalization is also called *network Tucker decomposition* (NTD).

In Tucker decomposition, the “all-orthogonality” and “ordering” lead to an SVD associated to a single tensor, which explains how the optimal truncations work from the decompositions in linear algebra. In the following, we will show that in the NTD, the SVD picture is generalized from a single tensor to a non-local (in fact, infinite) PEPS. Thus, the truncations are optimized in a non-local way.

Let us arbitrarily choose one virtual bond (say  $a$ ) of the PEPS. If the PEPS is on a tree, we can cut the bond and separate the TN into three disconnecting parts: the spectrum ( $\Lambda$ ) on this bond and two tree branches stretching on the two sides of the bond. Specifically speaking, each branch contains one virtual bond and all the physical bonds on the corresponding side, formally denoted as  $\Psi_{i_1 i_2 \dots, a}^L$  (and  $\Psi_{j_1 j_2 \dots, a}^R$  on the other side). Then the PEPS can be written as

$$\sum_a \Psi_{i_1 i_2 \dots, a}^L \Lambda_a \Psi_{j_1 j_2 \dots, a}^R. \quad (144)$$

To get the SVD picture, we need to prove that  $\Psi^L$  and  $\Psi^R$  in the above equation are isometries, satisfying the orthogonal conditions as

$$\begin{aligned} \sum_{i_1 i_2 \dots} \Psi_{i_1 i_2 \dots, a}^L \Psi_{i_1 i_2 \dots, a'}^L &= I_{aa'}, \\ \sum_{j_1 j_2 \dots} \Psi_{j_1 j_2 \dots, a}^R \Psi_{j_1 j_2 \dots, a'}^R &= I_{aa'}. \end{aligned} \quad (145)$$

Note that the spectrum  $\Lambda$  is positive-defined according to the algorithm (though this property is not included as one of the super-orthogonal conditions). To this end, we construct the

TN of  $\sum_{i_1 i_2 \dots} \Psi_{i_1 i_2 \dots, a}^{L(R)} \Psi_{i_1 i_2 \dots, a'}$  from its boundary. If the PEPS is super-orthogonal, the spectrums must be on the boundary of the TN because the super-orthogonal conditions are satisfied everywhere. Then the contractions of the tensors on the boundary of the TN are given exactly by Eq. (131), which gives identities. Then we have on the new boundary again the spectrums to iterate the contractions. All tensors can be contracted by iteratively using the super-orthogonal conditions, which in the end gives identities as Eq. (145). Thus, Eq. (144) indeed gives the SVD of the whole wavefunction. The truncations of the bond dimensions is globally optimized by taking the whole tree PEPS as the environment.

If the PEPS is infinite, we still assume that it has the spectrums on the “boundary” so that we can start the “contractions”. Note that we in fact neither have a well-defined boundary for infinite trees, nor need to actually do the contractions to prove Eq. (145). The deduction above still stands. Even if we do not put the spectrums, saying we put any matrices (full rank to avoid trivial fixed point), the results of the contractions will rapidly converge to identities, then the situation becomes equivalent to that where we put the spectrums on the boundary.

#### 4.5. Tree tensor network approximation on regular lattices and rank-1 decomposition

4.5.1. *Super-orthogonalization works well for truncating gapped PEPS: an intuitive discussion* From the discussions above, we can see that the “canonical” form of a TN state is strongly desired, because it is expected to give the entanglement and the optimal truncations of the bond dimensions. Recall that to contract a TN that cannot be contracted exactly, truncations are inevitable, and locating the optimal truncations is one of the main tasks in the computations. The super-orthogonal form provides a robust way to optimally truncate the bond dimensions of the PEPS defined on a tree.

Interestingly, the super-orthogonal form does not require the tree structure. For a PEPS defined on a regular lattice, for example the square lattice, one can still super-orthogonalize it using the same algorithm. What is different is that the SVD picture of the wave function (generally, see Eq. (108)) is gone, as well as the robustness of the optimal truncations. In other words, the super-orthogonal spectrum does not exactly give the entanglement. A question rises: can we still truncate iPEPS defined on a square lattice according to the super-orthogonal spectrum?

Surprisingly, numeric simulations show that the accuracy by truncating according to the super-orthogonal spectrum is still good in many cases. Let us take the ground-state simulation of a 2D system by imaginary-time evolution as an example. As discussed in Sec. 2.5.3, the simulation becomes the contraction of a 3D TN. One usual way to compute this contraction is to contract layer by layer to a PEPS (see, e.g., [204, 190]). The contraction will enlarge the virtual bond dimensions, and truncations are needed. When the ground state is gapped (see, e.g., [190, 124]), the truncations produce accurate results, which means the super-orthogonal spectrum approximates the true entanglement quite well.

The algorithms where the truncations are optimized by the super-orthogonal spectrum are often called *simple update* scheme [190, 124]. Note that in the original proposal [190], the super-orthogonalization was not used explicitly. Instead, the PEPS is gradually mapped

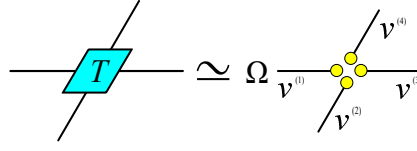


**Figure 32.** (Color online) The illustrations of rank-1 decomposition [Eq. (146)].

to the super-orthogonal form by the near-identical transformation  $e^{-\tau\hat{H}}$  with  $\tau \rightarrow 0$  and the truncations by the SVD's on local tensors.

The success of the simple update suggests that the optimal truncation method on trees still works well for regular lattices. Intuitively, this can be understood in the following way. Comparing a regular lattice with a tree, if it has the same coordination number, the two lattices look exactly the same if we only inspect locally on one site and its nearest neighbors. The difference appears when one goes round the closed loops on the regular lattice, since there are no loop in the tree. Thus, the error when we apply the optimal truncation schemes (such as super-orthogonalization) of a tree to a regular lattice should be characterized by some non-local features. This explains in a descriptive way why the simple update works well for gapped states, where the physics is dominated by short-range correlations. For the systems that possess small gaps or are gapless, simple update is not sufficiently accurate to determine physical properties such as the ground-state energy or gap. For example for calculating ground state, the variational energy can be reduced by improving the computation from simple update to cluster update [126].

*4.5.2. Rank-1 decomposition and the algorithm Rank-1 decomposition in MLA [225]* provides a more mathematic and rigorous way to understand the approximation when using simple update to truncate PEPS on regular lattices [122]. For a tensor  $T$ , its rank-1 decomposition (Fig. 32) is defined as

$$T_{a_1 a_2 \dots a_K} \simeq \Omega \prod_{k=1}^K v_{a_k}^{(k)}, \quad (146)$$

where  $v^{(k)}$  are normalized vectors and  $\Omega$  is a constant that satisfies

$$\Omega = \sum_{a_1 a_2 \dots a_K} T_{a_1 a_2 \dots a_K} \prod_{k=1}^K v_{a_k}^{(k)*}. \quad (147)$$

Rank-1 decomposition provides an approximation of  $T$ , where the distance between the rank-1 tensor and  $T$  is minimized, i.e.,

$$\min_{|v_{a_k}^{(k)}|=1} |T_{a_1 a_2 \dots a_K} - \Omega \prod_{k=1}^K v_{a_k}^{(k)}|. \quad (148)$$

The rank-1 decomposition gives the fixed point of a set of self-consistent equations (Fig. 33), which are

$$\sum_{\text{all except } a_k} T_{a_1 a_2 \dots a_K} \prod_{j \neq k} v_{a_j}^{(j)} = \Omega v_{a_k}^{(k)} \quad (\forall k). \quad (149)$$



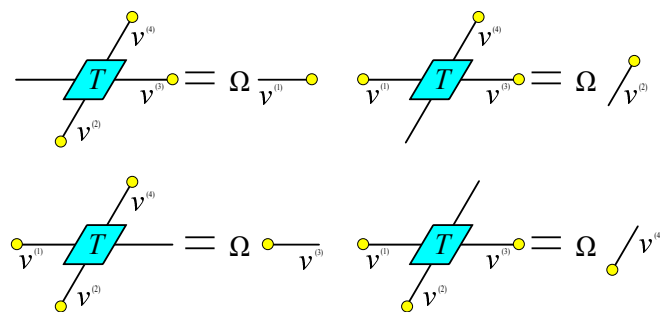


**Figure 33.** (Color online) The illustrations of self-consistent conditions for the rank-1 decomposition [Eq. (149)].

It means one will have  $v^{(k)}$  by contracting all other vectors with the tensor. This property provides us an algorithm to compute rank-1 decomposition.

Apart from some very special cases, such an optimization problem is concave, thus rank-1 decomposition is unique \*. Furthermore, if one arbitrarily choose a set of norm-1 vectors, they will converge to the fixed point exponentially fast with the iterations. To the best of knowledge, the exponential convergence has not been proved rigorously, but observed in most cases.

*4.5.3. Rank-1 decomposition, super-orthogonalization, and contractions of tree tensor networks* Let us still consider an translational invariant square TN that is formed by infinite copies of the 4th-order tensor  $T$ . The rank-1 decomposition of  $T$  provides an approximative scheme to compute the contraction of the TN, which is known as the *theory of network contractor dynamics* (NCD) [122].

The picture of NCD can be understood by iteratively using the self-consistent conditions [Eq. (149)] to “grow” tree TN, so that it covers the whole infinite square lattice (Fig. 34). Let us start from Eq. (147) that gives  $\Omega$ . Using Eq. (149), we substitute each of the four vectors by the contraction of  $T$  with the other three vectors. After doing so, Eq. (147) becomes the contraction of more than one  $T$ ’s with the vectors on the boundary. In other words, we “grow” the local TN contraction from one tensor plus four vectors to that with more tensors and vectors.

By repeating the substitution, the TN can be grown to cover the whole square lattice, where each site is allowed to put maximally one  $T$ . Inevitably, some sites will not have  $T$  but four vectors instead. These vectors (also called *contractors*) give the rank-1 decomposition of  $T$  as Eq. (146). One can see from the picture that some tensors in the square TN are replaced by its rank-1 approximation, so that all loops are destructed and the TN becomes a tree covering the square lattice. Thus, the square TN is approximated by such an optimal tree TN on square lattice in the sense of rank-1 decomposition.

In fact, the growing process as well as the optimal tree TN is only to understand the tree approximation with rank-1 decomposition. There is no need to practically implement such a

\*In fact the uniqueness of rank-1 decomposition has not been rigorously proven. Some related discussions from the perspective of eigenvalue degeneracy will be given in the next section.

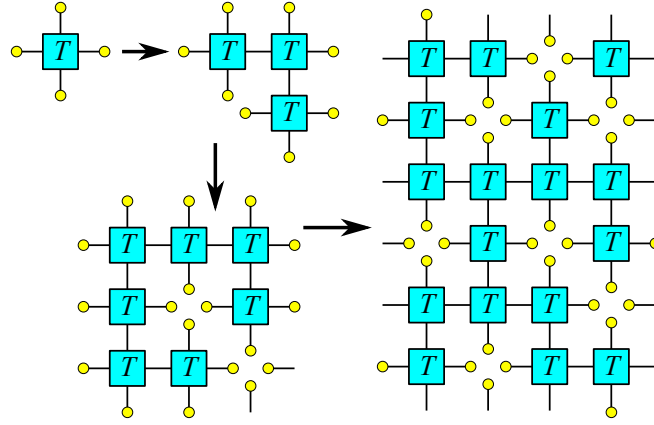


**Figure 34.** (Color online) Using the self-consistent conditions of the rank-1 decomposition, a tree TN with no loops can grow to cover the infinite square lattice. The four vectors gathering in a same site give the rank-1 approximation of the original tensor.

process. Thus, it does not matter how the TN is grown or where the rank-1 tensors are put to destroy the loops. All information we need is given by the rank-1 decomposition. The tree approximation of the TN is encoded in the rank-1 decomposition.

For growing the TN, we shall remark that using the contraction of one  $T$  with several vectors to substitute one vector is certainly not unique. However, the aim of “growing” is to reconstruct the TN formed by  $T$ . Thus, if  $T$  has to appear in the substitution, the vectors should be uniquely chosen as those given in the rank-1 decomposition due to its uniqueness. Secondly, there are hidden conditions when covering the lattice by “growing”. A stronger version is

$$T_{a_1 a_2 a_3 a_4} = T_{a_3 a_2 a_1 a_4}^* = T_{a_1 a_4 a_3 a_2}^* = T_{a_3 a_4 a_1 a_2}. \quad (150)$$

And a weaker one only requires the vectors to be conjugate to each other as

$$v^{(1)} = v^{(3)\dagger}, \quad v^{(2)} = v^{(4)\dagger}. \quad (151)$$

These conditions assure that the self-consistent equations encodes the correct tree that optimally approximates the square TN.

The super-orthogonal conditions in Eq. (131) are actually equivalent to the above self-consistent equations of rank-1 decomposition by defining the tensor  $T$  and vector  $v$  as

$$T_{a_1 a_2 \dots a_K} = \sum_s P_{s, a'_1 a'_2 \dots a'_K} P_{s, a''_1 a''_2 \dots a''_K}^* \prod_{k=1}^K \sqrt{\Lambda_{a'_k}^{(k)} \Lambda_{a''_k}^{(k)*}}, \quad (152)$$

$$v_{a_k}^{(k)} = \sqrt{\Lambda_{a'_k}^{(k)} \Lambda_{a''_k}^{(k)*}}, \quad (153)$$

with  $a_k = (a'_k, a''_k)$ . Thus, the super-orthogonal spectrum provides an optimal approximation for the truncations of the bond dimensions in the sense of the optimal tree. This provides a direct connection between the simple update scheme and the contraction of tree TN.

*4.5.4. Error of optimal tree approximation and tree-expansion theory based on rank-decomposition* . The error of NCD is another important and interesting issue. From the

**Figure 35.** (Color online) The illustrations of rank-1 decomposition [Eq. (154)].

first glance, the error seems to be the error of rank-1 decomposition  $\varepsilon = |T - \prod_k v^{(k)}|$ . This would be true if we replaced all tensors in the square TN by the rank-1 version. In the above scheme, however, we only replace a part of the tensors to destruct loops. These two ways of replacement seem to be equivalent if we only look at one tensor. Differences appear when we look at more tensors. This can be seen in a physical way by considering the correlations of classical Ising model, whose partition function can be written as a TN (see Chap. 2). The correlation of two spins can be obtained by the contraction of a TN, where the two tensor corresponding to the two spins are slightly modified and the rest are the same to the TN of the partition function. In the fully replaced case, there will be no correlations at all, but in the optimal tree approximation, a finite correlation length can be captured by the path allowed in the tree. When the TN represents the inner product of two PEPS, the fully replaced way approximates the PEPS by a separable state with zero entanglement. In the tree picture, the corresponding approximative PEPS is indeed entanglement, like a tree PEPS.

As the error of rank-1 decomposition cannot properly give the error of NCD, then, what can? To answer this question in a more rigorous way, let us introduce the *rank decomposition* (also called CANDECOMP/PARAFAC decomposition) of  $T$  in MLA (Fig. 35) that reads

$$T_{a_1 a_2 \dots} = \sum_{r=0}^{R-1} \Omega_r \prod_k v_{a_k}^{(k,r)}, \quad (154)$$

where  $v^{(k,r)}$  are normalized vectors. The idea of rank decomposition [347, 348] is to expand  $T$  into the summation of  $R$  number of rank-1 tensors with  $R$  called the *tensor rank*.  $\Omega$  can always be in the descending order according to the absolute values. Then the leading term  $\Omega_0 \prod_k v^{(k,0)}$  gives exactly the rank-1 decomposition of  $T$ , and the error of the rank-1 decomposition becomes  $|\sum_{r=1}^{R-1} \Omega_r \prod_k v_{a_k}^{(k,r)}|$ .

In the optimal tree TN, let us replace the rank-1 tensors back by the full rank tensor in Eq. (154). We suppose the rank decomposition is exact, thus we will recover the original TN by doing so. The TN contraction becomes the summation of  $R^{\tilde{N}}$  terms with  $\tilde{N}$  the number of rank-1 tensors in the optimal tree TN. Each term is the contraction of a tree TN, which is the same as the optimal tree TN except that certain vectors are changed to  $v^{(k,r)}$  instead of  $v^{(k,0)}$ . Note that in all terms, we use the same tree structure; the leading term in the summation is the optimal tree TN. It means with rank decomposition, we expand the contraction of the square TN by the summation of the contractions of many tree TN's.

Let us rewrite the expansion so that the contributions of the terms are given more explicitly. For simplicity, we assume that  $R = 2$ , meaning  $T$  can be exactly decomposed as the summation of two rank-1 tensors, which are the leading term given by the rank-1 decomposition, and the next-leading term denoted as  $T_1 = \Omega_1 \prod_k v^{(k,1)}$  (dubbed as the

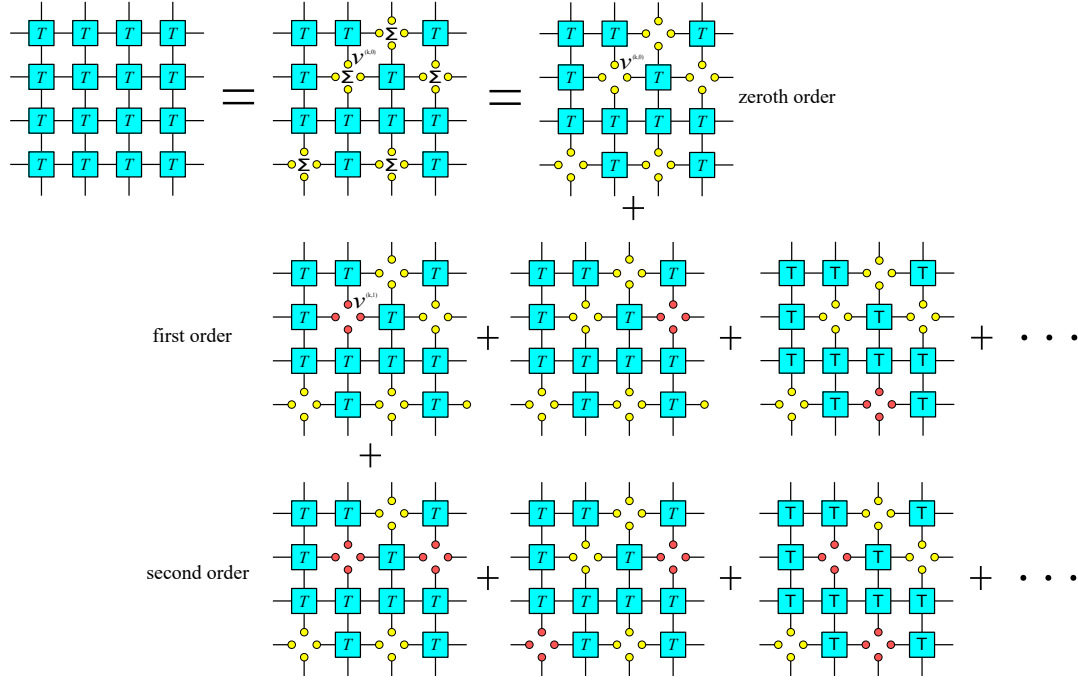


**Figure 36.** (Color online) The illustrations of the expansion with rank decomposition. The yellow and red circles stand for  $v_{a_k}^{(k,0)}$  (zeroth order terms in the rank decomposition) and  $v_{a_k}^{(k,1)}$  (first order terms), respectively. Here, we consider the tensor rank  $R = 2$  for simplicity.

*impurity tensor*). Defining  $\tilde{n}$  as the number of the next-leading terms appearing in one of the tree TN in the summation, the expansion can be written as

$$Z = \Omega_0^{\tilde{N}} \sum_{\tilde{n}=0}^{\tilde{N}} \left(\frac{\Omega_1}{\Omega_0}\right)^{\tilde{n}} \sum_{\mathcal{C} \in \mathcal{C}(\tilde{n})} Z_{\mathcal{C}}. \quad (155)$$

We call  $\mathcal{C}(\tilde{n})$  as the set of all possible *configurations* of  $\tilde{n}$  number of  $T_1$ 's, where there are  $\tilde{n}$  of  $T_1$ 's located in different positions in the tree. Then  $Z_{\mathcal{C}}$  denotes the contraction of such a tree TN with a specific configuration of  $T_1$ 's. We put the coefficients  $\Omega_r$  in front so that the descending order in the expansion becomes explicit since we have  $|\Omega_1/\Omega_0| < 1$ .

To proceed, we choose one tensor in the tree as the original point, and always contract the tree TN by ending at this tensor. Then the distance  $\mathcal{D}$  of a vector is defined as the number of tensors in the path that connects this vector to the original point. Note that one impurity tensor is the tensor product of several vectors, and each vector may have different distance to the original point. For simplicity, we take the shortest one to define the distance of the impurity tensor.

Now, let us utilize the exponential convergence of the rank-1 decomposition. After contracting any vectors with the tensor in the tree, the resulting vector approaches the fixed point (the vectors in the rank-1 decomposition) in an exponential speed. Define  $\mathcal{D}_0$  as the average number of the contractions that will project any vectors to the fixed point with a tolerable difference. Consider any impurity tensors with the distance  $\mathcal{D} > \mathcal{D}_0$ , their contributions to the contraction are the same, since after  $\mathcal{D}_0$  contractions, the vectors have

already been projected to the fixed point.

From the above argument, we can see that the error is related not only to the error of the rank-1 decomposition, but also to the speed of the convergence that defines  $\mathcal{D}_0$ . The smaller  $\mathcal{D}_0$  is, the smaller the error (the total contribution in the summation from the non-dominant terms) will be. The convergence speed is related to the correlation length (or gap) of the physical system. The rigorous relations between them have not been established yet. Such a picture also leads to an expansion theory of TN contraction. Unfortunately, it requires the rank decomposition, whose algorithm for arbitrary tensors has not been well understood.

#### 4.6. Contracting tensor network on square lattice: *iDMRG*, *iTEBD*, *CTMRG*, and tensor ring decomposition

We have shown that rank-1 decomposition solves the contraction of infinite-size tree TN and provides a mathematic explanation of the approximation made in the simple update algorithm. Then, it is natural to think: can we generalize this scheme beyond being only rank-1, in order to have better update schemes? In the following, we will show that besides the rank decomposition (Sec. 4.4.4), the so-called *tensor ring decomposition* (TRD) [123, 349] was suggested as another rank-N generalization for solving TN contraction problems.

TRD is defined by a set of SEE's and certain constraints required by the TN contraction. The original proposal of TRD requires all eigenvalue equations to be Hermitian [123]. Later, a generalization that allows non-Hermitian problems was proposed [349]. Since the non-Hermitian version provides more explicit connections to the existing NRG-based schemes, unifying the *iDMRG* [14, 15, 226], *iTEBD* [60], and *CTMRG* [201] algorithms in a same TN picture, we will concentrate on this version in the following.

*4.6.1. Revisiting iDMRG, iTEBD, and CTMRG: a uniform description with tensor ring decomposition* Consider an infinite square TN formed by the copies of the fourth-order tensor  $T$  (dubbed as *cell tensor*). In the following, we show that *iDMRG*, *iTEBD*, and *CTMRG* solve the TN contraction problem in three different ways, but lead to the same set of SEE's with proper constraints. Particularly, while doing *iDMRG* along one direction of the TN, we are actually implementing *iTEBD* in the other direction. We also show that similar to the definition of rank-1 decomposition, TRD is defined by the SEE's as a rank-N generalization.

The TN contraction can be solved using the *iDMRG* [14, 15, 226] by considering an infinite-size row of tensors in the TN as an MPO [170, 171, 173, 174, 175]. To write the self-consistent eigenvalue equations, we introduce three third-order variational tensors denoted by  $v^L$ ,  $v^R$  (dubbed as the *boundary* or *environmental tensors*) and  $\Psi$  (dubbed as the *central tensor*). These tensors are the fixed-point solution of the a set of eigenvalue equations.  $v^L$  and  $v^R$  are, respectively, the left and right dominant eigenvector of the following matrices (Fig.

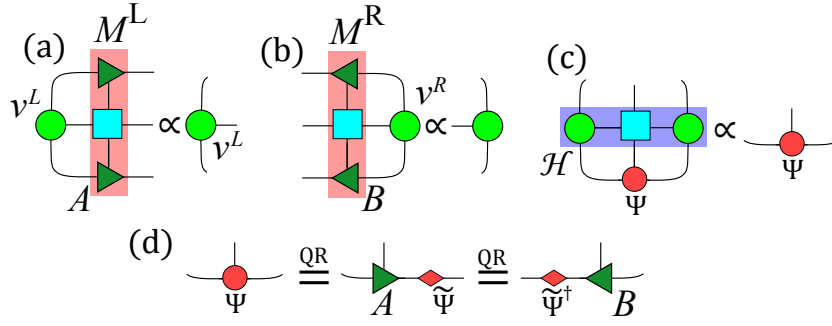


**Figure 37.** (Color online) The (a), (b) and (c) show the three local eigenvalue equations given by Eqs. (157) and (159). The isometries  $A$  and  $B$  are obtained by the QR decompositions of  $\Psi$  in two different ways in Eq. (158), as shown in (d).

37 (a) and (b))

$$M_{c'b'_1b_1,cb'_2b_2}^L = \sum_{aa'} T_{a'c'ac} A_{a'b'_1b'_2}^* A_{ab_1b_2}, \quad (156)$$

$$M_{c'b'_1b_1,cb'_2b_2}^R = \sum_{aa'} T_{a'c'ac} B_{a'b'_1b'_2}^* B_{ab_1b_2}, \quad (157)$$

where  $A$  and  $B$  are the left and right orthogonal parts by the QR decompositions of  $\Psi$  (Fig. 37 (d)) as

$$\Psi_{abb'} = \sum_{b''} A_{abb''} \tilde{\Psi}_{b''b'} = \sum_{b''} \tilde{\Psi}_{bb''}^\dagger B_{ab''b'}. \quad (158)$$

$\Psi$  is the dominant eigenvector of the Hermitian matrix (Fig. 37 (c)) that satisfies

$$\mathcal{H}_{a'b'_1b'_2,ab_1b_2} = \sum_{cc'} T_{a'c'ac} v_{c'b'_1b_1}^L v_{cb'_2b_2}^R. \quad (159)$$

One can see that each of the eigenvalue problems are parametrized by the solutions of others, thus we solve them in a recursive way. First, we initialize arbitrarily the central tensors  $\Psi$  and get  $A$  and  $B$  by Eq. (158). Note that a good initial guess can make the simulations faster and more stable. Then we update  $v^L$  and  $v^R$  by multiplying with  $M^L$  and  $M^R$  in Eqs. (156) and (157). Then we have the new  $\Psi$  by solving the first eigenvector of  $\mathcal{H}$  in Eq. (159) that is defined by the new  $v^L$  and  $v^R$ . We iterate such a process until all variational tensors converge.

Let us rephrase the iDMRG algorithm given above in the language of TN contraction/reconstruction. When the variational tensors give the fixed point, the eigenvalue equations “encodes” the infinite TN, i.e., the TN can be reconstructed from the equations. To do so, we start from a local contraction  $Z$  (Fig. 38) written as

$$Z \rightleftharpoons \sum T_{a'c'ac} \Psi_{a'b_1b_2}^* \Psi_{ab_3b_4} v_{c'b_1b_3}^L v_{cb_2b_4}^R. \quad (160)$$

The summation goes through all indexes. According to the fact that  $\Psi$  is the leading eigenvector of Eq. (159),  $Z$  is maximized with fixed  $v^L$  and  $v^R$ . We here use the symbol “ $\rightleftharpoons$ ” to represent the contraction relation up to a difference of a constant factor.

Then, we use the eigenvalue equations of  $v^L$  and  $v^R$  to add one  $M^L$  and one  $M^R$  [Eq. (156) and (157)] in the contraction, i.e., we substitute  $v^L$  by  $v^L M^L$  and  $v^R$  by  $M^R v^R$ . After

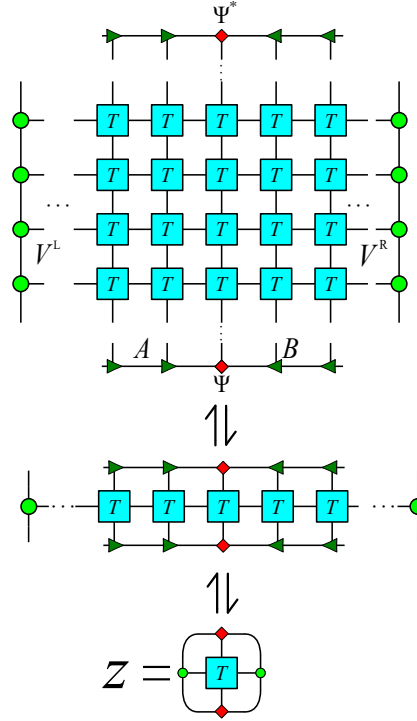


**Figure 38.** (Color online) The eigenvalue equations as illustrated “encode” the infinite TN.

doing so for one time, a finite central orthogonal MPS appears, formed by  $A$ ,  $B$  and  $\Psi$ . Such substitutions can be repeated for infinite times, then we will have an infinite central orthogonal MPS in  $Z$  formed by  $\Psi$ ,  $A$  and  $B$  as

$$\Phi_{\dots a_n \dots} = \sum_{\{b\}} \dots A_{a_{n-2} b_{n-2} b_{n-1}} A_{a_{n-1} b_{n-1} b_n} \Psi_{a_n b_n b_{n+1}} B_{a_{n+1} b_{n+1} b_{n+2}} B_{a_{n+2} b_{n+2} b_{n+3}} \dots \quad (161)$$

One can see that the bond dimension of  $b_n$  is in fact the dimension cut-off of the MPS

Now, we have

$$Z \rightleftharpoons \Phi^\dagger \rho \Phi, \quad (162)$$

where  $\rho$  is an infinite-dimensional matrix that has the form of an infinite MPO (middle of Fig. 38) as

$$\rho_{\dots a'_n \dots, \dots a_n \dots} = \sum_{\{c\}} \dots T_{a'_n c_n a_n c_{n+1}} T_{a'_{n+1} c_{n+1} a_{n+1} c_{n+2}} \dots \quad (163)$$

$\rho$  is in fact one infinite row of the TN. Compared with Eq. (160), the difference of  $Z$  is only a constant factor that can be given by the dominant eigenvalues of  $M^L$  and  $M^R$ .

After the substitutions from Eq. (160) to (162),  $Z$  is still maximized by the given  $\Phi$ , since  $v^L$  and  $v^R$  are the dominant eigenvectors. Note that such a maximization is optimized under the assumption that the dominant eigenvector  $\Phi$  can be well represented in an MPS with finite bond dimensions. Meanwhile, one can easily see that the MPS is normalized  $|\Phi_{\dots a_n \dots}| = 1$ , thanks to the orthogonality of  $A$  and  $B$ . Then we come to a conclusion that  $\Phi$  is the optimal MPS that gives the dominant eigenvector of  $\rho$ , satisfying  $\Phi \rightleftharpoons \rho \Phi$ . Then, we can rewrite the

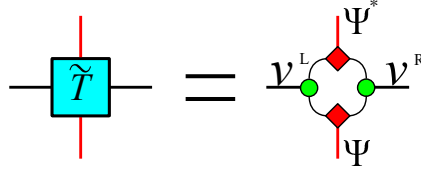


**Figure 39.** (Color online) The illustrations of the tensor ring decomposition in Eq. (164).

TN contraction as  $Z \rightleftharpoons \lim_{K \rightarrow \infty} \Phi^\dagger \rho^K \Phi$ , where the infinite TN appears as  $\rho^K$  (Fig. 38). Note we use the fact that for a matrix  $M$ , the normalized vector  $v$  is its dominant eigenvector (if exists) while  $v^T M v$  is maximized.

One can see that there are two important constraints in the process above:

- $Z$  [Eq. (160)] is maximized under the constraint that  $v^L$  and  $v^R$  are normalized.
- $\Phi^\dagger \rho \Phi$  is maximized under the constraint that  $\Phi$  is normalized.

The two eigenvalue problems with these two constraints define the *tensor ring decomposition* (Fig. 39) as

$$\tilde{T}_{a'c'ac} = \sum_{b_1 b_2 b_3 b_4} \Psi_{a'b_1 b_2}^* \Psi_{ab_3 b_4} v_{c'b_1 b_3}^L v_{cb_2 b_4}^R, \quad (164)$$

so that  $Z = \sum T_{a'c'ac} \tilde{T}_{a'c'ac}$  [Eq. (160)] is maximized. Like the NTD and rank-1 decomposition, TRD belongs to the decompositions that encode infinite TN's. By taking the dimensions of  $\{b\}$  as one, the eigenvalue equations of TRD reduce to those of rank-1 decomposition.

It has been revealed that the ground states obtained by iTEBD and iDMRG are different only up to a gauge transformation [226]. Here, TRD further unifies iDMRG and iTEBD in the same picture in the algorithmic sense. For iTEBD, after combining the contraction and truncation given by Eqs. (88) and (95), we have the equation for updating the tensor there as

$$A_{s,cc'} \rightleftharpoons \sum_{s'aba'b'} T_{sbs'b'} A_{s',aa'} X_{ab,c} Y_{a'b',c'}. \quad (165)$$

Looking at Eqs. (157) and (157), Eq. (165) is just the eigenvalue equation for updating  $v^{[L(R)]}$ , which is  $v^{[L(R)]} \rightleftharpoons M^{[L(R)]} v^{[L(R)]}$ , and the QR decomposition in Eq. (158) guaranties that the “truncations in iTEBD” are implemented by isometries. In other words, one can consider another MPS defined in the vertical direction, which is formed by  $v^{[L(R)]}$  and updated by the iTEBD algorithm. It means that while implementing iDMRG in the parallel direction of the TN, one is in fact simultaneously implementing iTEBD to update an MPS along the vertical direction. The relations between iTEBD and iDMRG has been discussed in other forms. It was shown that for the same system, the ground state obtained by iDMRG is equivalent to the ground state by iTEBD, up to a gauge transformation [226, 350]. A different relation is explained above, where the two algorithms themselves are unified in a same scheme.

Interestingly, when one uses iDMRG to solve the ground state of a 1D system, the MPS formed by  $v^{[L(R)]}$  in the imaginary-time direction satisfies the continuous structure [349] proposed for continuous field theories [45]. Such an iTEBD calculation can also be considered as the transverse contraction of the TN [339, 351].



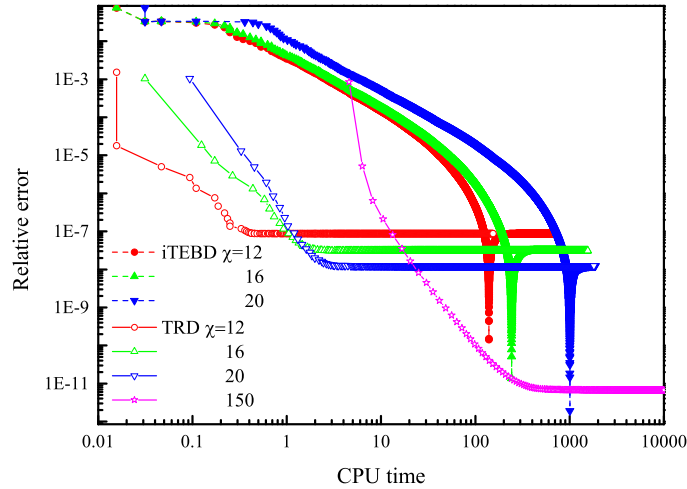


**Figure 40.** (Color online) The (absolute) relative error versus computational time of the standard iTEBD and the TRD by solving SEE's [123]. The data are obtained by contracting the 2D TN that represents the partition function of the classical Ising model at the critical temperature. The deeps of the iTEBD curves are because that the sign of the relative error is changed.

CTMRG [201, 209] is also closely related to the picture given above, which can lead to the CTMRG without corners. The tensors  $\Psi$ ,  $v^L$  and  $v^R$  correspond to the row and column tensors, and the equations for updating these tensors are the same to the equations of updating the row and column tensors in CTMRG (see Eqs. (97) and (101)). Such a relation becomes more explicit in the rank-1 case, when corners become simply scalars. The difference is that in the original CTMRG by Orús *et al* [201], the tensors are updated with a power method, i.e.,  $\Psi \leftarrow \mathcal{H}\Psi$  and  $v^{[L(R)]} \leftarrow M^{[L(R)]}v^{[L(R)]}$ . Recently, eigen-solvers instead of power method were suggested in CTMRG ([209] and a related review [352]), where the eigenvalue equations of the row and column tensors are the same to those given in TRD. The efficiency was shown to be largely improved with this modification.

*4.6.2. Improvement of efficiency by using self-consistent eigenvalue equations* Although iTEBD and TRD share the same set of SEE's, meaning the fixed points of these two methods are the same, their efficiencies are largely different. We use the standard iTEBD [60] and TRD to compute the free energy (per site) of 2D classical Ising model on square lattice at the critical temperature. Since the TN is not from unitary gates, we use canonicalization [61] in iTEBD. For TRD, we use the original proposal where the SEE's are Hermitian (up to a unitary transformation) [123]. The relative errors compared with the exact solution [353] are shown in Fig. 40. When using the same dimension cut-off  $\chi$ , these two algorithms converge to the same precision. The difference is at the level of machine error. However, the efficiency of TRD is much higher. Table 1 shows the CPU time with different  $\chi$ 's to reach the convergence. The CPU time of AOP is two orders of magnitude lower than that of iTEBD. If we restrain

**Table 1.** The CPU time using iTEBD and AOP to reach the convergence with different  $\chi$ 's.

CPU time	$\chi = 12$	$\chi = 16$	$\chi = 20$
iTEBD	$\sim 200$	$\sim 400$	$\sim 1000$
AOP	$\sim 1$	$\sim 3$	$\sim 4$

the CPU time to maximally be  $t_{CPU} = 1000$  for example, one is able to take  $\chi = 20$  (with the error  $\sim O(10^{-8})$ ) in iTEBD and  $\chi \simeq 150$  (with the error  $\sim O(10^{-11})$ ) in TRD. Similar results were reported in Ref. [209], where the authors calculated the variational tensors in CTMRG by solving eigenvalue equations. The efficiency was found to be largely improved.

*4.6.3. Extracting information of tensor networks* Before talking about cluster and full update schemes by TRD (meaning by iTEBD, iDMRG, or CTMRG, with no need to specify any more), let us explain in the following how to extract useful information of the TN from TRD. The information of the TN and the physical system are encoded in the variational tensors  $v^L$ ,  $v^R$  and  $\Psi$ . In the following, we introduce the *free energy* and *correlation length* of the TN. Note that the same or similar tricks of these quantities are well-known in the TN community and have been employed everywhere (see, e.g., a review [354]). In the following, we treated these two quantities as the properties of the TN itself. When the TN is used to represent different physical models, these quantities can be interpreted accordingly to get the physical properties. We assume that  $M^L$  and  $M^R$  share the same eigenvalues and eigenvectors for simplicity.

The first issue we concern is the contraction itself. To avoid diverging or vanishing to zero, we define the *free energy* per tensor of the TN as

$$f = - \lim_{N \rightarrow \infty} \frac{\ln \mathcal{Z}}{N}, \quad (166)$$

with  $\mathcal{Z}$  the value of the contraction in theory and  $N$  denoting the number of tensors. Such a definition is closely related to some physical quantities, such as the free energy of classical models and the average fidelity of quantum states. Meanwhile,  $f$  can enable us to compare the values of the contractions of two TN's without actually computing  $\mathcal{Z}$ .

The free energy is given by the dominant eigenvalues of  $M^L$  and  $M^R$ . Let us reverse the above reconstructing process to prove this. Firstly, we use the MPS in Eq. (161) to contract the TN in one direction, and have  $\mathcal{Z} = (\lim_{K \rightarrow \infty} \eta^K) \Phi^\dagger \Phi = \lim_{K \rightarrow \infty} \eta^K$  with  $\eta$  the dominant eigenvalue of  $\rho$ . The problem becomes getting  $\eta$ . By going from  $\Phi^\dagger \rho \Phi$  to Eq. (160), we can see that the eigenvalue problem of  $\Phi$  is transferred to that of  $\mathcal{H}$  in Eq. (159) multiplied by a constant  $\lim_{K_1 \rightarrow \infty} \kappa_0^{\tilde{K}}$  with  $\kappa_0$  the dominant eigenvalue of  $M^L$  and  $M^R$  and  $\tilde{K}$  the number of tensors in  $\rho$ . Thus, we have  $\eta = \eta_0 \kappa_0^{\tilde{K}}$  with  $\eta_0$  the dominant eigenvalue of  $\mathcal{H}$ . Finally, we have the TN contraction  $\mathcal{Z} = [\eta_0 \kappa_0^{\tilde{K}}]^K = \eta_0^K \kappa_0^{\tilde{K}K}$  with  $K\tilde{K} = N$ . By substituting into Eq. (166), we have  $f = - \ln \kappa_0 - \lim_{\tilde{K} \rightarrow \infty} (\ln \eta_0) / K_1 = - \ln \kappa_0$ .

The second issue is about the correlations of the TN. For the *correlation functions*, one possible definition is

$$F(\tilde{T}^{[\mathbf{r}_1]}, \tilde{T}^{[\mathbf{r}_2]}) = \mathcal{Z}(\tilde{T}^{[\mathbf{r}_1]}, \tilde{T}^{[\mathbf{r}_2]}) / \mathcal{Z} - \mathcal{Z}(\tilde{T}^{[\mathbf{r}_1]}, T^{[\mathbf{r}_2]}) \mathcal{Z}(T^{[\mathbf{r}_1]}, \tilde{T}^{[\mathbf{r}_2]}) / \mathcal{Z}^2, \quad (167)$$

where  $\mathcal{Z}(\tilde{T}^{[\mathbf{r}_1]}, \tilde{T}^{[\mathbf{r}_2]})$  denotes the contraction of the TN after substituting the original tensors in the positions  $\mathbf{r}_1$  and  $\mathbf{r}_2$  by two different tensors  $\tilde{T}^{[\mathbf{r}_1]}$  and  $\tilde{T}^{[\mathbf{r}_2]}$ .  $T^{[\mathbf{r}]}$  denotes the original tensor at the position  $\mathbf{r}$ .

Though the correlation functions depend on the tensors that are substituted with, and can be defined in many different ways, the long-range behavior share some universal properties. For a sufficiently large distance ( $|\mathbf{r}_1 - \mathbf{r}_2| \gg 1$ ), if  $\tilde{T}^{[\mathbf{r}_1]}$  and  $\tilde{T}^{[\mathbf{r}_2]}$  are in a same column,  $F$  satisfies

$$F \sim e^{-|\mathbf{r}_1 - \mathbf{r}_2| / \xi}, \quad (168)$$

and one has  $\xi = 1 / (\ln \eta_0 - \ln \eta_1)$  with  $\eta_0$  and  $\eta_1$  the two dominant eigenvalues of  $\mathcal{H}$ ; if  $\tilde{T}^{[\mathbf{r}_1]}$  and  $\tilde{T}^{[\mathbf{r}_2]}$  are in a same row, one has

$$\xi = 1 / (\ln \kappa_0 - \ln \kappa_1), \quad (169)$$

with  $\kappa_0$  and  $\kappa_1$  the two dominant eigenvalues of  $M^{L(R)}$ .

To prove the first case, we rewrite  $\mathcal{Z}(\tilde{T}^{[\mathbf{r}_1]}, \tilde{T}^{[\mathbf{r}_2]}) / \mathcal{Z}$  as

$$\mathcal{Z}(\tilde{T}^{[\mathbf{r}_1]}, \tilde{T}^{[\mathbf{r}_2]}) / \mathcal{Z} = [\Phi^\dagger \rho(\tilde{T}^{[\mathbf{r}_1]}, \tilde{T}^{[\mathbf{r}_2]}) \Phi] / (\Phi^\dagger \rho \Phi). \quad (170)$$

Then, introduce the transfer matrix  $M$  of  $\Phi^\dagger \rho \Phi$ , i.e.,  $\Phi^\dagger \rho \Phi = \text{Tr} M^{\tilde{K}}$  with  $\tilde{K} \rightarrow \infty$ . With the eigenvalue decomposition of  $\mathcal{M} = \sum_{j=0}^{D-1} \eta_j v_j v_j^\dagger$  with  $D$  the matrix dimension and  $v_j$  the  $j$ -th eigenvectors, one can further simply the equation as

$$\mathcal{Z}(\tilde{T}^{[\mathbf{r}_1]}, \tilde{T}^{[\mathbf{r}_2]}) / \mathcal{Z} = \sum_{j=0}^{D-1} (\eta_j / \eta_0)^{|\mathbf{r}_1 - \mathbf{r}_2|} v_0^\dagger \mathcal{M}(\tilde{T}^{[\mathbf{r}_1]}) v_j v_j^\dagger \mathcal{M}(\tilde{T}^{[\mathbf{r}_2]}) v_0, \quad (171)$$

with  $\mathcal{M}(\tilde{T}^{[\mathbf{r}]})$  the transfer matrix after substituting the original tensor at  $\mathbf{r}$  with  $\tilde{T}^{[\mathbf{r}]}$ . Similarly, one has

$$\mathcal{Z}(\tilde{T}^{[\mathbf{r}_1]}, T) / \mathcal{Z} = v_0^\dagger \mathcal{M}(\tilde{T}^{[\mathbf{r}_1]}) v_0, \quad (172)$$

$$\mathcal{Z}(T, \tilde{T}^{[\mathbf{r}_2]}) / \mathcal{Z} = v_0^\dagger \mathcal{M}(\tilde{T}^{[\mathbf{r}_2]}) v_0. \quad (173)$$

Note that one could transform the MPS into a translational invariant form (e.g., the left/right canonical form) to uniquely define the transfer matrix of  $\Phi^\dagger \rho \Phi$ . Substituting the equations above in Eq. (167), one has

$$F(\tilde{T}^{[\mathbf{r}_1]}, \tilde{T}^{[\mathbf{r}_2]}) = \sum_{j=1}^{D-1} (\eta_j / \eta_0)^{|\mathbf{r}_1 - \mathbf{r}_2|} v_0^\dagger \mathcal{M}(\tilde{T}^{[\mathbf{r}_1]}) v_j v_j^\dagger \mathcal{M}(\tilde{T}^{[\mathbf{r}_2]}) v_0. \quad (174)$$

When the distance is sufficiently large, i.e.,  $|\mathbf{r}_1 - \mathbf{r}_2| \gg 1$ , only the dominant term takes effects, which is

$$F(\tilde{T}^{[\mathbf{r}_1]}, \tilde{T}^{[\mathbf{r}_2]}) \simeq (\eta_1 / \eta_0)^{|\mathbf{r}_1 - \mathbf{r}_2|} v_0^\dagger \mathcal{M}(\tilde{T}^{[\mathbf{r}_1]}) v_1 v_1^\dagger \mathcal{M}(\tilde{T}^{[\mathbf{r}_2]}) v_0. \quad (175)$$

Compared with Eq. (168), one has  $\xi = 1 / (\ln \eta_0 - \ln \eta_1)$ . The second case can be proved similarly.

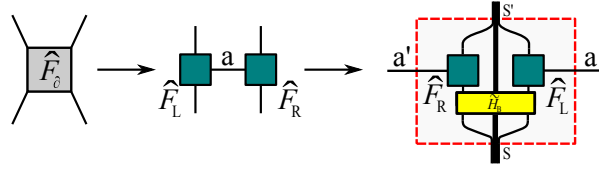


**Figure 41.** (Color online) Graphical representations of Eq.(176)-(179).

These two quantities are defined independently on specific physical models that the TN might represent, thus they can be considered as the mathematical properties of the TN. By introducing physical models, these quantities are closely related to the physical quantities. For example, when the TN represents the the partition function of a classical lattice model, Eq. (166) multiplied by the temperature is exactly the free energy. And the correlation lengths of the TN are also the physical correlation lengths of the model in two spatial directions. When the TN gives the imaginary time evolution of an infinite 1D quantum chain, the correlation lengths of the TN are the spatial and dynamical correlation length of the ground state.

#### 4.7. Application to the ground-state simulations of quantum lattice models

One of the main successful applications of TN algorithms is to simulate the ground states of quantum lattice models. There are already several reviews about this issue [57, 355, 354, 352, 17]. In the following, we explain a simple way of simulating the ground state based on the above unified scheme [227]. There are particularly two advantages: it allows classical, quantum, or classical-quantum mixed ways to efficiently implement the simulations; it allows to reproduce the physics of a large or even infinite-size model in the bulk of a few-body system.

*4.7.1. Simulating one-dimensional quantum systems.* Let us firstly take the ground-state simulation of the infinite-size 1D quantum system as an example, to show how to derive the few-body Hamiltonian from the infinite-size model. The Hamiltonian is the summation of two-body nearest-neighbor terms and is translationally invariant, which reads  $\hat{H}_{Inf} = \sum_n \hat{H}_{n,n+1}$ . The first step is to choose a supercell (e.g., a finite bulk of the chain with  $\tilde{N}$  sites). Then the Hamiltonian of the bulk is simply  $\hat{H}_B = \sum_{n=1}^{\tilde{N}} \hat{H}_{n,n+1}$ , and the Hamiltonian connecting the bulk to the rest part is  $\hat{H}_\partial = \hat{H}_{n',n'+1}$  (because the interactions are nearest-neighbor).

Define the operator  $\hat{F}^\partial$  as

$$\hat{F}_\partial = \hat{I} - \tau \hat{H}_\partial, \quad (176)$$

with  $\tau$  the Trotter-Suzuki step. This definition is to construct the Trotter-Suzuki decomposition [65, 66]. Instead of using the exponential form  $e^{-\tau \hat{H}}$ , we chose to shift  $\hat{H}_\partial$  for algorithmic consideration. The errors of these two ways concerning the ground state are at the same level ( $\mathcal{O}(\tau^2)$ ). Introduce an ancillary index  $a$  and rewrite  $\hat{F}_\partial$  as a sum of operators

as

$$\hat{F}_\partial = \sum_a \hat{F}_L(s)_a \otimes \hat{F}_R(s')_a, \quad (177)$$

where  $\hat{F}_L(s)_a$  and  $\hat{F}_R(s')_a$  are two sets of one-body operators (labeled by  $a$ ) acting on the left and right one of the two spins ( $s$  and  $s'$ ) associated with  $\hat{H}_\partial$ , respectively (Fig. 41). This is the same to the decomposition given in Sec. 2.5.3, but in a slightly different notation. Eq. (177) can be easily achieved by directly rewriting Eq. (176) or using eigenvalue decomposition.

Construct the operator  $\hat{\mathcal{F}}(S)_{a'a}$ , with  $S = (s_1, \dots, s_{\tilde{N}})$  representing the physical spins inside the super-cell, as

$$\hat{\mathcal{F}}(S)_{a'a} = \hat{F}_R(s_1)_{a'}^\dagger \tilde{H}_B \hat{F}_L(s_{\tilde{N}})_a, \quad (178)$$

with  $\tilde{H}_B = \hat{I} - \varepsilon \hat{H}_B$ .  $\hat{F}_R(s_1)_{a'}^\dagger$  and  $\hat{F}_L(s_{\tilde{N}})_a$  act on the first and last sites of the super-cell, respectively. One can see that  $\hat{\mathcal{F}}(S)_{a'a}$  represents a set of operators labeled by two indexes ( $a'$  and  $a$ ) that act on the supercell.

In the language of TN, the co-efficients of  $\hat{\mathcal{F}}(S)_{a'a}$  in the local basis is a forth-order cell tensor (Fig. 41) as

$$T_{S'a'Sa} = \langle S' | \hat{\mathcal{F}}(S)_{a'a} | S \rangle. \quad (179)$$

On the left-hand-side, the order of the indexes has been rearranged to be consistent with the definition used in the TN algorithm introduced above.  $T$  is the cell tensor, whose infinite copies form the TN of the imaginary-time evolution of the infinite system up to the first Trotter-Suzuki order. With the cell tensor  $T$ , the ground-state properties can be solved using the TN algorithms (e.g., TRD) introduced above. The ground state is given by the MPS given by Eq. (161).

Note that the above procedure of transforming the 1D ground-state simulation to TN contraction is similar to the one introduced in Sec. 2.5.3. The difference is that the above one allows to change the number of sites contained in the tensor  $T$ .

We use TRD (i.e., iTEBD, iDMRG, or corner-less CTMRG) to solve the TN contraction. Let us consider one of the eigenvalue equations [also see Eq. (159)]

$$\mathcal{H}_{S'b'_1b'_2, Sb_1b_2} = \sum_{aa'} T_{S'a'Sa} v_{a'b'_1b_1}^L v_{ab'_2b_2}^R. \quad (180)$$

To use a more concise notation, we use  $\mathcal{H}_{S'b'_1b'_2, Sb_1b_2}$  as the coefficients and define the operator

$$\hat{\mathcal{H}} = \sum_{SS'} \sum_{b_1b_2b'_1b'_2} \mathcal{H}_{S'b'_1b'_2, Sb_1b_2} |S'b'_1b'_2\rangle \langle Sb_1b_2|. \quad (181)$$

This Hamiltonian is the effective Hamiltonian in iDMRG [14, 15, 32] or some other methods which represent the RG of Hilbert space by MPS [350, 356]. The indexes  $\{b\}$  are considered as virtual spins by introducing the basis of space vectors  $\{|b\rangle\}$ . The virtual spins are called the *entanglement bath sites*.

By substituting the cell tensor  $T$  [Eqs. (178) and (179)] inside the above equation, we have

$$\hat{\mathcal{H}} = \hat{\mathcal{H}}_L \tilde{H}_B \hat{\mathcal{H}}_R, \quad (182)$$

where the Hamiltonians  $\hat{\mathcal{H}}_L$  and  $\hat{\mathcal{H}}_R$  on the boundaries satisfy

$$\begin{aligned}\langle b'_1 s'_1 | \hat{\mathcal{H}}_L | b_1 s_1 \rangle &= \sum_a v_{ab'_1 b_1}^L \langle s'_1 | \hat{F}_R(s_1)_a^\dagger | s_1 \rangle, \\ \langle s'_N b'_2 | \hat{\mathcal{H}}_R | s_N b_2 \rangle &= \sum_a \langle s'_N | \hat{F}_L(s_N)_a^\dagger | s_N \rangle v_{ab_2 b'_2}^R,\end{aligned}\tag{183}$$

$\hat{\mathcal{H}}_L$  and  $\hat{\mathcal{H}}_R$  are just two-body Hamiltonians, of which each acts on the bath site and the neighboring physical site on the boundary of the bulk. It has been applied to define the infinite boundary condition for simulating the time evolution of 1D quantum systems [357].

Ref. [227] shows that  $\hat{\mathcal{H}}_L$  and  $\hat{\mathcal{H}}_R$  can also be written in a shifted form as

$$\hat{\mathcal{H}}_{L(R)} = I - \tau \hat{H}_{L(R)}.\tag{184}$$

$\hat{H}_{L(R)}$  is independent on  $\tau$  and called the *physical-bath Hamiltonian*. Then  $\hat{\mathcal{H}}$  can be written as the shift of a few-body Hamiltonian as  $\hat{\mathcal{H}} = I - \tau \hat{H}_{FB}$ , where  $\hat{H}_{FB}$  has the standard summation form as

$$\hat{H}_{FB} = \hat{H}_L + \sum_{n=1}^L \hat{H}_{n,n+1} + \hat{H}_R.\tag{185}$$

After obtaining  $\hat{H}_L$  and  $\hat{H}_R$ , one can compute the coupling constants and magnetic fields by choosing the operator basis. If one takes the bath dimension to be  $\chi$ , the coefficient matrix of  $\hat{H}_{L(R)}$  is  $(2\chi \times 2\chi)$ . Then  $\hat{H}_{L(R)}$  can be generally expanded by  $\hat{S}^{\alpha_1} \otimes \hat{S}^{\alpha_2}$  with  $\{\hat{S}\}$  the generators of the  $SU(\chi)$  group.

Let us take the bond dimension  $\chi = 2$  as an example, and  $\hat{H}_{L(R)}$  just gives the Hamiltonian between two spin-1/2's. Thus, it can be expanded by the spin (or Pauli) operators  $\hat{S}^{\alpha_1} \otimes \hat{S}^{\alpha_2}$  as

$$\hat{H}_{L(R)} = \sum_{\alpha_1, \alpha_2=0}^3 J_{L(R)}^{\alpha_1 \alpha_2} \hat{S}^{\alpha_1} \otimes \hat{S}^{\alpha_2},\tag{186}$$

where the spin-1/2 operators are labeled as  $\hat{S}^0 = I$ ,  $\hat{S}^1 = \hat{S}^x$ ,  $\hat{S}^2 = \hat{S}^y$ , and  $\hat{S}^3 = \hat{S}^z$ . Then with  $\alpha_1 \neq 0$  and  $\alpha_2 \neq 0$ , we have  $J_{L(R)}^{\alpha_1 \alpha_2}$  as the coupling constants, and  $J_{L(R)}^{\alpha_1 0}$  and  $J_{L(R)}^{0 \alpha_2}$  the magnetic fields on the first and second sites, respectively.  $J_{L(R)}^{00}$  only provides a constant shift of the Hamiltonian which does not change the eigenstates.

As an example, we show the  $\hat{H}_L$  and  $\hat{H}_R$  for the infinite quantum Ising chain in a transverse field [358], which read

$$\begin{aligned}\hat{H}_L &= J_{xz}^L \hat{S}_1^x \hat{S}_2^z + J_{zz}^L \hat{S}_1^z \hat{S}_2^z - h_x^L \hat{S}_1^x - h_z^L \hat{S}_1^z - \tilde{h}_x^L \hat{S}_2^x, \\ \hat{H}_R &= J_{zx}^R \hat{S}_{N-1}^z \hat{S}_N^x + J_{zz}^R \hat{S}_{N-1}^z \hat{S}_N^z - h_x^R \hat{S}_N^x - h_z^R \hat{S}_N^z - \tilde{h}_x^R \hat{S}_{N-1}^x.\end{aligned}\tag{187}$$

The coupling constants and magnetic fields depend on the parameter  $\alpha$ , as shown in Fig. 42. The calculation shows that except the Ising interactions and the transverse field that originally appear in the infinite model, the  $\hat{S}^x \hat{S}^z$  coupling and a vertical field emerge in  $\hat{H}_L$  and  $\hat{H}_R$ . This is interesting, because the  $\hat{S}^x \hat{S}^z$  interaction is the stabilizer on the open boundaries of the cluster state, a highly entangled state that has been widely used in quantum information sciences [359, 360]. More relations with the cluster state are to be further explored.

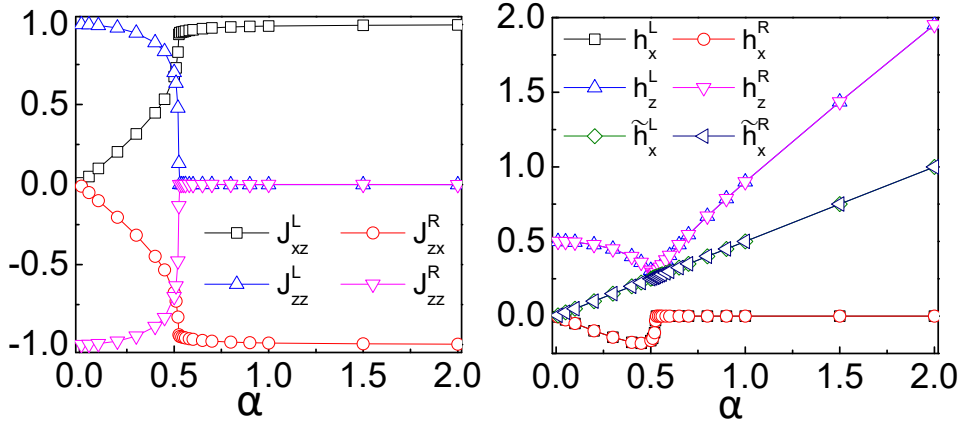


**Figure 42.** (Color online) The  $\alpha$ -dependence [358] of the coupling constants (left) and magnetic fields (right) of the few-body Hamiltonians [Eq. (187)]. Reused from [358] with permission.

The physical information of the infinite-size model can be extracted from the ground state of  $\hat{H}_{FB}$  (denoted by  $|\Psi(Sb_1b_2)\rangle$ ). The reduced density matrix of the bulk is written as

$$\hat{\rho}(S) = \text{Tr}_{b_1b_2} |\Psi(Sb_1b_2)\rangle \langle \Psi(Sb_1b_2)|. \quad (188)$$

We have  $|\Psi(Sb_1b_2)\rangle = \sum_{Sb_1b_2} \Psi_{Sb_1b_2} |Sb_1b_2\rangle$  with  $\Psi_{Sb_1b_2}$  the eigenvector of Eq. (180) or (159). It is easy to see that  $\Psi_{Sb_1b_2}$  is the central tensor in the central-orthogonal MPS [Eq. (161)], thus the  $\hat{\rho}(S)$  is actually the reduced density matrix of the MPS. Recall that the rest of the tensors are orthogonal. Meanwhile, the MPS optimally gives the ground state of the original model, thus,  $\hat{\rho}(S)$  from the few-body model optimally gives the reduced density matrix of original model.

In Eq. (185), the summation of the physical interactions are within the supercell that we choose to construct the cell tensor. If we want to increase the supercell to, e.g., capture longer correlations inside the bulk, the computational cost will obviously increase exponentially. A much efficient way is to increase directly the physical bulk in  $\hat{H}_{FB}$ . In other words,  $\hat{H}_L$  and  $\hat{H}_R$  are obtained by TRD from the supercell of a tolerable size  $L$ , and  $\hat{H}_{FB}$  is constructed with a larger bulk as  $\hat{H}_{FB} = \hat{H}_L + \sum_{n=1}^{\tilde{L}} \hat{H}_{n,n+1} + \hat{H}_R$  with  $\tilde{L} > L$ . Though  $\hat{H}_{FB}$  becomes more expensive to solve, we can use any finite-size algorithms to compute its dominant dominant eigenvector, avoiding the iterative computation of the eigenvectors of the SEE's. In principle,  $\hat{H}_{FB}$  can be simulated by quantum simulators. We will discuss this issue later.

**4.7.2. Simulating higher-dimensional quantum systems** For ( $D > 1$ )-dimensional quantum systems on, e.g., square lattice, one can use different update schemes to calculate the ground state. Here, we explain an alternative way by generalizing the above 1D simulation to higher dimensions [227]. The idea is to optimize the physical-bath Hamiltonians by simple update (i.e., iDMRG on tree lattices [129, 136] with a different gauge), and construct the few-body Hamiltonian  $\hat{H}_{FB}$  with a larger bulk. The interactions inside the bulk will be fully considered when solving the ground state of  $\hat{H}_{FB}$ , thus the precision will be significantly improved compared with the simple update.

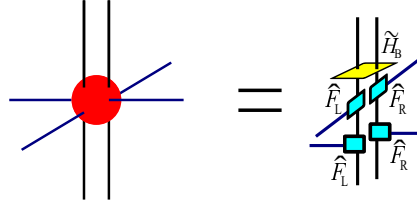


**Figure 43.** (Color online) Graphical representation of the cell tensor for 2D quantum systems [Eq. (190)].

The procedures for higher-dimensional models are similar to those for 1D models. The first step is to contract the cell tensor, so that the ground-state simulation is transformed to a TN contraction problem. To begin with, we choose a supercell that obeys the translational invariance, e.g. two sites connected by a parallel bond, and construct the tensor that parametrizes the eigenvalue equations. The bulk interaction is simply the coupling between these two spins, i.e.  $\hat{H}_B = \hat{H}_{i,j}$ , and the interaction between two neighboring supercells is the same, i.e.,  $\hat{H}_\partial = \hat{H}_{i,j}$ . By shifting  $\hat{H}_\partial$ , we define  $\hat{F}_\partial = I - \tau\hat{H}_\partial$  and decompose it as

$$\hat{F}_\partial = \sum_a \hat{F}_L(s)_a \otimes \hat{F}_R(s')_a. \quad (189)$$

$\hat{F}_L(s)_a$  and  $\hat{F}_R(s')_a$  are two sets of operators labeled by  $a$  that act on the two spins ( $s$  and  $s'$ ) in the supercell, respectively.

Define an operator that is the product of the (shifted) bulk Hamiltonian with  $\hat{F}_L(s)_a$  and  $\hat{F}_R(s)_a$  (Fig. 43) as

$$\hat{\mathcal{F}}(S)_{a_1 a_2 a_3 a_4} = \hat{F}_R(s)_{a_1} \hat{F}_R(s)_{a_2} \hat{F}_L(s')_{a_3} \hat{F}_L(s')_{a_4} \tilde{H}^B, \quad (190)$$

with  $S = (s, s')$  and  $\tilde{H}^B = I - \tau\hat{H}^B$ .  $\hat{\mathcal{F}}(S)$  can be understood as a set of quantum operators acting on the supercell (spins  $s$  and  $s'$ ) labeled by the boundary indexes  $a_1, a_2, a_3$  and  $a_4$ . Then the cell tensor that defines the TN is given by the coefficients of  $\hat{\mathcal{F}}(S)_{a_1 a_2 a_3 a_4}$  as

$$T_{S'S a_1 a_2 a_3 a_4} = \langle S' | \hat{\mathcal{F}}(S)_{a_1 a_2 a_3 a_4} | S \rangle. \quad (191)$$

One can see that  $T$  has six bonds, of which two ( $S$  and  $S'$ ) are physical and four ( $a_1, a_2, a_3$ , and  $a_4$ ) are non-physical. For comparison, the tensor in the 1D quantum case has four bonds, where two are physical and two are non-physical.

As discussed above in Sec. 2.5.3, the ground-state simulation becomes the contraction of a cubic TN formed by infinite copies of  $T$ . Each layer of the cubic TN gives the operator  $\hat{\rho}(\tau) = I - \tau\hat{H}$ , which is in a PEPO defined on a square lattice. Infinite layers of the PEPO  $\lim_{K \rightarrow \infty} \hat{\rho}(\tau)^K$  give the cubic TN. For the same model defined on the Bethe lattice, the 3D TN is formed by infinite layers of PEPO  $\hat{\rho}_{Bethe}(\tau)$  that is defined on the Bethe lattice. The cell tensor is defined exactly in the same way as Eq. (191).

The next step is to solve the SEE's of simple update. With the Bethe approximation, there are five variational tensors, which are  $\Psi$  (central tensor) and  $v^{[x]}$  ( $x = 1, 2, 3, 4$ , boundary tensors). Meanwhile, we have five self-consistent equations that encodes the 3D



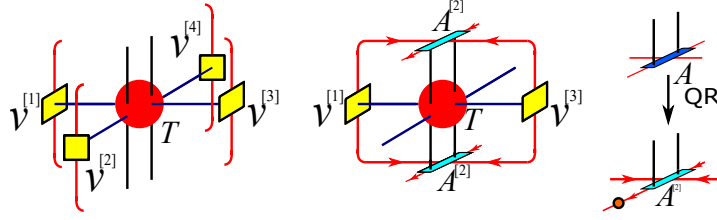


**Figure 44.** (Color online) The left figure is the graphic representations of  $\mathcal{H}_{S'b_1b_2b_3b_4, Sb_1b_2b_3b_4}$  in Eq.(192), and we take Eq.(194) from the self-consistent equations as an example shown in the middle. The QR decomposition in Eq.(197) is shown in the right figure, where the arrows indicate the direction of orthogonality of  $A^{[3]}$  in Eq.(198).

TN  $\lim_{K \rightarrow \infty} \hat{\rho}_{Bethe}(\tau)^K$ , which are given by five matrices as

$$\mathcal{H}_{S'b_1b_2b_3b_4, Sb_1b_2b_3b_4} = \sum_{a_1a_2a_3a_4} T_{S'Sa_1a_2a_3a_4} v_{a_1b_1b_1'}^{[1]} v_{a_2b_2b_2'}^{[2]} v_{a_3b_3b_3'}^{[3]} v_{a_4b_4b_4'}^{[4]}, \quad (192)$$

$$M_{a_1b_1b_1', a_3b_3b_3'}^{[1]} = \sum_{S'Sa_2a_4b_2b_2'b_4b_4'} T_{S'Sa_1a_2a_3a_4} A_{S'b_1b_2b_3b_4}^{[1]*} v_{a_2b_2b_2'}^{[2]} A_{Sb_1b_2b_3b_4}^{[1]} v_{a_4b_4b_4'}^{[4]} \quad (193)$$

$$M_{a_2b_2b_2', a_4b_4b_4'}^{[2]} = \sum_{S'Sa_1a_3b_1b_1'b_3b_3'} T_{S'Sa_1a_2a_3a_4} A_{S'b_1b_2b_3b_4}^{[2]*} v_{a_1b_1b_1'}^{[1]} A_{Sb_1b_2b_3b_4}^{[2]} v_{a_3b_3b_3'}^{[3]} \quad (194)$$

$$M_{a_1b_1b_1', a_3b_3b_3'}^{[3]} = \sum_{S'Sa_2a_4b_2b_2'b_4b_4'} T_{S'Sa_1a_2a_3a_4} A_{S'b_1b_2b_3b_4}^{[3]*} v_{a_2b_2b_2'}^{[2]} A_{Sb_1b_2b_3b_4}^{[3]} v_{a_4b_4b_4'}^{[4]} \quad (195)$$

$$M_{a_2b_2b_2', a_4b_4b_4'}^{[4]} = \sum_{S'Sa_1a_3b_1b_1'b_3b_3'} T_{S'Sa_1a_2a_3a_4} A_{S'b_1b_2b_3b_4}^{[4]*} v_{a_1b_1b_1'}^{[1]} A_{Sb_1b_2b_3b_4}^{[4]} v_{a_3b_3b_3'}^{[3]} \quad (196)$$

Eqs. (192) and (194) are illustrated in Fig. 44 as examples.  $A^{[x]}$  is an isometry obtained by the QR decomposition of the central tensor  $\Psi$  referring to the  $x$ -th virtual bond  $b_x$ . For example for  $x = 2$ , we have (Fig. 44)

$$\Psi_{Sb_1b_2b_3b_4} = \sum_b A_{Sb_1bb_3b_4}^{[2]} R_{bb_2}^{[2]}. \quad (197)$$

$A^{[2]}$  is orthogonal, satisfying

$$\sum_{Sb_1b_3b_4} A_{Sb_1bb_3b_4}^{[2]*} A_{Sb_1b'b_3b_4}^{[2]} = I_{bb'}. \quad (198)$$

Similar to the 1D case, the ground-state properties can already be extracted by the central tensor  $\Psi$ . For example, the reduced density matrix of the supercell  $\hat{\rho}(S) = \text{Tr}_{/(S)} |\Phi\rangle\langle\Phi|$  (with  $|\Phi\rangle$  denoting the ground state of the infinite model) is well approximated by the central tensor as

$$\hat{\rho}(S) \simeq \sum_{SS'b_1b_2b_3b_4} \Psi_{S'b_1b_2b_3b_4}^* \Psi_{Sb_1b_2b_3b_4} |S\rangle\langle S'|. \quad (199)$$

The self-consistent equations can be solved recursively. By solving the leading eigenvector of  $\mathcal{H}$  given by Eq. (192), we update the central tensor tensor  $\Psi$ . Then according to Eq. (197), we decompose  $\Psi$  to obtain  $A^{[x]}$ , update  $M^{[x]}$  in Eqs. (193)-(196), and update each  $v^{[x]}$  by  $M^{[x]}v^{[x]}$ . Repeat this process until all the five variational tensors converge. The

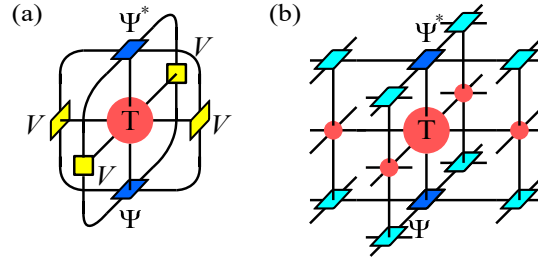


**Figure 45.** (Color online) The left figure shows the local contraction the encodes the infinite TN for simulating the 2D ground state. By substituting with the self-consistent equations, the TN representing  $\tilde{Z} = \langle \tilde{\Phi} | \hat{\rho}_{Bethe}(\tau) | \tilde{\Phi} \rangle$  can be reconstructed, with  $\hat{\rho}_{Bethe}(\tau)$  the TPDO of the Bethe model and  $|\tilde{\Phi}\rangle$  a tree PEPS.

algorithm is the generalized DMRG based on infinite tree PEPS [129, 136]. Each boundary tensor can be understood as the infinite environment of a tree branch, thus the original model is actually approximated at this stage by one defined on an infinite tree. Note that when only looking at the tree locally (from one site and its nearest neighbors), it looks the same to the original lattice. Thus, the loss of information is mainly long-range, i.e., from the destruction of loops.

The Bethe approximation can be understood better from the rank-1 decomposition (see Sec. 4.5). Firstly, Eqs. (193)-(196) encodes a Bethe TN, which is actually  $\tilde{Z} = \langle \tilde{\Phi} | \hat{\rho}_{Bethe}(\tau) | \tilde{\Phi} \rangle$  with  $\hat{\rho}_{Bethe}(\tau)$  the TPDO of the Bethe model and  $|\tilde{\Phi}\rangle$  a tree PEPS (Fig.45). To see this, let us start with the local contraction [Fig.45 (a)] as

$$Z_{Bethe} = \sum \Psi_{S'b_1b_2b_3b_4}^* \Psi_{Sb_1b_2b_3b_4} T_{S'Sa_1a_2a_3a_4} v_{a_1b_1b_1}^{[1]} v_{a_2b_2b_2}^{[2]} v_{a_3b_3b_3}^{[3]} v_{a_4b_4b_4}^{[4]}. \quad (200)$$

Then, each  $v^{[x]}$  can be replaced by  $M^{[x]}v^{[x]}$  because we are at the fixed point of the eigenvalue equations. By repeating this substitution in a similar way as the rank-1 decomposition in Sec. 4.5.3, we will have the TN for  $\tilde{Z} = \langle \tilde{\Phi} | \hat{\rho}_{Bethe}(\tau) | \tilde{\Phi} \rangle$ , which is maximized at the fixed point [Fig.45 (b)]. With the constraint  $\langle \tilde{\Phi} | \tilde{\Phi} \rangle = 1$  satisfied,  $|\tilde{\Phi}\rangle$  is the ground state of  $\hat{\rho}_{Bethe}(\tau)$ .

Now, we constrain the growth so that the TN covers the infinite square lattice. Inevitably, some  $v^{[x]}$ 's will gather at the same site. The tensor product of these  $v^{[x]}$ 's in fact gives the optimal rank-1 approximation of the “correct” full-rank tensor here. Suppose that one uses the full-rank tensor to replace its rank-1 version (the tensor product of four  $v^{[x]}$ 's), one will have the PEPO of  $I - \tau \hat{H}$  (with  $H$  the Hamiltonian on square lattice), and the tree iPEPS becomes the iPEPS defined on the square lattice. However, we do not know the “correct” tensor. Compared with the NCD scheme that employs rank-1 decomposition explicitly to solve TN contraction, one difference here for updating iPEPS is that the “correct” tensor to be decomposed by rank-1 decomposition contains the variational tensor, thus is in fact unknown before the equations are solved. For this reason, we cannot use rank-1 decomposition directly. Another difference is that the constraint, i.e., the normalization of the tree PEPS, should be fulfilled. By utilizing the iDMRG algorithm with the tree iPEPS, the rank-1 tensor is obtained without knowing the “correct” tensor, and meanwhile, the constraints are satisfied. The ground state is optimally given by the tree iPEPS  $|\tilde{\Phi}\rangle$ .

Now, we construct the few-body Hamiltonian in a larger cluster, so that the error brought

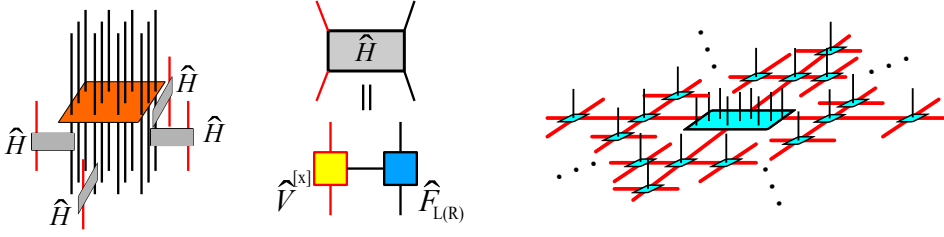


**Figure 46.** (Color online) The left figure shows the few-body Hamiltonian  $\hat{\mathcal{H}}$  in Eq.(201). The middle one shows the physical-bath Hamiltonian  $\hat{\mathcal{H}}_\partial$  that gives the interaction between the corresponding physical and bath site. The right one illustrates the state ansatz for the infinite system. Note that the boundary of the cluster should be surrounded by  $\hat{\mathcal{H}}_\partial$ 's, and each  $\hat{\mathcal{H}}_\partial$  corresponds to an infinite tree branch in the state ansatz. For simplicity, we only illustrate four of the  $\hat{\mathcal{H}}_\partial$ 's and the corresponding branches.

by Bethe approximation can be reduced. Similar to the 1D case, we embed a larger cluster in the middle of the entanglement bath. The few-body Hamiltonian (Fig. 46) reads

$$\hat{\mathcal{H}} = \prod_{\langle n \in \text{cluster}, \alpha \in \text{bath} \rangle} \hat{\mathcal{H}}_\partial(n, \alpha) \prod_{\langle i, j \rangle \in \text{cluster}} [I - \tau \hat{H}(s_i, s_j)]. \quad (201)$$

$\hat{\mathcal{H}}_\partial(n, \alpha)$  is defined as the physical-bath Hamiltonian between the  $\alpha$ -th bath site and the neighboring  $n$ -th physical site, and it is obtained by the corresponding boundary tensor  $v^{[x(\alpha)]}$  and  $\hat{F}_{L(R)}(s_n)$  (Fig. 46) as

$$\langle b'_\alpha s'_n | \hat{\mathcal{H}}_\partial(n, \alpha) | b_\alpha s_n \rangle = \sum_a v_{ab'_\alpha b_\alpha}^{[x(\alpha)]} \langle s'_n | \hat{F}_{L(R)}(s_n)_a | s_n \rangle. \quad (202)$$

Here,  $\hat{F}_{L(R)}(s_n)_a$  is the operator defined in Eq. (189), and  $v_{ab'_\alpha b_\alpha}^{[x(\alpha)]}$  are the solutions of the SEE's given in Eqs. (192)-(196).

$\hat{\mathcal{H}}$  in Eq. (201) can also be written as a shift of the few-body Hamiltonian  $\hat{H}_{FB}$ , i.e.  $\hat{\mathcal{H}} = I - \tau \hat{H}_{FB} + \mathcal{O}(\tau^2)$ , with  $\hat{H}_{FB}$  possessing the summation form as

$$\hat{H}_{FB} = \sum_{\langle i, j \rangle \in \text{cluster}} \hat{H}(s_i, s_j) + \sum_{\langle n \in \text{cluster}, \alpha \in \text{bath} \rangle} \hat{H}_{PB}(n, \alpha), \quad (203)$$

with  $\hat{\mathcal{H}}_\partial(n, \alpha) = I - \tau \hat{H}_{PB}(s_n, b_\alpha)$ . This equations gives a general form of the few-body Hamiltonian: the first term gives all the physical interactions inside the cluster, and the second gives the physical-bath interactions  $\hat{H}_{PB}(s_n, b_\alpha)$ .  $\hat{\mathcal{H}}$  can be solved by any finite-size algorithms, such as ED, DMRG, QMC, or finite-size PEPS [206] algorithms. Less error from the rank-1 decomposition will be caused since the interactions inside the cluster will be fully considered.

The ground state ansatz behind the few-body model is the iPEPS shown in Fig. 46, where the central cluster is entangled with the surrounding infinite-tree branches. Note that solving Eq. (192) in Stage one is equivalent to solving Eq. (201) by choose the cluster as small as a supercell. After acquiring the ground state of  $\hat{H}_{FB}$ , we calculate the reduced density matrix by tracing over the bath degrees of freedom, where the physical information of the original model can be extracted.

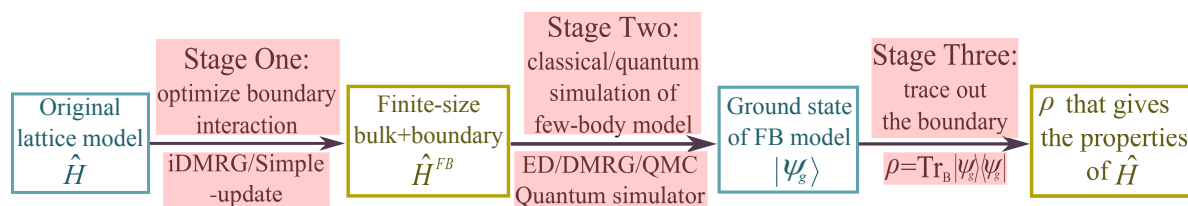


**Figure 47.** (Color online) The “*ab-initio* optimization principle” to simulate quantum many-body systems.

Some benchmark results of simulating 2D and 3D spin models can be found in Ref. [227]. For the ground state of Heisenberg model on honeycomb lattice, results of the magnetization and bond energy show that the few-body model of 18 physical and 12 bath sites only have the effect of  $O(10^{-3})$  to these quantities. For the ground state of Heisenberg model on cubic lattice, the difference of the energy per site is  $O(10^{-3})$  between the few-body model of 8 physical plus 24 bath sites and the model of 1000 sites by QMC. The quantum phase transition of the quantum Ising model on cubic lattice can also be accurately captured by such a few-body model, including determining the critical field and the critical exponent from the magnetization. This means that the critical phenomena is reproduced in the bulk of such a small system.

**4.7.3. “Ab-initio optimization principle” of tensor network for simulating quantum many-body systems** Here, we summarize the simulation procedures explained above, and give the “*ab-initio* optimization principle” (AOP) [123, 227] for simulating quantum many-body systems with few-body models.

The AOP simulation contains three stages (Fig. 47). The first stage is to optimize the physical-bath interactions in the few-body model by classical computations. The algorithm can be iDMRG or simple update. The second stage is to construct the few-body model by embedding a finite-size cluster in the entanglement bath, and simulate the ground state of this few-body model. One can employ any well-established finite-size algorithms (such as ED, finite-size DMRG, or QMC) by classical computations, or build quantum simulations. The third stage is to extract physical information by tracing over all bath degrees of freedom.

As to the classical computations in the AOP scheme, one will have a high flexibility to balance between the computational complexity and accuracy, according to the required precision and the computational resources at hand. On one hand, thanks to the infinite-tree branches of the PEPS ansatz, one can avoid the conventional finite-size effects faced by the previous ED, QMC or DMRG algorithms in standard finite-size models. In the few-body way, the system size is actually infinite. The approximation is that the loops beyond the supercell are destroyed in the manner of rank-1 approximation for a high efficiency with classical computations. On the other hand, the error from the destruction of the loops can be reduced in the second stage by considering a cluster larger than the supercell chosen in the simple update. It is important to note that the second stage would introduce no improvement if no larger loops are contained while increasing the size of the cluster. From this point of view,

we have no “finite-size effects” here but the errors caused by the finiteness of the considered loops. In addition, this “loop” scheme explains why we can flexibly change the size of the cluster. As shown in Sec. 4.5.3, it is to restore the rank-1 tensors inside the chosen cluster with the full tensor.

The relations among the related algorithms are illustrated in Fig. 48, by taking certain limits of the computational parameters. The simplest situation is to take the dimension of the bath sites  $\dim(b) = 1$ , and then  $\hat{\mathcal{H}}_\partial$  can be written as a linear combination of spin operators (and identity). Thus in this case,  $v^{[x]}$  simply plays the role of a mean field. If one only uses the bath calculation of the first stage to obtain the ground-state properties, the algorithm will be reduced to the tree DMRG. If one takes the minimal supercell with  $D = 1$  in stage one, the entanglement bath will be reduced to a magnetic mean field. By choosing a large cluster, the DMRG simulation in stage two becomes equivalent to the standard DMRG for solving the cluster in a mean field. If one uses  $D = 1$  and chooses a supercell of a tolerably large size in the first stage without entering stage two, or if one chooses a small cluster with  $D = 1$  in stage one and uses ED in stage two to solve the few-body Hamiltonian with a tolerably large cluster, our approach will become the ED on the corresponding finite system in a mean field. By taking proper supercell, cluster, algorithms and computational parameters, the AOP approach outperforms others.

The AOP approach with classical computations can be categorized as a cluster update scheme in the aspect of classical computations. Compared with the “traditional” cluster update schemes [135, 210, 211, 206], there are some similarities, where both optimally approximate the infinite environment by a finite one defined on a cluster. Importantly, there exist some essential differences. The key of the “traditional” cluster update schemes is to use the super-orthogonal spectrum to approximate the environment of the iPEPS for its optimal truncations during the evolution or variation. The central idea of AOP is different. In the second stage, what is approximated is the environment of the original Hamiltonian, not an iPEPS. And the environment is mimicked by the physical-bath Hamiltonians, not spectrums.

In addition, it is possible to use full update in the first stage to optimize the interactions related to the entanglement bath. For example, one may use TRD (iDMRG, iTEBD or CTMRG) to compute the environment tensors, instead of rank-1 decomposition in the simple update. This idea has not been realized yet, but it can be seen easily that the interactions among the bath sites will appear in  $\hat{H}_{FB}$ . Surely the computation will become much more expensive. It is not clear yet how the performance would be.

As reviewed in Sec. 1, the idea of “bath” has been utilized in many approaches and gained tremendous successes. The general idea these approaches share is to mimic the target model of high complexity by a simpler model embedded in a bath. The physics of the target model can be extracted by integrating over the bath degrees of freedom. The approximations are reflected by the underlying effective model. In Table 2, we show the effective models of two recognized methods (DFT and DMFT) as well as the AOP. An essential difference is that the effective models of the former two methods are under single-particle approximations, and the effective model of AOP is strongly correlated.

As to the quantum simulations, the AOP scheme possesses several unique advantages.

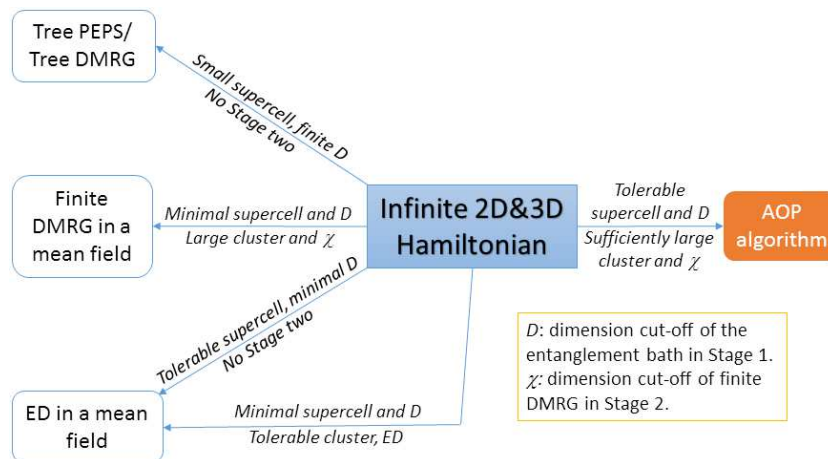


**Figure 48.** (Color online) Relations between several related algorithms (PEPS, DMRG and ED) for the ground-state simulations of 2D and 3D Hamiltonian. The corresponding computational set-ups in the first (bath calculation) and second (solving the few-body Hamiltonian) stages are given above and under the arrows, respectively. Reused from [227] with permission.

**Table 2.** The effective models under several bath-related methods: density functional theory (DFT, also known as the *ab-initio* calculations), dynamical mean-field theory (DMFT) and *ab-initio* optimization principle (AOP) of TN.

Methods	DFT	DMFT	AOP
<b>Effective models</b>	Tight binding model	Single impurity model	Interacting few-body model

The first advantage concerns the size. One main difficulty of building a quantum simulator is to access a large size. In this scheme, a few-body model of only  $O(10)$  sites shows a high accuracy with the error  $< O(10^{-3})$  [123, 227]. Such sizes are accessible by current experiments. Secondly, the interactions in the few-body model are simple. The bulk just contains the interactions of the original physical model. The physical-bath interactions are only nearest-neighbor. But there exist several challenges. Firstly, the physical-bath interaction for simulating, e.g., spin-1/2 models, is between a spin-1/2 and a higher spin. This may require the realization of the interactions between  $SU(N)$  spins, which is difficult but possible with current experimental techniques [361, 362, 363, 364]. The second challenge concerns the non-standard form in the physical-bath interaction, for example the  $\hat{S}^z \hat{S}^z$  coupling in  $\hat{H}_{FB}$  for simulating quantum Ising chain [see Eq. (187)] [358]. With the experimental realization of the few-body models, the numerical simulations of many-body systems will not only be useful to study natural materials. It would become possible to firstly study the many-body phenomena by numerics, and then realize, control, and even utilize these phenomena in small quantum devices.

## 5. Conclusion

The explosive progresses of the TN that have been made in recent years opened an interdisciplinary diagram for studying variates of subjects such as quantum many-body physics. What is more, the theories and techniques in the TN algorithms are now evolving into a new numerical field, providing a systematic framework of TN. This review is aimed at extracting this framework from the TN algorithms that was regarded independent to each other.

We review the TN contraction algorithms inspired by the numerical renormalization group (NRG). The idea is to contract the TN and truncate to bound the dimensions. For the contraction procedure, the key is the contraction order, which leads to the exponential, linearized, and polynomial contraction algorithms according to how the size of the TN decreases. For the truncation, the key is the environment, which plays the role of the reference when determining the importance of the basis. We have the simple, cluster, and full decimation schemes, where the environment is chosen to be a local tensor, a local but larger cluster, and the whole TN, respectively. When the environment becomes larger, the accuracy increases, but so do the computational costs. Thus, it is important to balance between the efficiency and accuracy. Then, we show that by explicitly writing the truncations in the TN, we are essentially contracting exactly contractible TN's, which provides a bridge to the TN schemes in Sec. 4.

In Sec. 4, we review the TN algorithms based on self-consistent eigenvalue equations (SEE's), aiming mainly at the optimal truncations of the bond dimensions of TN states, i.e., update algorithms. Such algorithms follow another clue that is different from the NRG-inspired methods to solve TN contraction. The TN contraction is solved without actually contracting, but by building a set of local self-consistent equations that could reconstruct the target TN. The SEE's are parameterized by both the cell tensor that defines the TN and the variational tensors (the solution), thus can be solved in a recursive manner. The relations between the SSE's-based TN algorithms and the multi-linear algebra (including network Tucker decomposition, rank-1 decomposition, and tensor ring decomposition (TRD)) are discussed. This provides a systematic way of understanding the simple, cluster and full update algorithms. Finally, we explain the *ab-initio* optimization principle for the optimal classical/quantum simulations of many-body systems by few-body models.

With the review, we expect that the readers could use the existing TN algorithms to solve their problems. Moreover, we hope that those who are interested in TN itself could get the ideas and connections behind the algorithms to develop new TN schemes.

## Acknowledgments

We are indebted to Ignacio Cirac, Mari-Carmen Bañuls, Jan von Delft, Andreas Weichselbaum, Tomotoshi Nishino, Tao Xiang, José Ignacio Latorre, Didier Poilblanc, Wei Li, Yichen Huang, Michael Lubasch, Xin Yan for helpful discussions and suggestions. This work was supported by ERC AdG OSYRIS (ERC-2013-AdG Grant No. 339106),

Spanish Ministry MINECO (National Plan 15 Grant: FISICATEAMO No. FIS2016-79508-P, SEVERO OCHOA No. SEV-2015-0522), Generalitat de Catalunya (AGAUR Grant No. 2017 SGR 1341 and CERCA/Program), Fundació Privada Cellex, EU FETPRO QUIC (H2020-FETPROACT-2014 No. 641122), the National Science Centre, and Poland-Symfonia Grant No. 2016/20/W/ST4/00314. SJR acknowledges Fundació Catalunya - La Pedrera · Ignacio Cirac Program Chair. CP, XC, and GS were supported in part by the MOST (Grant No. 2018YFA0305800), NSFC (Grant No. 11474279), and the Key Research Program of the CAS (Grant No. XDB07010100 and No. XDPB08).

- [1] C. David Sherrill. Frontiers in electronic structure theory. *J. Chem. Phys.*, 132:110902, 2010.
- [2] Kieron Burke. Perspective on density functional theory. *J. Chem. Phys.*, 136:150901, 2012.
- [3] Axel D. Becke. Perspective: Fifty years of density-functional theory in chemical physics. *J. Chem. Phys.*, 140, 2014.
- [4] Christian P. Robert. *Monte carlo methods*. Wiley Online Library, 2004.
- [5] Patrick A. Lee, Naoto Nagaosa, and Xiao-Gang Wen. Doping a Mott insulator: Physics of high-temperature superconductivity. *Rev. Mod. Phys.*, 78:17–85, January 2006.
- [6] Bernhard Keimer, Steven A. Kivelson, Michael R. Norman, Shinichi Uchida, and J. Zaanen. From quantum matter to high-temperature superconductivity in copper oxides. *Nature*, 518(7538):179, 2015.
- [7] Robert B. Laughlin. Nobel Lecture: Fractional quantization. *Rev. Mod. Phys.*, 71:863–874, July 1999.
- [8] Kenneth G. Willson. The renormalization group: Critical phenomena and the Kondo problem. *Rev. Mod. Phys.*, 47:773, 1975.
- [9] Mitchel D. Kovarik. Numerical solution of large  $s = 1/2$  and  $s = 1$  heisenberg antiferromagnetic spin chains using a truncated basis expansion. *Phys. Rev. B*, 41:6889–6898, April 1990.
- [10] Tao Xiang and Gillian A. Gehring. Real space renormalisation group study of Heisenberg spin chain. *J. Magn. Magn. Mater.*, 104:861–862, 1992.
- [11] Tao Xiang and Gillian A. Gehring. Numerical solution of  $S = 1$  antiferromagnetic spin chains using a truncated basis expansion. *Phys. Rev. B*, 48:303–310, July 1993.
- [12] Jun Kondo. Resistance Minimum in Dilute Magnetic Alloys. *Prog. Theor. Phys.*, 32:37–49, 1964.
- [13] Steven R. White and Reinhard M. Noack. Real-space quantum renormalization groups. *Phys. Rev. Lett.*, 68:3487, 1992.
- [14] Steven R. White. Density matrix formulation for quantum renormalization groups. *Phys. Rev. Lett.*, 69:2863, 1992.
- [15] Steven R. White. Density-matrix algorithms for quantum renormalization groups. *Phys. Rev. B*, 48:10345–10356, October 1993.
- [16] Ulrich Schollwöck. The density-matrix renormalization group. *Rev. Mod. Phys.*, 77:259–315, Apr 2005.
- [17] Ulrich Schollwöck. The density-matrix renormalization group in the age of matrix product states. *Ann. Phys.*, 326:96–192, 2011.
- [18] Xiaoqun Wang and Tao Xiang. Transfer-matrix density-matrix renormalization-group theory for thermodynamics of one-dimensional quantum systems. *Phys. Rev. B*, 56(9):5061, 1997.
- [19] Tomotoshi Nishino and Kouichi Okunishi. Corner transfer matrix renormalization group method. *J. Phys. Soc. Jpn.*, 65:891–894, 1996.
- [20] Charles H. Bennett and David P. DiVincenzo. Quantum information and computation. *Nature*, 404:247–255, 2000.
- [21] Michael. A. Nielsen and Isaac L. Chuang. *Quantum Computation and Quantum Communication*. Cambridge University Press, Cambridge, England, 2000.
- [22] Luigi Amico, Rosario Fazio, Andreas Osterloh, and Vlatko Vedral. Entanglement in many-body systems. *Rev. Mod. Phys.*, 80:517, 2008.
- [23] Ryszard Horodecki, Pawel Horodecki, Michal Horodecki, and Karol Horodecki. Quantum entanglement. *Rev. Mod. Phys.*, 81:865, 2009.



- [24] Stellan Östlund and Stefan Rommer. Thermodynamic limit of density matrix renormalization. Phys. Rev. Lett., 75:3537, 1995.
- [25] Tobias J. Osborne and Michael A. Nielsen. Entanglement, Quantum Phase Transitions, and Density Matrix Renormalization. Quantum Information Processing, 1(1):45–53, April 2002.
- [26] Guifré Vidal. Efficient Classical Simulation of Slightly Entangled Quantum Computations. Phys. Rev. Lett., 91:147902, October 2003.
- [27] Frank Verstraete, Diego Porras, and J. Ignacio Cirac. Density Matrix Renormalization Group and Periodic Boundary Conditions: A Quantum Information Perspective. Phys. Rev. Lett., 93:227205, November 2004.
- [28] Guifré Vidal. Efficient Simulation of One-Dimensional Quantum Many-Body Systems. Phys. Rev. Lett., 93:040502, July 2004.
- [29] Mark Fannes, Bruno Nachtergaele, and Reinhard F. Werner. Finitely correlated states on quantum spin chains. Comm. Math. Phys., 144:443–490, 1992.
- [30] Stefan Rommer and Stellan Östlund. Class of ansatz wave functions for one-dimensional spin systems and their relation to the density matrix renormalization group. Phys. Rev. B, 55:2164, 1997.
- [31] Jorge Dukelsky, Miguel A. Martín-Delgado, Tomotoshi Nishino, and Germán Sierra. Equivalence of the variational matrix product method and the density matrix renormalization group applied to spin chains. Europhys. Lett., 43:457, 1998.
- [32] Ian P. McCulloch. From density-matrix renormalization group to matrix product states. J. Stat. Mech. Theory Exp., 10, 2007.
- [33] David Pérez-García, Frank Verstraete, Michael M. Wolf, and J. Ignacio Cirac. Matrix Product State Representations. Quantum Inf. Comput., 7:401, 2007.
- [34] Rodney J. Baxter. Dimers on a Rectangular Lattice. J. Math. Phys., 9:650, 1968.
- [35] M. P. Nightingale and H. W. J. Blöte. Gap of the linear spin-1 Heisenberg antiferromagnet: A Monte Carlo calculation. Phys. Rev. B, 33:659–661, January 1986.
- [36] Bernard Derrida and Martin R. Evans. Exact correlation functions in an asymmetric exclusion model with open boundaries. Journal de Physique I, 3(2):311–322, 1993.
- [37] Bernard Derrida, Martin R. Evans, Vincent Hakim, and Vincent Pasquier. Exact solution of a 1D asymmetric exclusion model using a matrix formulation. J. Phys. A: Mathematical and General, 26(7):1493, 1993.
- [38] Ian Affleck, Tom Kennedy, Elliott H. Lieb, and Hal Tasaki. Rigorous results on valence-bond ground states in antiferromagnets. Phys. Rev. Lett., 59:799, 1987.
- [39] Ian Affleck, Tom Kennedy, Elliott H. Lieb, and Hal Tasaki. Valence bond ground states in isotropic quantum antiferromagnets. Comm. Math. Phys., 115(3):477–528, 1988.
- [40] Mark Fannes, Bruno Nachtergaele, and Reinhard F. Werner. Ground states of VBS models on Cayley trees. J. Stat. Phys., 66:939, 1992.
- [41] Harald Niggemann, Andreas Klümper, and Johannes Zittartz. Quantum phase transition in spin-3/2 systems on the hexagonal lattice—optimum ground state approach. Z. Phys. B, 104:103, 1997.
- [42] Harald Niggemann, Andreas Klümper, and Johannes Zittartz. Ground state phase diagram of a spin-2 antiferromagnet on the square lattice. Eur. Phys. J. B, 13:15, 2000.
- [43] Frank Verstraete, Miguel A. Martín-Delgado, and J. Ignacio Cirac. Diverging entanglement length in gapped quantum spin systems. Phys. Rev. Lett., 92:087201, 2004.
- [44] Vahid Karimipour and Laleh Memarzadeh. Matrix product representations for all valence bond states. Phys. Rev. B, 77:094416, 2008.
- [45] Frank Verstraete and J. Ignacio Cirac. Continuous Matrix Product States for Quantum Fields. Phys. Rev. Lett., 104:190405, 2010.
- [46] Matthew B. Hastings. Locality in quantum and Markov dynamics on lattices and networks. Phys. Rev. Lett., 93:140402, 2004.
- [47] Matthew B. Hastings. Lieb-Schultz-Mattis in higher dimensions. Phys. Rev. B, 69:104431, 2004.
- [48] Matthew B. Hastings. An area law for one-dimensional quantum systems. J. Stat. Mech.: Theory and Experiment, 2007(08), 2007.

- [49] Yichen Huang. Classical simulation of quantum many-body systems. University of California, Berkeley, 2015.
- [50] Frank Verstraete and J. Ignacio Cirac. Matrix product states represent ground states faithfully. Phys. Rev. B, 73:094423, 2006.
- [51] Jacob D. Bekenstein. Black Holes and Entropy. Phys. Rev. D, 7:2333–2346, April 1973.
- [52] Mark Srednicki. Entropy and area. Phys. Rev. Lett., 71:666–669, August 1993.
- [53] José I. Latorre, Enrique Rico, and Guifré Vidal. Ground state entanglement in quantum spin chains. Quant. Inf. Comp., 4:48, 2004.
- [54] Pasquale Calabrese and John Cardy. Entanglement entropy and quantum field theory. J. Stat. Mech.: Theory and Experiment, 2004(06), 2004.
- [55] Martin B. Plenio, Jens Eisert, J. Dreissig, and Marcus Cramer. Entropy, Entanglement, and Area: Analytical Results for Harmonic Lattice Systems. Phys. Rev. Lett., 94:060503, February 2005.
- [56] Jens Eisert, Marcus Cramer, and Martin B. Plenio. Colloquium: Area laws for the entanglement entropy. Rev. Mod. Phys., 82:277, 2010.
- [57] Frank Verstraete, Valentin Murg, and J. Ignacio Cirac. Matrix product states, projected entangled pair states, and variational renormalization group methods for quantum spin systems. Advances in Physics, 57:143–224, 2008.
- [58] Guifré Vidal. Efficient classical simulation of slightly entangled quantum computations. Phys. Rev. Lett., 91:147902, 2003.
- [59] Guifré Vidal. Efficient Simulation of One-Dimensional Quantum Many-Body Systems. Phys. Rev. Lett., 93:040502, 2004.
- [60] Guifré Vidal. Classical Simulation of Infinite-Size Quantum Lattice Systems in One Spatial Dimension. Phys. Rev. Lett., 98:070201, 2007.
- [61] Roman. Orús and Guifré Vidal. Infinite time-evolving block decimation algorithm beyond unitary evolution. Phys. Rev. B, 78:155117, October 2008.
- [62] Jutho Haegeman, J. Ignacio Cirac, Tobias J. Osborne, Iztok Pižorn, Henri Verschelde, and Frank Verstraete. Time-dependent variational principle for quantum lattices. Phys. Rev. Lett., 107:070601, 2011.
- [63] Sung G. Chung and Lihua Wang. Entanglement perturbation theory for the elementary excitation in one dimension. Phys. Lett. A, 373(26):2277–2280, 2009.
- [64] Hale F. Trotter. On the product of semi-groups of operators. Proceedings of the American Mathematical Society, 10(4):545–551, 1959.
- [65] M. Suzuki and M. Inoue. The ST-transformation approach to analytic solutions of quantum systems. I general formulations and basic limit theorems. Prog. Theor. Phys., 78:787, 1987.
- [66] Makoto Inoue and Masuo Suzuki. The ST-transformation approach to analytic solutions of quantum systems. II: Transfer-matrix and Pfaffian methods. Progress of theoretical physics, 79(3):645–664, 1988.
- [67] Michael Levin and Cody P. Nave. Tensor renormalization group approach to two-dimensional classical lattice models. Phys. Rev. Lett., 99:120601, 2007.
- [68] Christoph Holzhey, Finn Larsen, and Frank Wilczek. Geometric and renormalized entropy in conformal field theory. Nuclear Physics B, 424(3):443–467, 1994.
- [69] Guifré Vidal, José I. Latorre, Enrique Rico, and Alexei Kitaev. Entanglement in Quantum Critical Phenomena. Phys. Rev. Lett., 90:227902, June 2003.
- [70] Luca Tagliacozzo, Thiago de Oliveira, Sofyan Iblisdir, and José I. Latorre. Scaling of entanglement support for matrix product states. Phys. Rev. B, 78:024410, July 2008.
- [71] Frank Pollmann, Subroto Mukerjee, Ari M. Turner, and Joel E. Moore. Theory of Finite-Entanglement Scaling at One-Dimensional Quantum Critical Points. Phys. Rev. Lett., 102:255701, June 2009.
- [72] J. Ignacio Cirac and Germán Sierra. Infinite matrix product states, conformal field theory, and the haldane-shastry model. Phys. Rev. B, 81:104431, Mar 2010.
- [73] Hong-Hao Tu and Germán Sierra. Infinite matrix product states, boundary conformal field theory, and the open haldane-shastry model. Phys. Rev. B, 92:041119, Jul 2015.

- [74] Shi-Ju Ran, Cheng Peng, Wei Li, Maciej Lewenstein, and Gang Su. Criticality in two-dimensional quantum systems: Tensor network approach. *Phys. Rev. B*, 95:155114, April 2017.
- [75] Steven R. White, Douglas J. Scalapino, Robert L. Sugar, E. Y. Loh, James E. Gubernatis, and Richard T. Scalettar. Numerical study of the two-dimensional Hubbard model. *Phys. Rev. B*, 40:506–516, 1989.
- [76] Matthias Troyer and Uwe-Jens Wiese. Computational complexity and fundamental limitations to fermionic quantum Monte Carlo simulations. *Phys. Rev. Lett.*, 94:170201, 2005.
- [77] Steven R. White and Douglas J. Scalapino. Density matrix renormalization group study of the striped phase in the 2D t-J model. *Phys. Rev. Lett.*, 80:1272, 1998.
- [78] Tao Xiang, Jizhong Lou, and Zhaobin Su. Two-dimensional algorithm of the density-matrix renormalization group. *Phys. Rev. B*, 64:104414, August 2001.
- [79] Edwin M. Stoudenmire and Steven R. White. Studying two-dimensional systems with the density matrix renormalization group. *Ann. Rev. Cond. Matter Phys.*, 3:111–128, 2012.
- [80] Norbert Schuch, Michael M. Wolf, Frank Verstraete, and J. Ignacio Cirac. Entropy Scaling and Simulability by Matrix Product States. *Phys. Rev. Lett.*, 100:030504, January 2008.
- [81] Frédéric Mila. Quantum spin liquids. *Europ. J. Phys.*, 21(6):499, 2000.
- [82] Leon Balents. Spin liquids in frustrated magnets. *Nature*, 464:199, 2010.
- [83] Lucile Savary and Leon Balents. Quantum spin liquids: a review. *Reports on Progress in Physics*, 80:016502, 2017.
- [84] Hong-Chen Jiang, Zheng-Yu Weng, and Donna N. Sheng. Density matrix renormalization group numerical study of the kagome antiferromagnet. *Phys. Rev. Lett.*, 101:117203, 2008.
- [85] Simeng Yan, David A. Huse, and Steven R. White. Spin-liquid ground state of the  $s=1/2$  kagome heisenberg antiferromagnet. *Science*, 332(6034):1173–1176, 2011.
- [86] Hong-Chen Jiang, Zhenghan Wang, and Leon Balents. Identifying topological order by entanglement entropy. *Nat. Phys.*, 8:902–905, 2012.
- [87] Stefan Depenbrock, Ian P. McCulloch, and Ulrich Schollwöck. Nature of the spin-liquid ground state of the  $s = 1/2$  heisenberg model on the kagome lattice. *Phys. Rev. Lett.*, 109:067201, August 2012.
- [88] Satoshi Nishimoto, Naokazu Shibata, and Chisa Hotta. Controlling frustrated liquids and solids with an applied field in a kagome Heisenberg antiferromagnet. *Nat. Comm.*, 4:2287, 2012.
- [89] Yin-Chen He, Michael P. Zaletel, Masaki Oshikawa, and Frank Pollmann. Signatures of Dirac Cones in a DMRG Study of the Kagome Heisenberg Model. *Phys. Rev. X*, 7:031020, July 2017.
- [90] Yasuhiro Hieida, Kouichi Okunishi, and Yasuhiro Akutsu. Numerical renormalization approach to two-dimensional quantum antiferromagnets with valence-bond-solid type ground state. *New J. Phys.*, 1(1):7, 1999.
- [91] Miguel. A. Martín-Delgado, Marco. Roncaglia, and German. Sierra. Stripe ansätze from exactly solved models. *Phys. Rev. B*, 64:075117, Jul 2001.
- [92] Tomotoshi Nishino, Yasuhiro Hieida, Kouichi Okunishi, Nobuya Maeshima, Yasuhiro Akutsu, and Andrej Gendiar. Two-Dimensional Tensor Product Variational Formulation. *Prog. Theor. Phys.*, 105(3):409–417, 2001.
- [93] Nobuya Maeshima, Yasuhiro Hieida, Yasuhiro Akutsu, Tomotoshi Nishino, and Kouichi Okunishi. Vertical density matrix algorithm: A higher-dimensional numerical renormalization scheme based on the tensor product state ansatz. *Phys. Rev. E*, 64:016705, Jun 2001.
- [94] Franc Verstraete and J. Ignacio Cirac. Valence-bond states for quantum computation. *Phys. Rev. A*, 70:060302, December 2004.
- [95] Frank Verstraete and J. Ignacio Cirac. Renormalization algorithms for Quantum-Many Body Systems in two and higher dimensions.
- [96] Tom Kennedy, Elliott H. Lieb, and Hal Tasaki. A two-dimensional isotropic quantum antiferromagnet with unique disordered ground state. *J. Stat. Phys.*, 53(1):383–415, Oct 1988.
- [97] Frank Verstraete, Michael M. Wolf, David Pérez-García, and J. Ignacio Cirac. Criticality, the area law, and the computational power of projected entangled pair states. *Phys. Rev. Lett.*, 96:220601, 2006.
- [98] Didier Poilblanc, Norbert Schuch, David Pérez-García, and J. Ignacio Cirac. Topological and entanglement properties of resonating valence bond wave functions. *Phys. Rev. B*, 86:014404, 2012.

- [99] Norbert Schuch, Didier Poilblanc, J. Ignacio Cirac, and David Pérez-García. Resonating valence bond states in the PEPS formalism. Phys. Rev. B, 86:115108, 2012.
- [100] Ling Wang, Didier Poilblanc, Zheng-Cheng Gu, Xiao-Gang Wen, and Frank Verstraete. Constructing a gapless spin-liquid state for the spin-1/2  $j_1$ - $j_2$  heisenberg model on a square lattice. Phys. Rev. Lett., 111:037202, 2013.
- [101] Didier Poilblanc, Philippe Corboz, Norbert Schuch, and J. Ignacio Cirac. Resonating-valence-bond superconductors with fermionic projected entangled pair states. Phys. Rev. B, 89:241106, R.
- [102] Philip W. Anderson. Resonating valence bonds: A new kind of insulator? Materials Research Bulletin, 8(2):153–160, 1973.
- [103] Patrick Fazekas and Philip W. Anderson. On the ground state properties of the anisotropic triangular antiferromagnet. Philos. Mag., 30:423, 1974.
- [104] Philip W. Anderson. The resonating valence bond state in  $la_2cuo_4$  and superconductivity. Science, 235:1196, 1987.
- [105] Ganapathy Baskaran, Zhou. Zou, and Philip W. Anderson. The resonating valence bond state and high- $t_c$  superconductivity: A mean field theory. Solid State Communications, 63(11):973–976, 1987.
- [106] Philip W. Anderson, Ganapathy Baskaran, Zhou. Zou, and T. Hsu. Resonating-valence-bond theory of phase transitions and superconductivity in  $la_2cuo_4$ -based compounds. Phys. Rev. Lett., 58:2790–2793, 1987.
- [107] Zheng-Cheng Gu, Michael Levin, Brian Swingle, and Xiao-Gang Wen. Tensor-product representations for string-net condensed states. Phys. Rev. B, 79:085118, 2009.
- [108] Oliver Buerschaper, Miguel Aguado, and Guifré Vidal. Explicit tensor network representation for the ground states of string-net models. Phys. Rev. B, 79:085119, 2009.
- [109] Xie Chen, Bei Zeng, Zheng-Cheng Gu, Isaac L. Chuang, and Xiao-Gang Wen. Tensor product representation of a topological ordered phase: Necessary symmetry conditions. Phys. Rev. B, 82:165119, 2010.
- [110] Xiao-Gang Wen. Vacuum degeneracy of chiral spin states in compactified space. Phys. Rev. B, 40:7387, 1989.
- [111] Xiao-Gang Wen. Topological orders in rigid states. Int. J. Mod. Phys. B, 4:239, 1990.
- [112] Xiao-Gang Wen and Qian Niu. Ground-state degeneracy of the fractional quantum Hall states in the presence of a random potential and on high-genus Riemann surfaces. Phys. Rev. B, 41:9377, 1990.
- [113] Xiao-Gang Wen. Topological orders and edge excitations in fractional quantum Hall states. Advanc. Phys., 44:405, 1995.
- [114] Michael Levin and Xiao-Gang Wen. String-net condensation: A physical mechanism for topological phases. Phys. Rev. B, 71:045110, 2005.
- [115] Michael Levin and Xiao-Gang Wen. Colloquium: Photons and electrons as emergent phenomena. Rev. Mod. Phys., 77:871–879, 2005.
- [116] Xiao-Gang Wen. An introduction to quantum order, string-net condensation, and emergence of light and fermions. Ann. Phys., 316:1–29, 2005.
- [117] Norbert Schuch, Michael M. Wolf, Frank Verstraete, and J. Ignacio Cirac. Computational complexity of projected entangled pair states. Phys. Rev. Lett., 98:140506, 2007.
- [118] Artur García-Sáez and José I. Latorre. An exact tensor network for the 3SAT problem. arXiv:1105.3201, 2011.
- [119] Thomas Hucklea, Konrad Waldherra, and Thomas Schulte-Herbrüggen. Computations in quantum tensor networks. Linear Algebra Application, 438:750–781, 2013.
- [120] Anders W. Sandvik and Guifre Vidal. Variational Quantum Monte Carlo Simulations with Tensor-Network States. Phys. Rev. Lett., 99:220602, November 2007.
- [121] Laurens Vanderstraeten, Jutho Haegeman, Philippe Corboz, and Frank Verstraete. Gradient methods for variational optimization of projected entangled-pair states. Phys. Rev. B, 94:155123, 2016.
- [122] Shi-Ju Ran, Bin Xi, Tie-Yan Liu, and Gang Su. Theory of network contractor dynamics for exploring thermodynamic properties of two-dimensional quantum lattice models. Phys. Rev. B, 88:064407, 2013.
- [123] Shi-Ju Ran. Ab initio optimization principle for the ground states of translationally invariant strongly

- correlated quantum lattice models. Phys. Rev. E, 93:053310, 2016.
- [124] Shi-Ju Ran, Wei Li, Bin Xi, Zhe Zhang, and Gang Su. Optimized decimation of tensor networks with super-orthogonalization for two-dimensional quantum lattice models. Phys. Rev. B, 86:134429, 2012.
- [125] Edwin Stoudenmire and David J. Schwab. Supervised learning with tensor networks. In Advances in Neural Information Processing Systems, pages 4799–4807, 2016.
- [126] Zhi-Yuan Xie, Jack Chen, Jing F. Yu, Xianghua Kong, Bruce Normand, and Tao Xiang. Tensor renormalization of quantum many-body systems using projected entangled simplex states. Phys. Rev. X, 4(1):011025, 2014.
- [127] Hai-Jun Liao, Zhi-Yuan Xie, Jack Chen, Zheng-Xin Liu, Hai-Dong Xie, Rui-Zhen Huang, Bruce Normand, and Tao Xiang. Gapless spin-liquid ground state in the  $s = 1/2$  kagome antiferromagnet. Phys. Rev. Lett., 118(13):137202, 2017.
- [128] Barry Friedman. A density matrix renormalization group approach to interacting quantum systems on Cayley trees. J. Phys.: Condens. Matter, 9:9021, 1997.
- [129] Marie-Bernadette Lepetit, Maixent Cousy, and Gustavo M. Pastor. Density-matrix renormalization study of the Hubbard model on a Bethe lattice. Eur. Phys. J. B, 13:421, 2000.
- [130] Miguel A. Martin-Delgado, Javier Rodriguez-Laguna, and Germán Sierra. Density-matrix renormalization-group study of excitons in dendrimers. Phys. Rev. B, 65:155116, 2002.
- [131] Yaoyun Y. Shi, Luming M. Duan, and Guifré Vidal. Classical simulation of quantum many-body systems with a tree tensor network. Phys. Rev. A, 74:022320, 2006.
- [132] Daniel Nagaj, Edward Farhi, Jeffrey Goldstone, Peter Shor, and Igor Sylvester. Quantum transverse-field Ising model on an infinite tree from matrix product states. Phys. Rev. B, 77:214431, 2008.
- [133] Luca Tagliacozzo, Glen Evenbly, and Guifré Vidal. Simulation of two-dimensional quantum systems using a tree tensor network that exploits the entropic area law. Phys. Rev. B, 80:235127, 2009.
- [134] Valentin Murg, Frank Verstraete, Örs Legeza, and Reinhard M. Noack. Simulating strongly correlated quantum systems with tree tensor networks. Phys. Rev. B, 82:205105, 2010.
- [135] Wei Li, Jan von Delft, and Tao Xiang. Efficient simulation of infinite tree tensor network states on the Bethe lattice. Phys. Rev. B, 86:195137, 2012.
- [136] Naoki Nakatani and Garnet K. L. Chan. Efficient tree tensor network states (TTNS) for quantum chemistry: Generalizations of the density matrix renormalization group algorithm. J. Chem. Phys., 138:134113, 2013.
- [137] Iztok Pižorn, Frank Verstraete, and Robert M. Konik. Tree tensor networks and entanglement spectra. Phys. Rev. B, 88:195102, 2013.
- [138] Valentin Murg, Frank Verstraete, Reinhold Schneider, Peter R. Nagy, and Örs Legeza. Tree Tensor Network State with Variable Tensor Order: An Efficient Multireference Method for Strongly Correlated Systems. J. Chem. Theory Comput., 11:1027–1036, 2015.
- [139] Guifré Vidal. Entanglement renormalization. Phys. Rev. Lett., 99:220405, 2007.
- [140] Guifré Vidal. Class of quantum many-body states that can be efficiently simulated. Phys. Rev. Lett., 101:110501, 2008.
- [141] Lukasz Cincio, Jacek Dziarmaga, and Marek M. Rams. Multiscale entanglement renormalization ansatz in two dimensions: quantum Ising model. Phys. Rev. Lett., 100:240603, 2008.
- [142] Glen Evenbly and Guifré Vidal. Entanglement renormalization in two spatial dimensions. Phys. Rev. Lett., 102:180406, 2009.
- [143] Miguel Aguado and Guifré Vidal. Entanglement renormalization and topological order. Phys. Rev. Lett., 100:070404, 2008.
- [144] Glen Evenbly and Guifré Vidal. Algorithms for entanglement renormalization. Phys. Rev. B, 79:144108, 2009.
- [145] Philippe Corboz and Guifré Vidal. Fermionic multiscale entanglement renormalization ansatz. Phys. Rev. B, 80:165129, 2009.
- [146] Glen Evenbly and Guifré Vidal. Entanglement renormalization in free bosonic systems: real-space versus momentum-space renormalization group transforms. New J. Phys., 12:025007, 2010.
- [147] Glen Evenbly and Guifré Vidal. Entanglement renormalization in noninteracting fermionic systems.

- Phys. Rev. B, 81:235102, 2010.
- [148] Robert N. C. Pfeifer, Glen Evenbly, and Guifré Vidal. Entanglement renormalization, scale invariance, and quantum criticality. Phys. Rev. A, 79:040301, April 2009.
- [149] Simone Montangero, Matteo Rizzi, Vittorio Giovannetti, and Rosario Fazio. Critical exponents with a multiscale entanglement renormalization Ansatz channel. Phys. Rev. B, 80:113103, September 2009.
- [150] Glen Evenbly, Philippe Corboz, and Guifré Vidal. Nonlocal scaling operators with entanglement renormalization. Phys. Rev. B, 82:132411, 2010.
- [151] Pietro Silvi, Vittorio Giovannetti, Pasquale Calabrese, Giuseppe E. Santoro, and Rosario Fazio. Entanglement renormalization and boundary critical phenomena. J. Statist. Mechan., 2010, 2010.
- [152] G. Evenbly, R. N. C. Pfeifer, V. Picó, S. Iblisdir, L. Tagliacozzo, I. P. McCulloch, and G. Vidal. Boundary quantum critical phenomena with entanglement renormalization. Phys. Rev. B, 82(16):161107, 2010.
- [153] Glen Evenbly and Guifré Vidal. Quantum criticality with the multi-scale entanglement renormalization ansatz. Strongly Correlated Systems, Springer, 176:99–130, 2013.
- [154] Glen Evenbly and Guifré Vidal. Quantum Criticality with the Multi-scale Entanglement Renormalization Ansatz, pages 99–130. Springer Berlin Heidelberg, Berlin, Heidelberg, 2013.
- [155] Glen. Evenbly and Guifré. Vidal. Algorithms for entanglement renormalization: Boundaries, impurities and interfaces. J. Stat. Phys., 157(4):931–978, Dec 2014.
- [156] Jacob C. Bridgeman, Aroon O’Brien, Stephen D. Bartlett, and Andrew C. Doherty. Multiscale entanglement renormalization ansatz for spin chains with continuously varying criticality. Phys. Rev. B, 91:165129, 2015.
- [157] Glen Evenbly and Guifré Vidal. Tensor Network States and Geometry. J. Stat. Phys., 145:891–918, 2011.
- [158] Brian Swingle. Entanglement renormalization and holography. Phys. Rev. D, 86:065007, 2012.
- [159] Brian Swingle. Constructing holographic spacetimes using entanglement renormalization. arXiv:1209.3304, 2012.
- [160] Masahiro Nozaki, Shinsei Ryu, and Tadashi Takayanagi. Holographic geometry of entanglement renormalization in quantum field theories. Journal of High Energy Physics, 2012(10):193, 2012.
- [161] Cedric Beny. Causal structure of the entanglement renormalization ansatz. New J. Phys., 15:023020, 2013.
- [162] Xiao-Liang Qi. Exact holographic mapping and emergent space-time geometry. arXiv:1309.6282.
- [163] Masamichi Miyaji, Tokiro Numasawa, Noburo Shiba, Tadashi Takayanagi, and Kento Watanabe. Continuous Multiscale Entanglement Renormalization Ansatz as Holographic Surface-State Correspondence. Phys. Rev. Lett., 115:171602, 2015.
- [164] Ning Bao, ChunJun Cao, Sean M. Carroll, Aidan Chatwin-Davies, Nicholas Hunter-Jones, Jason Pollack, and Grant N. Remmen. Consistency conditions for an AdS multiscale entanglement renormalization ansatz correspondence. Phys. Rev. D, 91:125036, 2015.
- [165] Bartłomiej Czech, Lampros Lamprou, Samuel McCandlish, and James Sully. Integral Geometry and Holography. arXiv:1505.05515.
- [166] Makoto Natsuume. Ads/CFT Duality User Guide, Lect. Notes in Phys. 903. Springer, Tokyo, 2015.
- [167] Jozef Genzor, Andrej Gendiar, and Tomotoshi Nishino. Phase transition of the Ising model on a fractal lattice. Phys. Rev. E, 93:012141, January 2016.
- [168] Meng Wang, Shi-Ju Ran, Tao Liu, Yang Zhao, Qing-Rong Zheng, and Gang Su. Phase diagram and exotic spin-spin correlations of anisotropic Ising model on the Sierpiński gasket. Europ. Phys. J. B, 89(2):1–10, 2016.
- [169] Samuel J. Denny, Jacob D. Biamonte, Dieter Jaksch, and Stephen R. Clark. Algebraically contractible topological tensor network states. J. Phys. A: Math. Theor., 45:015309, 2012.
- [170] Frank Verstraete, Juan J. García-Ripoll, and J. Ignacio Cirac. Matrix Product Density Operators: Simulation of Finite-Temperature and Dissipative Systems. Phys. Rev. Lett., 93:207204, November 2004.
- [171] Michael Zwolak and Guifré Vidal. Mixed-State Dynamics in One-Dimensional Quantum Lattice Systems: A Time-Dependent Superoperator Renormalization Algorithm. Phys. Rev. Lett., 93:207205, November 2004.

- [172] Bogdan Pirvu, Valentin Murg, Ignacio J. Cirac, and Frank Verstraete. Matrix product operator representations. New J. Phys., 12(2):025012, 2010.
- [173] Wei Li, Shi-Ju Ran, Shou-Shu Gong, Yang Zhao, Bin Xi, Fei Ye, and Gang Su. Linearized tensor renormalization group algorithm for the calculation of thermodynamic properties of quantum lattice models. Phys. Rev. Lett., 106:127202, 2011.
- [174] Jonas Becker, Thomas Köhler, Alexander C. Tiegel, Salvatore R. Manmana, Stefan Wessel, and Andreas Honecker. Finite-temperature dynamics and thermal intraband magnon scattering in Haldane spin-one chains. Phys. Rev. B, 96:060403, August 2017.
- [175] Adil A. Gangat, Te I, and Ying-Jer Kao. Steady States of Infinite-Size Dissipative Quantum Chains via Imaginary Time Evolution. Phys. Rev. Lett., 119:010501, July 2017.
- [176] Bin-Bin Chen, Yun-Jing Liu, Ziyu Chen, and Wei Li. Series-expansion thermal tensor network approach for quantum lattice models. Phys. Rev. B, 95:161104, Apr 2017.
- [177] Yong-Liang Dong, Lei Chen, Yun-Jing Liu, and Wei Li. Bilayer linearized tensor renormalization group approach for thermal tensor networks. Phys. Rev. B, 95:144428, Apr 2017.
- [178] Florian Fröwis, Volckmar Nebendahl, and Wolfgang Dür. Tensor operators: Constructions and applications for long-range interaction systems. Phys. Rev. A, 81:062337, June 2010.
- [179] Roman Orús. Exploring corner transfer matrices and corner tensors for the classical simulation of quantum lattice systems. Phys. Rev. B, 85:205117, 2012.
- [180] Piotr Czarnik, Lukasz Cincio, and Jacek Dziarmaga. Projected entangled pair states at finite temperature: Imaginary time evolution with ancillas. Phys. Rev. B, 86:245101, 2012.
- [181] Piotr Czarnik and Jacek Dziarmaga. Fermionic projected entangled pair states at finite temperature. Phys. Rev. B, 90:035144, July 2014.
- [182] Piotr Czarnik and Jacek Dziarmaga. Variational approach to projected entangled pair states at finite temperature. Phys. Rev. B, 92:035152, July 2015.
- [183] Piotr Czarnik and Jacek Dziarmaga. Projected entangled pair states at finite temperature: Iterative self-consistent bond renormalization for exact imaginary time evolution. Phys. Rev. B, 92:035120, Jul 2015.
- [184] Piotr Czarnik, Jacek Dziarmaga, and Andrzej M. Oleś. Variational tensor network renormalization in imaginary time: Two-dimensional quantum compass model at finite temperature. Phys. Rev. B, 93:184410, May 2016.
- [185] Piotr Czarnik, Marek M. Rams, and Jacek Dziarmaga. Variational tensor network renormalization in imaginary time: Benchmark results in the Hubbard model at finite temperature. Phys. Rev. B, 94:235142, December 2016.
- [186] Yan-Wei Dai, Qian-Qian Shi, Sam Y. Cho, Murray T. Batchelor, and Huan-Qiang Zhou. Finite-temperature fidelity and von Neumann entropy in the honeycomb spin lattice with quantum Ising interaction. Phys. Rev. B, 95:214409, June 2017.
- [187] Piotr Czarnik, Jacek Dziarmaga, and Andrzej M. Oleś. Overcoming the sign problem at finite temperature: Quantum tensor network for the orbital  $e_g$  model on an infinite square lattice. Phys. Rev. B, 96:014420, July 2017.
- [188] Wen-Cong Gan, Fu-Wen Shu, and Meng-He Wu. Thermal geometry from CFT at finite temperature. Phys. Lett. B, 760:796–799, 2016.
- [189] Ali Mollabashi, Masahiro Naozaki, Shinsei Ryu, and Tadashi Takayanagi. Holographic geometry of cMERA for quantum quenches and finite temperature. Journal of High Energy Physics, 2014(3):98, 2014.
- [190] Hong-Chen Jiang, Zheng-Yu Weng, and Tao Xiang. Accurate determination of tensor network state of quantum lattice models in two dimensions. Phys. Rev. Lett., 101:090603, 2008.
- [191] Zheng-Cheng Gu, Michael Levin, and Xiao-Gang Wen. Tensor-entanglement renormalization group approach as a unified method for symmetry breaking and topological phase transitions. Phys. Rev. B, 78:205116, 2008.
- [192] Zheng-Cheng Gu and Xiao-Gang Wen. Tensor-Entanglement-Filtering Renormalization Approach and Symmetry Protected Topological Order. Phys. Rev. B, 80:155131, 2009.

- [193] Hui-Hai Zhao, Zhi-Yuan Xie, Qihong N. Chen, Zhong-Chao Wei, Jianwei W. Cai, and Tao Xiang. Renormalization of tensor-network states. Phys. Rev. B, 81:174411, 2010.
- [194] Qian N. Chen, Ming-Pu Qin, Jack Chen, Zhong-Chao Wei, Hui-Hai Zhao, Bruce Normand, and Tao Xiang. Partial order and finite-temperature phase transitions in Potts models on irregular lattices. Phys. Rev. Lett., 107(16):165701, 2011.
- [195] Zhi-Yuan Xie, Jing Chen, Ming-Pu Qin, Jing W. Zhu, Li-Ping Yang, and Tao Xiang. Coarse-graining renormalization by higher-order singular value decomposition. Phys. Rev. B, 86:045139, 2012.
- [196] Artur García-Sáez and José I. Latorre. Renormalization group contraction of tensor networks in three dimensions. Phys. Rev. B, 87:085130, February 2013.
- [197] Ming-Pu Qin, Qian N. Chen, Zhi-Yuan Xie, Jack Chen, Jing F. Yu, Hui-Hai Zhao, Bruce Normand, and Tao Xiang. Partial long-range order in antiferromagnetic Potts models. Phys. Rev. B, 90(14):144424, 2014.
- [198] Wang Shun, Zhi-Yuan Xie, Jack Chen, Bruce Normand, and Tao Xiang. Phase Transitions of Ferromagnetic Potts Models on the Simple Cubic Lattice. Chinese Physics Lett., 31(7):070503, 2014.
- [199] Hui-Hai Zhao, Zhi-Yuan Xie, Tao Xiang, and Masatoshi Imada. Tensor network algorithm by coarse-graining tensor renormalization on finite periodic lattices. Phys. Rev. B, 93:125115, March 2016.
- [200] Scott Yang, Zheng-Cheng Gu, and Xiao-Gang Wen. Loop Optimization for Tensor Network Renormalization. Phys. Rev. Lett., 118:110504, 2017.
- [201] Roman Orús and Guifré Vidal. Simulation of two-dimensional quantum systems on an infinite lattice revisited: Corner transfer matrix for tensor contraction. Phys. Rev. B, 80:094403, 2009.
- [202] Rodney J. Baxter. Variational approximations for square lattice models in statistical mechanics. J. Stat. Phys., 19:461, 1978.
- [203] Zhi-Yuan Xie, Hong-Chen Jiang, Qinjun N. Chen, Zheng-Yu Weng, and Tao Xiang. Second renormalization of tensor-network states. Phys. Rev. Lett., 103:160601, 2009.
- [204] Jacob Jordan, Roman Orús, Guifré Vidal, Frank Verstraete, and J. Ignacio Cirac. Classical simulation of infinite-size quantum lattice systems in two spatial dimensions. Phys. Rev. Lett., 101:250602, 2008.
- [205] Iztok Pižorn, Ling Wang, and Frank Verstraete. Time evolution of projected entangled pair states in the single-layer picture. Phys. Rev. A, 83:052321, 2011.
- [206] Michael Lubasch, J. Ignacio Cirac, and Mari-Carmen Bañuls. Algorithms for finite projected entangled pair states. Phys. Rev. B, 90:064425, 2014.
- [207] Ho N. Phien, Johann A. Bengua, Hoang D. Tuan, Philippe Corboz, and Roman Orús. Infinite projected entangled pair states algorithm improved: Fast full update and gauge fixing. Phys. Rev. B, 92:035142, 2015.
- [208] Philippe Corboz. Variational optimization with infinite projected entangled-pair states. Phys. Rev. B, 94:035133, 2016.
- [209] Matthew T. Fishman, Laurens Vanderstraeten, Valentin Zauner-Stauber, Jutho Haegeman, and Frank Verstraete. Faster methods for contracting infinite 2d tensor networks. arXiv:1711.05881, 2017.
- [210] Ling Wang and Frank Verstraete. Cluster update for tensor network states. arXiv:1110.4362, 2011.
- [211] Michael Lubasch, J. Ignacio Cirac, and Mari-Carmen Bañuls. Unifying projected entangled pair state contractions. New J. Phys., 16:033014, 2014.
- [212] Llewellyn H. Thomas. The calculation of atomic fields. Math. Proc. Cambridge Philos. Soc., 23:542, 1927.
- [213] Enrico Fermi. Eine statistische methode zur bestimmung einiger eigenschaften des atoms und ihre anwendung auf die theorie des periodischen systems der elemente. Zeitschrift für Physik, 48(1-2):73–79, 1928.
- [214] Walter Metzner and Dieter Vollhardt. Correlated lattice fermions in  $d = \infty$  dimensions. Phys. Rev. Lett., 62:324, 1989.
- [215] Antoine Georges and Gabriel Kotliar. Hubbard model in infinite dimensions. Phys. Rev. B, 45:6479, 1992.
- [216] Antoine Georges, Gabriel Kotliar, Werner Krauth, and Marcelo J. Rozenberg. Dynamical mean-field theory of strongly correlated fermion systems and the limit of infinite dimensions. Rev. Mod. Phys.,



- 13:68, 1996.
- [217] Jorge E. Hirsch and R. Martin Fye. Monte Carlo method for magnetic impurities in metals. Phys. Rev. Lett., 56:2521, 1986.
- [218] Daniel J. García, Karen Hallberg, and Marcelo J. Rozenberg. Dynamical mean field theory with the density matrix renormalization group. Phys. Rev. Lett., 93:246403, 2004.
- [219] Gerald Knizia and Garnet K. L. Chan. Density matrix embedding: A simple alternative to dynamical mean-field theory. Phys. Rev. Lett., 109:186404, 2012.
- [220] Gerald Knizia and Garnet K. L. Chan. Density matrix embedding: A strong-coupling quantum embedding theory. J. Chem. Theor. Comp., 9:1428–1432, 2013.
- [221] Rodney J. Baxter. Corner transfer matrices of the eight-vertex model. I. Low-temperature expansions and conjectured properties. J. Stat. Phys., 15:485–503, 1976.
- [222] Rodney J. Baxter. Corner transfer matrices of the eight-vertex model. II. The Ising model case. J. Stat. Phys., 17:1–14, 1977.
- [223] Tomotoshi Nishino, Kouichi Okunishi, Yasuhiro Hieida, Nobuya Maeshima, and Yasuhiro Akutsu. Self-consistent tensor product variational approximation for 3D classical models. Nuclear Physics B, 575(3):504–512, 2000.
- [224] Andrej Gendiar, Nobuya Maeshima, and Tomotoshi Nishino. Stable optimization of a tensor product variational state. Progress of theoretical physics, 110(4):691–699, 2003.
- [225] Lieven Lathauwer, Lieven De Moor, and Joos Vandewalle. A multilinear singular value decomposition. SIAM J. Matrix Analysis Application, 21:1253–1278, 2000.
- [226] Ian P. McCulloch. Infinite size density matrix renormalization group, revisited. arXiv:0804.2509, 2008.
- [227] Shi-Ju Ran, Angelo Piga, Cheng Peng, Gang Su, and Maciej Lewenstein. Few-body systems capture many-body physics: Tensor network approach. Phys. Rev. B, 96:155120, Oct 2017.
- [228] Tamara G. Kolda and Brett W. Bader. Tensor Decompositions and Applications. SIAM Review, 51(3):455–500, 2009.
- [229] Lieven De Lathauwer, Bart De Moor, and Joos Vandewalle. On the best rank-1 and rank- $(r_1, r_2, \dots, r_n)$  approximation of higher-order tensors. SIAM journal on Matrix Analysis and Applications, 21(4):1324–1342, 2000.
- [230] Lieven D. Lathauwer and Joos Vandewalle. Dimensionality reduction in higher-order signal processing and rank- $(r_1, r_2, \dots, r_n)$  reduction in multilinear algebra. Linear Algebra and its Applications, 391:31–55, 2004. Special Issue on Linear Algebra in Signal and Image Processing.
- [231] Lieven De Lathauwer. A Link between the Canonical Decomposition in Multilinear Algebra and Simultaneous Matrix Diagonalization. SIAM. J. Matrix Anal. & Appl., 28(3):642–666, 2006.
- [232] Evrim Acar, Seyit A. Çamtepe, Mukkai S. Krishnamoorthy, and Bülent Yener. Modeling and Multiway Analysis of Chatroom Tensors, pages 256–268. Springer Berlin Heidelberg, Berlin, Heidelberg, 2005.
- [233] Liu Ning, Zhang Benyu, Yan Jun, Chen Zheng, Liu Wenyin, Bai Fengshan, and Chien Leefeng. Text representation: from vector to tensor. November 2005.
- [234] Jian-Tao Sun, Hua-Jun Zeng, Huan Liu, Yuchang Lu, and Zheng Chen. CubeSVD: A Novel Approach to Personalized Web Search. pages 382–390, 2005.
- [235] Evrim Acar, Seyit A. Çamtepe, and Bülent Yener. Collective Sampling and Analysis of High Order Tensors for Chatroom Communications, pages 213–224. Springer, Berlin, Heidelberg, 2006.
- [236] Jimeng Sun, Spiros Papadimitriou, and Philip S. Yu. Window-based Tensor Analysis on High-dimensional and Multi-aspect Streams. pages 1076–1080, December 2006.
- [237] Tamara G Kolda, Brett W Bader, and Joseph P Kenny. Higher-order web link analysis using multilinear algebra. In Data Mining, Fifth IEEE International Conference on, page 8. IEEE, 2005.
- [238] Tamara Kolda and Brett Bader. The tophits model for higher-order web link analysis. In Workshop on link analysis, counterterrorism and security, volume 7, pages 26–29, 2006.
- [239] Brett W. Bader, Richard A. Harshman, and Tamara G. Kolda. Temporal Analysis of Semantic Graphs Using ASALSAN. In Seventh IEEE International Conference on Data Mining (ICDM 2007), pages 33–42, October 2007.

- [240] Bo Du, Mengfei Zhang, Lefei Zhang, Ruimin Hu, and Dacheng Tao. PLTD: Patch-based low-rank tensor decomposition for hyperspectral images. *IEEE Transactions on Multimedia*, 19(1):67–79, 2017.
- [241] Nicholas D. Sidiropoulos, Lieven De Lathauwer, Xiao Fu, Kejun Huang, Evangelos E. Papalexakis, and Christos Faloutsos. Tensor decomposition for signal processing and machine learning. *IEEE Transactions on Signal Processing*, 65(13):3551–3582, 2017.
- [242] Thorsten B. Wahl, Hong-Hao Tu, Norbert Schuch, and J. Ignacio Cirac. Projected entangled-pair states can describe chiral topological states. *Phys. Rev. Lett.*, 111(23):236805, 2013.
- [243] Jerome Dubail and Nicholas Read. Tensor network trial states for chiral topological phases in two dimensions and a no-go theorem in any dimension. *Phys. Rev. B*, 92(20):205307, 2015.
- [244] Shuo Yang, Thorsten B. Wahl, Hong-Hao Tu, Norbert Schuch, and J. Ignacio Cirac. Chiral projected entangled-pair state with topological order. *Phys. Rev. Lett.*, 114(10):106803, 2015.
- [245] Didier Poilblanc, J. Ignacio Cirac, and Norbert Schuch. Chiral topological spin liquids with projected entangled pair states. *Phys. Rev. B*, 91(22):224431, 2015.
- [246] Matthieu Mambrini, Román Orús, and Didier Poilblanc. Systematic construction of spin liquids on the square lattice from tensor networks with SU(2) symmetry. *Phys. Rev. B*, 94:205124, November 2016.
- [247] Ching-Yu Huang and Tzu-Chieh Wei. Detecting and identifying two-dimensional symmetry-protected topological, symmetry-breaking, and intrinsic topological phases with modular matrices via tensor-network methods. *Phys. Rev. B*, 93:155163, April 2016.
- [248] Matthias Gerster, Matteo Rizzi, Pietro Silvi, Marcello Dalmonte, and Simone Montangero. Fractional quantum hall effect in the interacting hofstadter model via tensor networks. *Phys. Rev. B*, 96(19):195123, 2017.
- [249] Hai-Jun Liao, Zhi-Yuan Xie, Jing Chen, Zhi-Yuan Liu, Hai-Dong Xie, Rui-Zhen Huang, Bruce Normand, and Tao Xiang. Gapless Spin-Liquid Ground State in the  $S = 1/2$  Kagome Antiferromagnet. *Phys. Rev. Lett.*, 118:137202, March 2017.
- [250] Cheng Peng, Shi-Ju Ran, Tao Liu, Xi Chen, and Gang Su. Fermionic algebraic quantum spin liquid in an octa-kagome frustrated antiferromagnet. *Phys. Rev. B*, 95:075140, February 2017.
- [251] Tao Liu, Shi-Ju Ran, Wei Li, Xin Yan, Yang Zhao, and Gang Su. Featureless quantum spin liquid, 1/3-magnetization plateau state, and exotic thermodynamic properties of the spin-1/2 frustrated Heisenberg antiferromagnet on an infinite Husimi lattice. *Phys. Rev. B*, 89:054426, February 2014.
- [252] Shi-Ju Ran, Wei Li, Shou-Shu Gong, Andreas Weichselbaum, Jan von Delft, and Gang Su. Emergent spin-1 trimerized valence bond crystal in the spin-1/2 heisenberg model on the star lattice. [arXiv:1508.03451](https://arxiv.org/abs/1508.03451), 2015.
- [253] Andreas Weichselbaum. Non-abelian symmetries in tensor networks: A quantum symmetry space approach. *Ann. Phys.*, 327:2972–3047, 2012.
- [254] Norbert Schuch, J. Ignacio Cirac, and David Pérez-García. PEPS as ground states: Degeneracy and topology. *Ann. Phys.*, 325(10):2153–2192, 2010.
- [255] Sukhwinder Singh, Robert N. C. Pfeifer, and Guifré Vidal. Tensor network decompositions in the presence of a global symmetry. *Phys. Rev. A*, 82:050301, November 2010.
- [256] Jutho Haegeman, Karel Van Acoleyen, Norbert Schuch, J. Ignacio Cirac, and Frank Verstraete. Gauging Quantum States: From Global to Local Symmetries in Many-Body Systems. *Phys. Rev. X*, 5:011024, February 2015.
- [257] Manuel Rispler, Kasper Duivenvoorden, and Norbert Schuch. Long-range order and symmetry breaking in projected entangled-pair state models. *Phys. Rev. B*, 92:155133, October 2015.
- [258] Shenghan Jiang and Ying Ran. Symmetric tensor networks and practical simulation algorithms to sharply identify classes of quantum phases distinguishable by short-range physics. *Phys. Rev. B*, 92:104414, September 2015.
- [259] Erez Zohar, Michele Burrello, Thorsten B. Wahl, and J. Ignacio Cirac. Fermionic projected entangled pair states and local U(1) gauge theories. *Ann. Phys.*, 363:385–439, 2015.
- [260] Hyunyong Lee and Jung H. Han. Classification of trivial spin-1 tensor network states on a square lattice. *Phys. Rev. B*, 94:115150, September 2016.
- [261] Luca Tagliacozzo, Alessio Celi, and Maciej Lewenstein. Tensor Networks for Lattice Gauge Theories

- with Continuous Groups. Phys. Rev. X, 4:041024, November 2014.
- [262] Enrique Rico, Thomas Pichler, Marcello Dalmonte, Peter Zoller, and Simone Montangero. Tensor Networks for Lattice Gauge Theories and Atomic Quantum Simulation. Phys. Rev. Lett., 112:201601, May 2014.
- [263] Xie Chen and Ashvin Vishwanath. Towards Gauging Time-Reversal Symmetry: A Tensor Network Approach. Phys. Rev. X, 5:041034, November 2015.
- [264] Thomas Pichler, Marcello Dalmonte, Enrique Rico, Peter Zoller, and Simone Montangero. Real-Time Dynamics in U(1) Lattice Gauge Theories with Tensor Networks. Phys. Rev. X, 6:011023, March 2016.
- [265] Boye Buyens, Simone Montangero, Jutho Haegeman, Frank Verstraete, and Karel Van Acoleyen. Finite-representation approximation of lattice gauge theories at the continuum limit with tensor networks. Phys. Rev. D, 95:094509, May 2017.
- [266] Kai Zapp and Román Orús. Tensor network simulation of qed on infinite lattices: Learning from  $(1+1)d$ , and prospects for  $(2+1)d$ . Phys. Rev. D, 95:114508, June 2017.
- [267] Román Orús. Advances on tensor network theory: symmetries, fermions, entanglement, and holography. Eur. Phys. J. B, 87(11):280, November 2014.
- [268] Steven R. White and Adrian E. Feiguin. Real-time evolution using the density matrix renormalization group. Phys. Rev. Lett., 93:076401, Aug 2004.
- [269] Juan José García-Ripoll. Time evolution of matrix product states. New J. Phys., 8(12):305, 2006.
- [270] Matteo Rizzi, Simone Montangero, and Guifre Vidal. Simulation of time evolution with multiscale entanglement renormalization ansatz. Phys. Rev. A, 77:052328, May 2008.
- [271] Tomaž Prosen and Marko Žnidarič. Matrix product simulations of non-equilibrium steady states of quantum spin chains. Journal of Statistical Mechanics: Theory and Experiment, 2009(02):P02035, 2009.
- [272] Peter Barmettler, Matthias Punk, Vladimir Gritsev, Eugene Demler, and Ehud Altman. Quantum quenches in the anisotropic spin-Heisenberg chain: different approaches to many-body dynamics far from equilibrium. New J. Phys., 12(5):055017, 2010.
- [273] Marko Žnidarič. Solvable quantum nonequilibrium model exhibiting a phase transition and a matrix product representation. Phys. Rev. E, 83:011108, Jan 2011.
- [274] Andreas Holzner, Andreas Weichselbaum, Ian P. McCulloch, Ulrich Schollwöck, and Jan von Delft. Chebyshev matrix product state approach for spectral functions. Phys. Rev. B, 83:195115, May 2011.
- [275] Damian Draxler, Jutho Haegeman, Tobias J. Osborne, Vid Stojevic, Laurens Vanderstraeten, and Frank Verstraete. Particles, holes, and solitons: A matrix product state approach. Phys. Rev. Lett., 111:020402, Jul 2013.
- [276] Jian Cui, J. Ignacio Cirac, and Mari Carmen Bañuls. Variational matrix product operators for the steady state of dissipative quantum systems. Phys. Rev. Lett., 114:220601, Jun 2015.
- [277] Mari-Carmen. Bañuls, Krzysztof. Cichy, J. Ignacio. Cirac, Karl. Jansen, and Hiroki. Saito. Thermal evolution of the schwinger model with matrix product operators. Phys. Rev. D, 92:034519, Aug 2015.
- [278] Jad C. Halimeh, Fabian Kolley, and Ian P. McCulloch. Chebyshev matrix product state approach for time evolution. Phys. Rev. B, 92:115130, Sep 2015.
- [279] Moritz Binder and Thomas Barthel. Minimally entangled typical thermal states versus matrix product purifications for the simulation of equilibrium states and time evolution. Phys. Rev. B, 92:125119, Sep 2015.
- [280] Antonius Dorda, Martin Ganahl, Hans Gerd Evertz, Wolfgang von der Linden, and Enrico Arrigoni. Auxiliary master equation approach within matrix product states: Spectral properties of the nonequilibrium anderson impurity model. Phys. Rev. B, 92:125145, Sep 2015.
- [281] Eduardo Mascarenhas, Hugo Flayac, and Vincenzo Savona. Matrix-product-operator approach to the nonequilibrium steady state of driven-dissipative quantum arrays. Phys. Rev. A, 92:022116, Aug 2015.
- [282] Laurens Vanderstraeten, Jutho Haegeman, Tobias J. Osborne, and Frank Verstraete.  $s$  matrix from matrix product states. Phys. Rev. Lett., 112:257202, Jun 2014.
- [283] Alexander C. Tiegel, Salvatore R. Manmana, Thomas Pruschke, and Andreas Honecker. Matrix product

- state formulation of frequency-space dynamics at finite temperatures. Phys. Rev. B, 90:060406, Aug 2014.
- [284] Lars Bonnes, Daniel Charrier, and Andreas M. Läuchli. Dynamical and steady-state properties of a bose-hubbard chain with bond dissipation: A study based on matrix product operators. Phys. Rev. A, 90:033612, Sep 2014.
- [285] Albert. H. Werner, Daniel. Jaschke, Pietro. Silvi, Martin. Kliesch, Tommaso. Calarco, Jens Eisert, and Simone Montangero. Positive tensor network approach for simulating open quantum many-body systems. Phys. Rev. Lett., 116:237201, Jun 2016.
- [286] Augustine Kshetrimayum, Hendrik Weimer, and Román Orús. A simple tensor network algorithm for two-dimensional steady states. Nat. Comm., 8(1):1291, 2017.
- [287] Cédric Bény. Deep learning and the renormalization group. [arXiv:1301.3124](https://arxiv.org/abs/1301.3124), 2013.
- [288] Ding Liu, Shi-Ju Ran, Peter Wittek, Cheng Peng, Raul B. Garcia, Gang Su, and Maciej Lewenstein. Machine learning by two-dimensional hierarchical tensor networks: A quantum information theoretic perspective on deep architectures. [arXiv:1710.04833](https://arxiv.org/abs/1710.04833), 2017.
- [289] Jing Chen, Song Cheng, Haidong Xie, Lei Wang, and Tao Xiang. On the equivalence of restricted Boltzmann machines and tensor network states. [arXiv:1701.04831](https://arxiv.org/abs/1701.04831), 2017.
- [290] Yichen Huang and Joel E. Moore. Neural network representation of tensor network and chiral states. [arXiv:1701.06246](https://arxiv.org/abs/1701.06246), 2017.
- [291] Zhao-Yu Han, Jun Wang, Heng Fan, Lei Wang, and Pan Zhang. Unsupervised Generative Modeling Using Matrix Product States. [arXiv:1709.01662](https://arxiv.org/abs/1709.01662), 2017.
- [292] Yoav Levine, David Yakira, Nadav Cohen, and Amnon Shashua. Deep Learning and Quantum Physics: A Fundamental Bridge. [arXiv:1704.01552](https://arxiv.org/abs/1704.01552), 2017.
- [293] Angel J. Gallego and Roman Orús. The physical structure of grammatical correlations: equivalences, formalizations and consequences. [arXiv:1708.01525](https://arxiv.org/abs/1708.01525), 2017.
- [294] Yuhan Liu, Xiao Zhang, Maciej Lewenstein, and Shi-Ju Ran. Learning architectures based on quantum entanglement: a simple matrix product state algorithm for image recognition. [arXiv:1803.09111](https://arxiv.org/abs/1803.09111), 2018.
- [295] Andrzej Cichocki, Namgil Lee, Ivan Oseledets, Anh-Huy Phan, Qibin Zhao, Danilo P. Mandic, and Others. Tensor networks for dimensionality reduction and large-scale optimization: Part 1 low-rank tensor decompositions. Foundations and Trends@ in Machine Learning, 9(4-5):249–429, 2016.
- [296] Andrzej Cichocki, Anh-Huy Phan, Qibin Zhao, Namgil Lee, Ivan Oseledets, Masashi Sugiyama, Danilo P. Mandic, and Others. Tensor Networks for Dimensionality Reduction and Large-scale Optimization: Part 2 Applications and Future Perspectives. Foundations and Trends@ in Machine Learning, 9(6):431–673, 2017.
- [297] Jacob Biamonte and Ville Bergholm. Tensor networks in a nutshell. [arXiv:1708.00006](https://arxiv.org/abs/1708.00006), 2017.
- [298] Erhard Schmidt. Zur Theorie der linearen und nichtlinearen Integralgleichungen. I. Teil: Entwicklung willkürlicher Funktionen nach Systemen vorgeschriebener. Mathematische Annalen, 63:433–476, 1907.
- [299] Artur Ekert and Peter L. Knight. Entangled quantum systems and the Schmidt decomposition. American Journal of Physics, 63(5):415–423, 1995.
- [300] Asher Peres. Quantum Theory: Concepts and Methods. Springer Netherlands, 2002.
- [301] Charles H. Bennett, Herbert J. Bernstein, Sandu Popescu, and Benjamin Schumacher. Concentrating partial entanglement by local operations. Phys. Rev. A, 53:2046–2052, April 1996.
- [302] Ivan V. Oseledets. Tensor-Train Decomposition. SIAM Journal on Scientific Computing, 33(5):2295–2317, 2011.
- [303] Johan J. de Swart. The Octet Model and its Clebsch-Gordan Coefficients. Rev. Mod. Phys., 35:916–939, October 1963.
- [304] Steven T. Bramwell and Michel J. P. Gingras. Spin Ice State in Frustrated Magnetic Pyrochlore Materials. Science, 294(5546):1495–1501, 2001.
- [305] John D. Bernal and Ralph H. Fowler. A Theory of Water and Ionic Solution, with Particular Reference to Hydrogen and Hydroxyl Ions. The Journal of Chemical Physics, 1(8):515–548, 1933.
- [306] Tom Fennell, Pascale Deen, A. R. Wildes, K. Schmalzl, D. Prabhakaran, A. T. Boothroyd, R. J. Aldus,

- D. F. McMorrow, and S. T. Bramwell. Magnetic coulomb phase in the spin ice  $ho_2ti_2o_7$ . Science, 326(5951):415–417, 2009.
- [307] Rodney J. Baxter. Eight-Vertex Model in Lattice Statistics. Phys. Rev. Lett., 26:832–833, April 1971.
- [308] Gregory M. Crosswhite and Dave Bacon. Finite automata for caching in matrix product algorithms. Phys. Rev. A, 78:012356, July 2008.
- [309] Gregory M. Crosswhite, A. C. Doherty, and Guifré Vidal. Applying matrix product operators to model systems with long-range interactions. Phys. Rev. B, 78:035116, July 2008.
- [310] Walter Kohn. Nobel Lecture: Electronic structure of matter: wave functions and density functionals. Rev. Mod. Phys., 71:1253–1266, October 1999.
- [311] Ingo Peschel, Matthias Kaulke, and Örs Legeza. Density-matrix spectra for integrable models. Annalen der Physik, 8(2):153–164, 1999.
- [312] Giuseppe Vitagliano, Arnau Riera, and José I. Latorre. Volume-law scaling for the entanglement entropy in spin-1/2 chains. New J. Phys., 12(11):113049, 2010.
- [313] Frank Pollmann and Joel E. Moore. Entanglement spectra of critical and near-critical systems in one dimension. New J. Phys., 12(2):025006, 2010.
- [314] Frank Pollmann and Ari M. Turner. Detection of symmetry-protected topological phases in one dimension. Phys. Rev. B, 86(12):125441, 2012.
- [315] Dominique Delande, Krzysztof Sacha, Marcin Płodzień, Sanat K. Avazbaev, and Jakub Zakrzewski. Many-body Anderson localization in one-dimensional systems. New J. Phys., 15(4):045021, 2013.
- [316] Jens H. Bardarson, Frank Pollmann, and Joel E. Moore. Unbounded growth of entanglement in models of many-body localization. Phys. Rev. Lett., 109(1):017202, 2012.
- [317] Pedro Ponte, Zlatko Papić, François Huveneers, and Dmitry A. Abanin. Many-body localization in periodically driven systems. Phys. Rev. Lett., 114(14):140401, 2015.
- [318] Balázs Pozsgay, Márton Mestyán, Miklós A. Werner, Márton Kormos, Gergely Zaránd, and Gábor Takács. Correlations after Quantum Quenches in the X X Z Spin Chain: Failure of the Generalized Gibbs Ensemble. Phys. Rev. Lett., 113(11):117203, 2014.
- [319] Peter Barmettler, Matthias Punk, Vladimir Gritsev, Eugene Demler, and Ehud Altman. Relaxation of antiferromagnetic order in spin-1/2 chains following a quantum quench. Phys. Rev. Lett., 102(13):130603, 2009.
- [320] Maurizio Fagotti, Mario Collura, Fabian H. L. Essler, and Pasquale Calabrese. Relaxation after quantum quenches in the spin-1 2 Heisenberg XXZ chain. Phys. Rev. B, 89(12):125101, 2014.
- [321] Fabian H. L. Essler and Maurizio Fagotti. Quench dynamics and relaxation in isolated integrable quantum spin chains. Journal of Statistical Mechanics: Theory and Experiment, 2016(6):064002, 2016.
- [322] Frank Pollmann and Joel E. Moore. Entanglement spectra of critical and near-critical systems in one dimension. New J. Phys., 12(2):025006, 2010.
- [323] Rodney J. Baxter. Exactly solved models in statistical mechanics. Elsevier, 2016.
- [324] Rodney J. Baxter. Corner transfer matrices of the chiral Potts model. J. Stat. Phys., 63:433–453, 1991.
- [325] Rodney J. Baxter. Chiral Potts model: corner transfer matrices and parametrizations. Int. J. Mod. Phys. B, 7:3489–3500, 1993.
- [326] Rodney J. Baxter. Corner transfer matrices of the chiral Potts model. II. The triangular lattice. J. Stat. Phys., 70:535–582, 1993.
- [327] Rodney J. Baxter and Peter J. Forrester. A variational approximation for cubic lattice models in statistical mechanics. J. Phys. A: Math. Gen., 17:2675–2685, 1984.
- [328] Tomotoshi Nishino and Kouichi Okunishi. Corner transfer matrix algorithm for classical renormalization group. Journal of the Physical Society of Japan, 66(10):3040–3047, 1997.
- [329] Tomotoshi Nishino and Kouichi Okunishi. Numerical latent heat observation of the  $q=5$  Potts model. arXiv preprint cond-mat/9711214, 1997.
- [330] Tomotoshi Nishino and Kouichi Okunishi. A density matrix algorithm for 3D classical models. Journal of the Physical Society of Japan, 67(9):3066–3072, 1998.
- [331] Norihiro Tsushima and Tsuyoshi Horiguchi. Phase diagrams of spin-3/2 Ising model on a square lattice in terms of corner transfer matrix renormalization group method. Journal of the Physical Society of

- Japan, 67(5):1574–1582, 1998.
- [332] Kouichi Okunishi, Yasuhiro Hieida, and Yasuhiro Akutsu. Universal asymptotic eigenvalue distribution of density matrices and corner transfer matrices in the thermodynamic limit. Phys. Rev. E, 59(6), 1999.
- [333] Kouichi Okunishi and Tomotoshi Nishino. Kramers-Wannier approximation for the 3D Ising model. Progress of Theoretical Physics, 103(3):541–548, 2000.
- [334] Tomotoshi Nishino, Yasuhiro Hieida, Kouichi Okunishi, Nobuya Maeshima, Yasuhiro Akutsu, and Andrej Gendiar. Two-dimensional tensor product variational formulation. Prog. Theor. Phys., 105(3):409–417, 2001.
- [335] Z. B. Li, Z. Shuai, Q. Wang, H. J. Luo, and Lothar Schülke. Critical exponents of the two-layer Ising model. Journal of Physics A: Mathematical and General, 34(31):6069, 2001.
- [336] Andrej Gendiar and Tomotoshi Nishino. Latent heat calculation of the three-dimensional  $q=3, 4$ , and 5 Potts models by the tensor product variational approach. Phys. Rev. E, 65(4):046702, 2002.
- [337] Glen Evenbly and Guifré Vidal. Tensor Network Renormalization. Phys. Rev. Lett., 115:180405, October 2015.
- [338] Glen Evenbly and Guifré Vidal. Tensor Network Renormalization Yields the Multiscale Entanglement Renormalization Ansatz. Phys. Rev. Lett., 115:200401, November 2015.
- [339] Mari-Carmen Bañuls, Matthew B. Hastings, Frank Verstraete, and J. Ignacio Cirac. Matrix Product States for Dynamical Simulation of Infinite Chains. Phys. Rev. Lett., 102:240603, June 2009.
- [340] Glen Evenbly and Robert N. C. Pfeifer. Improving the efficiency of variational tensor network algorithms. Phys. Rev. B, 89:245118, June 2014.
- [341] Robert N. C. Pfeifer, Jutho Haegeman, and Frank Verstraete. Faster identification of optimal contraction sequences for tensor networks. Phys. Rev. E, 90:033315, September 2014.
- [342] Paul A. M. Dirac. Note on exchange phenomena in the thomas atom. Mathematical Proceedings of the Cambridge Philosophical Society, 26(3):376385, 1930.
- [343] Arthur K. Kerman and Steven E. Koonin. Hamiltonian formulation of time-dependent variational principles for the many-body system. Ann. Phys., 100(1):332 – 358, 1976.
- [344] Roman Jackiw and Arthur K. Kerman. Time-dependent variational principle and the effective action. Physics Lett. A, 71(2):158–162, 1979.
- [345] P. W. Langhoff, S. T. Epstein, and M. Karplus. Aspects of time-dependent perturbation theory. Rev. Mod. Phys., 44:602–644, Jul 1972.
- [346] Ho N. Phien, Ian P. McCulloch, and Guifré Vidal. Fast convergence of imaginary time evolution tensor network algorithms by recycling the environment. Phys. Rev. B, 91:115137, Mar 2015.
- [347] Frank L. Hitchcock. The expression of a tensor or a polyadic as a sum of products. Studies in Applied Mathematics, 6(1-4):164–189, 1927.
- [348] Frank L. Hitchcock. Multiple Invariants and Generalized Rank of a P-Way Matrix or Tensor. Studies in Applied Mathematics, 7(1-4):39–79, 1928.
- [349] Emanuele Tirrito, Maciej Lewenstein, and Shi-Ju Ran. Criticality and excitation gap in quantum systems: Applications of continuous matrix product states in imaginary time. arXiv:1608.06544.
- [350] Jutho Haegeman, Christian Lubich, Ivan Oseledets, Bart Vandereycken, and Frank Verstraete. Unifying time evolution and optimization with matrix product states. Phys. Rev. B, 94:165116, October 2016.
- [351] Alexander Müller-Hermes, J. Ignacio Cirac, and Mari-Carmen Bañuls. Tensor network techniques for the computation of dynamical observables in one-dimensional quantum spin systems. New J. Phys., 14(7):075003, 2012.
- [352] Jutho Haegeman and Frank Verstraete. Diagonalizing transfer matrices and matrix product operators: A medley of exact and computational methods. Annual Review of Condensed Matter Physics, 8(1):355–406, 2017.
- [353] Lars Onsager. Crystal statistics. i. a two-dimensional model with an order-disorder transition. Phys. Rev., 65(3-4):117, 1944.
- [354] Roman Orús. A practical introduction to tensor networks: Matrix product states and projected entangled pair states. Ann. Phys., 349:117, 2014.
- [355] J. Ignacio Cirac and Frank Verstraete. Renormalization and tensor product states in spin chains and

- lattices. J. Phys. A: Math. Theor., 42:504004, 2009.
- [356] Valentin Zauner-Stauber, Laurens Vanderstraeten, Matthew T Fishman, Frank Verstraete, and Jutho Haegeman. Variational optimization algorithms for uniform matrix product states. Phys. Rev. B, 97(4):045145, 2018.
- [357] Ho N. Phien, Guifré Vidal, and Ian P. McCulloch. Infinite boundary conditions for matrix product state calculations. Phys. Rev. B, 86:245107, December 2012.
- [358] Shi-Ju Ran, Cheng Peng, Gang Su, and Maciej Lewenstein. Controlling phase diagram of finite spin-1/2 chains by tuning boundary interactions. arXiv:1707.07838, 2017.
- [359] Hans J. Briegel and Robert Raussendorf. Persistent Entanglement in Arrays of Interacting Particles. Phys. Rev. Lett., 86:910–913, January 2001.
- [360] Robert Raussendorf and Hans J. Briegel. A One-Way Quantum Computer. Phys. Rev. Lett., 86:5188–5191, May 2001.
- [361] Alexey Vyacheslavovich Gorshkov, M Hermele, V Gurarie, C Xu, Paul S Julienne, J Ye, Peter Zoller, Eugene Demler, Mikhail D Lukin, and AM Rey. Two-orbital  $SU(n)$  magnetism with ultracold alkaline-earth atoms. Nat. Phys., 6(4):289, 2010.
- [362] Debasish Banerjee, Michael Bögli, Marcello Dalmonte, Enrique Rico, Pascal Stebler, Uwe-Jens Wiese, and Peter Zoller. Atomic quantum simulation of  $U(n)$  and  $SU(n)$  non-abelian lattice gauge theories. Phys. Rev. Lett., 110:125303, Mar 2013.
- [363] Francesco Scazza, Christian Hofrichter, Moritz Höfer, PC De Groot, Immanuel Bloch, and Simon Fölling. Observation of two-orbital spin-exchange interactions with ultracold  $SU(n)$ -symmetric fermions. Nat. Phys., 10(10):779, 2014.
- [364] Xiaohang Zhang, Michael Bishof, Sarah L. Bromley, Christina V. Kraus, Marianna S. Safronova, Peter Zoller, Ana Maria Rey, and Jun Ye. Spectroscopic observation of  $SU(n)$ -symmetric interactions in Sr orbital magnetism. Science, 345(6203):1467–1473, 2014.

